Superfund Records Center
SITE: Centredale
BREAK: 3.4
OTHER: 25.357

SDMS DocID 253337

US ARMY CORPS
OF ENGINEERS
New England District

Contract No. DACW33-01-D-0004
Delivery Order No. 01
March 2006

Interim Final

Sediment Stability Study
Phase II Report

Centredale Manor Restoration Project Superfund Site
North Providence, Rhode Island

INTERIM FINAL

Sediment Stability Study
Phase II Report

Centredale Manor Restoration Project Superfund Site
North Providence, Rhode Island

CONTRACT NUMBER: DACW33-01-D-0004
DELIVERY ORDER NO. 01

Submitted to

Department of the Army
U.S. Army Corps of Engineers
North Atlantic Division
New England District

March 2006

Prepared by

Quantitative Environmental Analysis, LLC
Montvale, NJ

Under contract to

BATTELLE
397 Washington Street
Duxbury, MA 02332
(781) 934-0571

TABLE OF CONTENTS

1.0 INTRODUCTION 1-1
1.1 Objective and Approach 1-1
1.2 Report Organization 1-2

2.0 DATA-BASED STABILITY ANALYSES 2-1
2.1 Bulk Bed Property Data 2-1
2.1.1 Allendale Pond 2-1
2.1.2 Lyman Mill Pond 2-2
2.1.3 Comparison of Bulk Bed Properties 2-2
2.2 Geochronology Analyses 2-2
2.2.1 ^{210}Pb Data Analysis 2-2
2.2.2 ^{137}Cs Data Analysis 2-4
2.2.3 Comparison of Sedimentation Rates Based on ^{210}Pb and ^{137}Cs Data 2-5
2.3 Dioxin Bed Concentration Data 2-5
2.4 Dioxin Water-Column Concentration Data 2-6

3.0 MODEL-BASED STABILITY ANALYSES 3-1
3.1 Hydrodynamic Model Development 3-1
3.1.1 Geometry and Bathymetry 3-1
3.1.2 Boundary Conditions 3-1
3.1.3 Model Calibration 3-2
3.2 Flood Flow Simulations 3-5
3.2.1 Estimates of Flood Flow Rates 3-5
3.2.2 Methods for Estimating Potential Bed Scour 3-5
3.2.3 Allendale Pond Results 3-9
3.2.4 Lyman Mill Pond Results 3-10
3.3 Sensitivity Analysis 3-11
3.3.1 Sensitivity Analysis: Bottom Roughness 3-12
3.3.2 Sensitivity Analysis: Dry Density 3-12
3.4 Summary of Model Results 3-12
3.5 Model Limitations 3-13

4.0 CONCEPTUAL SITE MODEL FOR SEDIMENT TRANSPORT 4-1

5.0 CONCLUSIONS RELATED TO BED STABILITY 5-1

6.0 REFERENCES 6-1

LIST OF TABLES

Table 2-1. Average Content of Clay/Silt, Sand and Gravel in Allendale and Lyman Mill Ponds 2-2
Table 2-2. Estimated Sedimentation Rates Based on 210Pb Data 2-3
Table 2-3. Estimated Ranges of Sedimentation Rates. 2-4
Table 2-4. Spatial Extent of Zones Used in Non-Resuspending Dioxin Flux Analysis. 2-7
Table 2-5. Statistics for Dioxin Concentration in Five Zones (Oct-Nov 1999 Data). 2-7
Table 2-6. Statistics for Dioxin Load in Five Zones (Oct-Nov 1999 Data) 2-7
Table 2-7. Statistics for Dioxin Concentration in Three Zones (December 2004 Data) 2-8
Table 2-8. Statistics for Dioxin Load in Three Zones (December 2004 Data). 2-8
Table 3-1. Current Velocity Sampling Locations. 3-3
Table 3-2. Current Velocity and Water Depth Measurements in Allendale Pond. 3-3

Table 3-3. Current Velocity and Water Depth Measurements in Lyman Mill Pond. 3-4
Table 3-4. Flow Rates for Flood Event Simulations. 3-5
Table 3-5. Shaker Core Locations and Descriptions. 3-7
Table 3-6. Measured Resuspension Potential in Allendale and Lyman Mill Ponds. 3-8
Table 3-7. Resuspension Parameters Used in Scour Depth Analysis. 3-8
Table 3-8. Potential Scour Areas in Allendale Pond. 3-9
Table 3-9. Areas of Potential-Measurable-Erosion in Allendale Pond. 3-9
Table 3-10. Impacts of Bed Scour in Allendale Pond. 3-10
Table 3-11. Potential Scour Areas in Lyman Mill Pond. 3-10
Table 3-12. Areas of Potential-Measurable-Erosion in Lyman Mill Pond. 3-11
Table 3-13. Impacts of Bed Scour in Lyman Mill Pond. 3-11
Table 3-14. Sensitivity to Bottom Roughness Variation: Allendale Pond, 100-Year Flood. 3-12
Table 3-15. Sensitivity to Bottom Roughness Variation: Lyman Mill Pond, 100-Year Flood. 3-12

Appendix A: Figures

Appendix B: Potential Impact of Upstream Reservoir Releases on Bed Stability in Allendale and Lyman Mill Ponds

ABBREVIATIONS AND ACRONYMS

1940-TH	1940 time horizon
95% CI	95 percent confidence interval
cfs	Cubic feet per second
COC	Chemical-of-concern
CSM	Conceptual site model
D50	50th percentile (median) particle diameter
D90	90th percentile particle diameter
EFDC	Environmental Fluid Dynamics Code
FEMA	Federal Emergency Management Agency
FIS	Flood Insurance Study
FS	Feasibility Study
NGVD	National Geodetic Vertical Datum
QEA	Quantitative Environmental Analysis, LLC
RI	Remedial Investigation
TEQ	Toxic Equivalency Quotient
USACE	United States Army Corps of Engineers
USEPA	United States Environmental Protection Agency
USGS	United States Geological Survey

This page intentionally left blank.

1.0 INTRODUCTION

The U.S. Environmental Protection Agency (USEPA) Region I and U.S. Army Corps of Engineers (USACE) New England District are conducting a Remedial Investigation and Feasibility Study (RI/FS) for the Centredale Manor Restoration Project Superfund Site (i.e., the site), located in North Providence, Rhode Island. As part of the RI/FS, a sediment stability study was conducted at the site. The results of Phase I of that study were presented in Quantitative Environmental Analysis (QEA) (2004c). Additional work was conducted during Phase II of the sediment stability study, and that work is presented in this report, which is an updated version of the Phase I report (i.e., QEA 2004c). The Phase II work includes: calibration of the hydrodynamic model; collection and analysis of site-specific bed erosion data; collection and analysis of bed probing data; revised model simulations using the calibrated model and site-specific erosion data; and inclusion of additional dioxin water column concentration data in Section 2.4.

A sediment stability evaluation is used to assess the impacts of sediment erosion, transport, and deposition processes on surficial sediment bed and water column concentrations of a chemical-of-concern (COC) within a river channel. Thus, a general understanding of sediment transport processes is important when conducting a sediment stability study. Stability evaluations consider both the hydrodynamic forces that induce sediment resuspension and properties of the sediment bed that influence erosion rates. Erosion from a sediment bed occurs through two modes of transport: 1) bed load transport, which is the near-bed transport of sand and gravel; and 2) suspended load transport, which is resuspension of clay, silt and fine sand into the water column. The eroded sediment particles eventually deposit, or return to the sediment bed, at a different location.

The assessment of the efficacy of remedial alternatives for contaminated sediment deposits generally includes a sediment stability analysis. Determining whether a sediment deposit is stable or unstable typically involves evaluating the impact of sediment transport processes on COC concentrations in the bioavailable layer and the associated effects of remedial alternatives on mitigating those impacts. Erosion potential of the overlying portion of the sediment bed will determine whether or not the elevated COC concentrations become bioavailable at some point in the future. Re-exposure of the elevated concentrations to the bioavailable layer may occur due to bed elevation changes occurring over two time scales: 1) net erosion during a high-energy event (e.g., flood in a river); and 2) long-term bed degradation (e.g., changes on decadal time scales). Another process that must be considered is natural recovery, which is the burial of high-concentration COC deposits by subsequent deposition of low-concentration COC (i.e., cleaner) sediment. Erosion, transport, and deposition, and therefore natural recovery, are generally both temporally and spatially variable within a contaminated sediment site.

Erosion is caused by physical forces on the sediment bed. These forces are typically generated by two hydrodynamic processes: current velocity and surface waves. These processes induce erosion by applying a shear stress (i.e., force per unit area) on the sediment bed that exceeds the critical value for the bed to remain in place (i.e., critical shear stress). The sediment bed resists erosion through a combination of gravitational force on particles, physical structure of the bed, and cohesive forces holding the bed together. These cohesive forces depend on various sediment physical properties, including bulk density, mineralogy, grain size distribution, gas content, and organic content.

1.1 Objective and Approach

Sediment stability is an important issue when considering the efficacy of various remedial alternatives at the site. While this study considers site-specific issues or questions, the primary issues that this study focuses on, with respect to remedial alternative evaluation, are:

- Potential for short- and long-term sediment transport processes to re-distribute bed contaminants within Allendale and Lyman Mill Ponds and downstream of Lyman Mill Dam.

- The impact of sediment transport processes on the natural recovery rate of bed concentrations in the surface layer.

The specific questions addressed in this sediment stability evaluation are as follows:

- What is the impact of floods of various magnitudes on surficial dioxin toxic equivalency quotient (TEQ) concentrations in Allendale and Lyman Mill Ponds?
    - What scour depth will be caused by floods of various magnitudes?
    - Where is scour likely to occur within the ponds?

- What effect will different remedial alternatives have on mitigating the impacts of a rare (i.e., 100-year) flood?

A two-phased approach was used to address these questions as described in the Final Sediment Stability Work Plan (QEA 2004a). In Phase A, site data were compiled, analyzed and synthesized to develop a coherent understanding of sediment transport in the study area. The results of the data synthesis task were used to develop a Conceptual Site Model (CSM) for sediment transport. A CSM is an important component of a sediment stability analysis because consistency must be maintained between the CSM and the results of quantitative and qualitative sediment stability analyses. The sediment transport CSM is a qualitative description of the processes (e.g., deposition and erosion) and system characteristics (e.g., upstream and tributary sediment loads, spatial distribution of bed properties) that control sediment dynamics within the study area.

In Phase B, a hydrodynamic model was developed and applied. The hydrodynamic model was used to evaluate the potential impacts of a range of floods on bed stability. Impacts of floods with 5-, 10-, 25-, 50- and 100-year return periods were investigated. For each flood simulation, two methods were used to analyze the potential impacts on bed stability: 1) comparison of bottom shear stress and current velocity to critical values for those parameters; and 2) estimation of scour depth.

1.2 Report Organization

This report consists of six sections and two appendices, as follows:

Section 1:	Introduction
Section 2:	Data-Based Stability Analyses
Section 3:	Model-Based Stability Analyses
Section 4:	Conceptual Site Model for Sediment Transport
Section 5:	Conclusions Related to Bed Stability
Section 6:	References
Appendix A:	Figures
Appendix B:	Potential Impact of Upstream Reservoir Releases on Bed Stability in Allendale and Lyman Mill Ponds

2.0 DATA-BASED STABILITY ANALYSES

The main objective of the data-based analyses presented in this section is to develop an understanding of data and processes related to bed stability in Allendale and Lyman Mill Ponds. The primary data sets used in these analyses were collected in May 2003 and include data on bulk bed properties, radioisotope activities and dioxin concentrations. In addition, dioxin water-column concentration data obtained during low-flow periods in October-November 1999 and December 2004 were analyzed to develop an understanding of bed fluxes from the pond under non-resuspending conditions.

2.1 Bulk Bed Property Data

Sediment core samples were collected in Allendale and Lyman Mill Ponds during May 2003. Core sample locations are shown on Figures 2-1 and 2-2. Bulk bed property data from these samples were evaluated to develop a general understanding of the type of sediment in the ponds and associated physical properties. A detailed mapping of sediment bed type, i.e., delineation of cohesive and non-cohesive bed areas, within the two ponds is not possible at the present time due to technical difficulties associated with the side-scan sonar survey conducted during October 2002 (Shields 2003). Shields (2003) indicated that 'the presence of dense organic growth and/or a thick layer of decaying material, which was also filled with gas bubbles, probably greatly attenuated the transmitted signal'.

2.1.1 Allendale Pond

The sediment bed in Allendale Pond is generally composed of cohesive sediment, i.e. muddy sediment with some sand and gravel. Surface-layer sediment (i.e., approximately top 6-12 inches) in Allendale Pond is primarily composed of fine-grained cohesive sediment with sandy sediment found in the deeper portions of the bed. Core logs presented in Corcoran (2004) show that, generally, surficial sediment is classified as peat. Grain size distribution data for surficial sediments were collected from 15 cores, with 13 cores being classified as cohesive sediment. A core was classified as cohesive if it met the following criteria: median particle diameter (D_{50}) < 250 μm and clay/silt content > 15 percent (Ziegler and Nisbet 1994). The two cores classified as non-cohesive had D_{50} values of 900 and 23,500 μm (cores CMS-SD-4214 and CMS-SD-4208, respectively), with clay/silt content less than 3 percent.

Frequency distributions of four bulk bed properties for the 13 surficial cores classified as cohesive are shown on Figure 2-3: organic matter content, dry (bulk) density, median particle diameter (D_{50}), and 90th percentile particle diameter (D_{90}). Organic matter content ranges from about 23 to 57 percent, with a median value of 33 percent. Dry (bulk) density of surficial layer sediment has an average value of 0.76 g/cm^3, with a range of 0.47 to 1.11 g/cm^3. The 95 percent confidence interval (95% CI) about the mean value is 0.63 to 0.89 g/cm^3. For the 13 cohesive cores, D_{50} values range from 10 to 113 μm and the clay/silt content varies from 39 to 98 percent.

In addition to the surficial data described above, grain size distribution information was collected from deeper segments of sediment cores in both ponds. Frequency distributions of clay/silt, sand and gravel content of surficial and subsurface Allendale Pond sediments are presented on Figure 2-4. Average contents of the three sediment classes are listed in Table 2-1.

Table 2-1. Average Content of Clay/Silt, Sand and Gravel in Allendale and Lyman Mill Ponds.

Sediment Type	Allendale Pond	Lyman Mill Pond
Clay/silt	41	67
Sand	49	30
Gravel	10	3

2.1.2 Lyman Mill Pond

The Lyman Mill Pond bed is primarily composed of cohesive sediment. Core logs indicate that the upper 6-12 inches of the bed is generally classified as muck, with coarser material occurring deeper in the bed (Corcoran 2004). Figure 2-5 presents frequency distributions of bed property data measured in surface-layer samples from cores collected from this pond. The median value of organic matter content is approximately 25 percent, with most of the data ranging from about 18 to 27 percent (one sample has an organic content of 60 percent). The mean dry density value of surficial sediment is 0.59 g/cm^3, with the 95% CI varying from 0.47 to 0.71 g/cm^3. Seven cores with grain distribution data are classified as cohesive sediment. The D_{50} values of surficial sediment in these cores range from 7 to 122 µm, with clay/silt content varying between 26 and 99 percent. Frequency distributions of clay/silt, sand and gravel content of Lyman Mill Pond sediments (all depths) are presented on Figure 2-6. Average contents of the three sediment classes are listed in Table 2-1.

2.1.3 Comparison of Bulk Bed Properties

The sediment bed in Lyman Mill Pond is generally finer (i.e., more clay/silt and less sand/gravel) than the bed in Allendale Pond. A large fraction of the coarse sediment (sand and gravel) entering the upstream pond (Allendale) will be deposited in that pond; the sand content of the suspended sediment load entering Lyman Mill Pond will be significantly less than the sand content flowing into Allendale Pond. This situation is typical for a river with a series of impoundments, such as occurs within the study area.

2.2 Geochronology Analyses

The radioisotopes cesium-137 (^{137}Cs) and lead-210 (^{210}Pb) are used to age-date sediments and to establish sedimentation rates in estuarine and freshwater systems (Olsen et al. 1978, Orson et al. 1990). Descriptions of the geochronology analyses that are used to evaluate radioisotope cores collected in Allendale and Lyman Mill Ponds are provided below. Ten of the sediment cores collected in the two ponds during May 2003 were analyzed for radioisotopes (i.e., ^{210}Pb and ^{137}Cs activity). Nine cores are from Allendale Pond and one core is from Lyman Mill Pond (LPX-SD-4201, Figure 2-2). A preliminary evaluation of sedimentation rates for the cores was conducted by USACE (Corcoran 2004). The analyses presented in this section expand upon the USACE analysis, with an emphasis on evaluating uncertainty in the estimated sedimentation rates.

2.2.1 ^{210}Pb Data Analysis

Lead-210 (^{210}Pb), which is a decay product of volatilized atmospheric radon-222 (^{222}Rn), is present in sediments primarily as a result of recent atmospheric deposition. Radon-222 is a volatile, short-lived, intermediate daughter of uranium-238 (^{238}U), a naturally-occurring radioisotope found in the earth's crust. The ^{210}Pb activity in a sediment sample represents the total ^{210}Pb activity, which is measured indirectly by analysis of its radioactive decay products bismuth-210 or polonium-210. Total ^{210}Pb activity ($^{210}Pb_T$), is composed of two components: 1) unsupported ^{210}Pb ($^{210}Pb_u$), which represents ^{210}Pb that is deposited on the earth's surface at an approximately constant rate via atmospheric deposition; and 2) supported ^{210}Pb ($^{210}Pb_s$), which is the background ^{210}Pb activity in the sediment. In aquatic environments, the approximately constant atmospheric flux of ^{210}Pb, and its decay half-life of 22.3 years, results in relatively

homogeneous ^{210}Pb activities within the biologically-active surface layer of the sediment bed and activities that decay exponentially below this depth. For this reason, ^{210}Pb serves as a useful tracer for estimating sedimentation rates in aquatic systems (Olsen et al. 1978, Orson et al. 1990, Robbins 1978).

Two models may be used to calculate sedimentation rates using ^{210}Pb data: 1) constant rate of supply (CRS); and 2) constant initial concentration (CIC). The CRS model assumes that the ^{210}Pb supply from the atmosphere to the sediment bed is constant and is independent of changes in sedimentation rate. Variation in the sedimentation rate causes either dilution (i.e., increased sedimentation rate) or concentration (i.e., decreased sedimentation rate) of ^{210}Pb levels. The CIC model assumes that the initial unsupported ^{210}Pb activity is constant and it is not dependent on changes in sedimentation rate. Thus, variation in the amount of ^{210}Pb removed from the water column to the sediment bed is correlated to the variation in sedimentation rate (Allen et al. 1993).

For this study, the CIC model is used. The first step in the analysis is to determine $^{210}Pb_s$ for a core in order to calculate $^{210}Pb_u$:

$$^{210}Pb_u = {}^{210}Pb_T - {}^{210}Pb_s \qquad (2\text{-}1)$$

Average values of $^{210}Pb_s$ were determined for each core (see Table 2-2). Data points used to calculate the average value in each core are shown as open circles on the left-hand panels of Figures 2-7 to 2-16.

Table 2-2. Estimated Sedimentation Rates Based on ^{210}Pb Data.

Core Number	Average $^{210}Pb_s$ Activity (pCi/g dry)	QEA Estimated Sedimentation Rate (cm/yr)	USACE Estimated Sedimentation Rate (cm/yr)
CMS-SD-4204	2.1	0.17	0.23
CMS-SD-4206	1.7	0.24	0.29
CMS-SD-4209	1.0	0.65	0.49
CMS-SD-4210	1.2	2.8	2.8
CMS-SD-4212	0.95	0.34	0.34
CMS-SD-4213	0.97	0.43	0.43
CMS-SD-4218	1.3	0.68	0.40
CMS-SD-4219	0.52	0.90	0.33
CMS-SD-4222	0.95	0.76	0.52
LPX-SD-4201	0.56	0.30	0.33

The next step in the analysis is to evaluate the vertical profile of $^{210}Pb_u$ (unsupported) activity, which is presented for each of the ten cores on the left-hand panels of Figures 2-7 to 2-16. Unsupported $^{210}Pb_u$ activity data are transformed to $\ln(^{210}Pb_u)$ and plotted as a function of depth in the sediment bed (d_{bed}). A linear regression analysis of $\ln(^{210}Pb_u)$ versus d_{bed} (in feet) is conducted and the slope of the regression line (m) is determined. Sedimentation rate (^{Pb}R) is calculated using:

$$^{Pb}R = -0.948/m \qquad (2\text{-}2)$$

where ^{Pb}R has units of cm/yr.

The estimated sedimentation rates for the ten cores range from 0.17 to 2.8 cm/yr (Table 2-2). Table 2-2 also includes sedimentation rates determined from the USACE analysis (Corcoran 2004). Comparison of the QEA and USACE results indicate that significant differences in estimated rates exist for several of the cores. These differences are primarily due to the choice of $^{210}Pb_u$ data points used in the regression

analysis. Because an objective method for picking a unique set of $^{210}Pb_u$ data points for the regression analysis does not exist, professional judgment must be used to select these data points.

Differences in the QEA and USACE sedimentation rate results illustrate the uncertainty inherent in the analysis of ^{210}Pb data. While each rate presented in Table 2-2 may be thought of as the 'best' estimate of average sedimentation rate for a particular core, the uncertainty associated with that 'best' estimate should be quantified. Thus, the following procedure was developed for evaluating uncertainty in the sedimentation rate analysis.

For each core, a total of N $^{210}Pb_u$ data points were used in the regression analysis to determine m and ^{Pb}R. For convenience, the sedimentation rate determined from the regression analysis conducted with N data points is denoted as $^{Pb}R_N$. Because a large portion of the uncertainty in results is due to the subset of data points used in the regression analysis, the variability in ^{Pb}R is estimated by creating N sub-samples, with each sub-sample consisting of (N-1) data points. A sub-sample is generated by removing one data point from the original group of N values. This process is repeated until each data point has been removed one time. For each of the sub-samples from a particular core, the regression analysis is conducted and a regression slope is determined, producing N values of m (i.e., m_n for n = 1, N). Statistical analysis of m_n yields a 95% CI for m for each core. The range of sedimentation rates for a particular core was estimated by using the upper- and lower-bound values of the 95% CI for m in Equation (2-2). The resulting ranges of sedimentation rates are tabulated in Table 2-3.

Table 2-3. Estimated Ranges of Sedimentation Rates.

Core Number	Sedimentation Rate Range: ^{210}Pb Analysis (cm/yr)	Sedimentation Rate Range: ^{137}Cs Analysis (cm/yr)
CMS-SD-4204	0.11 → 0.30	0.33 → 0.52
CMS-SD-4206	0.20 → 0.31	NA
CMS-SD-4209	0.63 → 0.96	0.48 → 1.04
CMS-SD-4210	1.55 → 7.29	0.56 → 1.12
CMS-SD-4212	0.26 → 0.45	0.26 → 0.52
CMS-SD-4213	0.53 → 0.59	0.56 → 0.82
CMS-SD-4218	0.53 → 0.84	0.67 → 1.04
CMS-SD-4219	0.58 → 1.41	NA
CMS-SD-4222	0.73 → 1.02	0.33 → 0.74
LPX-SD-4201	0.26 → 0.35	0.11 → 0.45

NA = no analysis due to non-interpretable ^{137}Cs profile

2.2.2 ^{137}Cs Data Analysis

Cesium-137 (^{137}Cs) levels in sediments are derived from atmospheric fallout during nuclear weapons testing. The first occurrence of detectable ^{137}Cs in sediments generally marks the year 1954, while peak levels correspond to 1963 (Simpson et al. 1976). Based on these dates, the best estimate of the long-term average sedimentation rate for a particular core is computed by dividing the depth of sediment between the sediment surface and the buried ^{137}Cs peak by the number of years between 1963 and the time of core collection (e.g., 40 years for a core collected in 2003). A ^{137}Cs vertical profile may also be examined to identify the first detectable presence of ^{137}Cs, which generally signifies the year 1954, to corroborate, where possible, the sedimentation rates estimated from the locations of the ^{137}Cs peaks. For this evaluation, the sedimentation rate for a particular core is computed by dividing the depth of sediment between the sediment surface and the first detectable presence of ^{137}Cs (found deeper in the core) by the number of years between 1954 and the time of core collection (e.g., 49 years for a core collected in 2003).

The average sedimentation rate based on location of the peak ^{137}Cs concentration in a core (^{Cs}R, in cm/yr) is calculated using:

$$^{Cs}R = d_p / 40 \qquad (2\text{-}3)$$

where d_p is depth of the peak concentration (cm) and 40 years is the lapsed time period between 1963 and core collection in 2003. Vertical profiles of ^{137}Cs activity are presented on the middle panels of Figures 2-7 to 2-16. Examination of these profiles shows that peak ^{137}Cs concentrations are evident in eight of the ten cores, with cores CMS-SD-4206 and CMS-SD-4219 having non-interpretable profiles. The ^{137}Cs peaks, however, are generally not well defined or highly resolved, i.e., relatively large vertical distances exist between sample points in the core. Thus, the average sedimentation rate cannot be estimated with a high-degree of accuracy based on the depth of the ^{137}Cs peak.

The uncertainty in the location of the ^{137}Cs peak in a core is addressed as follows. As with the ^{210}Pb uncertainty analysis, the ^{137}Cs data are used to determine a range of sedimentation rates for a particular core. The first step in the analysis is to identify the peak ^{137}Cs concentration ($^{137}Cs_{peak}$) in a core. This value represents the average activity in a sediment segment that is typically 0.05 ft (1.5 cm) thick. Vertical spacing between segments is generally greater than 0.05 ft. The next step is to define the 1963 time horizon in a core as the zone in which the maximum ^{137}Cs concentration exists. This zone (i.e., 1963 time horizon) is assumed to extend from the lower-edge of the segment immediately above $^{137}Cs_{peak}$ to the upper-edge of the segment immediately below $^{137}Cs_{peak}$ (see middle panels of Figures 2-7 to 2-16); the 1963 time horizon extends from d_{lower} to d_{upper} in the core. Finally, these two depths are used in Equation (2-3) to calculate a range for ^{Cs}R in a particular core. The results of this analysis are tabulated in Table 2-3.

2.2.3 Comparison of Sedimentation Rates Based on ^{210}Pb and ^{137}Cs Data

Independent estimates of sedimentation rate are provided by the ^{210}Pb and ^{137}Cs analyses. Combining the estimated rates from these two approaches yields an improved understanding of the depositional environment in Allendale and Lyman Mill Ponds. Frequency distributions of upper- and lower-bound estimates of sedimentation rates based on the ^{210}Pb and ^{137}Cs analyses (see Table 2-3) in Allendale Pond are presented on Figure 2-17. Note that the results for core CMS-SD-4210 are excluded from Figure 2-17 because those results are exceptionally high, inconsistent with ^{137}Cs results for that core, and, hence, are considered to be unreliable. These results indicate that, generally, the ^{210}Pb and ^{137}Cs analyses produce consistent upper- and lower-bound estimates of sedimentation rate. Median values of lower- and upper-bound sedimentation rates are about 0.5 and 0.8 cm/yr, respectively. While there is variability in sedimentation rate in Allendale Pond, with an approximate overall range of 0.1 to 1.5 cm/yr, a reasonable estimate of a representative (or average) range of sedimentation rate for this pond is 0.5 to 0.8 cm/yr.

2.3 Dioxin Bed Concentration Data

Sediment samples from the geochronology cores discussed in Section 2.2 were also analyzed for dioxin concentrations. For convenience, dioxins in this analysis are expressed as toxic equivalency quotient (TEQ) concentration. Vertical profiles of dioxin TEQ concentration in the ten geochronology cores are displayed on the right-hand panel of Figures 2-7 to 2-16. In general, maximum TEQ concentrations in the cores are less than 20 μg/kg, with the exception of core CMS-SD-4213 (maximum value of approximately 50 μg/kg). In addition, maximum concentrations usually occur in the upper 1 ft (30 cm) of the core.

Chemical manufacturing activities at the Centredale Manor site began in approximately 1940. Therefore, it is reasonable to assume that negligible dioxin concentrations will occur below the 1940 time horizon

(1940-TH) in the sediment bed. Thus, determining the 1940-TH in the sediment bed may provide useful information for developing certain remedial alternatives for Allendale and Lyman Mill Ponds.

The depth of the 1940-TH is calculated by multiplying sedimentation rate by the time period between 1940 and 2003. Uncertainty in the estimated sedimentation rate, however, must be incorporated into the time horizon, which is accomplished by using the ranges listed in Table 2-3. This approach yields the 1940-TH ranges, based on the ^{210}Pb and ^{137}Cs analyses, shown on Figures 2-7 to 2-16 (represented as the cross-hatched zones on the figures). Examination of these figures shows that the 1940-TH is relatively thick in some cores (approximately 1 ft) due to uncertainty in sedimentation rate. The range of 1940-TH depths in Allendale Pond is indicated on Figure 2-18, which presents the frequency distributions of minimum and maximum depths of the 1940-TH. These results indicate that a representative estimate for the 1940-TH in Allendale Pond is a depth between 1 and 2 ft.

2.4 Dioxin Water-Column Concentration Data

Water column samples were collected at various locations in the study area during October and November 1999 (TTNUS 2000). Flow rates in the river during the water column sampling ranged from about 25 to 110 cubic feet per second (cfs). The average flow rate at the U.S. Geological Survey (USGS) Centredale gaging station is approximately 73 cfs (USGS 1996). Thus, the sampling was carried out during low to moderate flow conditions during which it is expected that sediment resuspension does not occur. Under non-resuspending conditions, COC flux (e.g., dioxin flux) from the bed to the water column occurs due to a combination of various processes, including diffusion, bioturbation and groundwater flux. To evaluate the validity of the assumption that dioxin is not being added to the water column via bed erosion, the correlation between total dioxin water-column concentration and flow rate during the 1999 sampling period is shown on Figure 2-19. If significant bed erosion were occurring, it is expected that dioxin water-column concentration would increase with increasing flow rate; no increase in concentration with flow rate is evident during the sampling period. Therefore, this data set may be used to evaluate non-resuspension loading of dioxin to the water column within the study area.

Significant variation in dioxin water-column concentrations occurred within the study area during the 14 days that samples were collected between October 25 and November 10, 1999; total dioxin concentrations ranged from 11 to 8,900 pg/L. Note that the water column samples were not filtered, so the concentration values represent total dioxin concentration (i.e., sum of particulate and dissolved components). The spatial distribution of total dioxin concentration during the low-flow sampling period in 1999 is shown on Figure 2-20. Examination of this spatial distribution suggests that the study area may be separated into five zones, which are defined in Table 2-4 and shown on Figures 2-21 and 2-22. Frequency distributions of total dioxin concentrations in the five zones are shown on Figure 2-23, while statistics for concentrations in each zone are tabulated in Table 2-5. These results indicate an interesting spatial pattern in total dioxin concentration. A significant increase in dioxin concentration occurs between Zones 1 and 2 (i.e., from the upstream area to the source/upstream portion of Allendale Pond area), with average concentrations increasing from 27 to 1,160 pg/L. Moving from Zone 2 to 3 (i.e., from upstream portion to downstream portion in Allendale Pond), concentrations decrease to levels observed in Zone 1. In Zone 4 (i.e., upstream portion of Lyman Mill Pond), dioxin water-column concentrations increase again (average value of 105 pg/L). Similar to the pattern in Allendale Pond, concentrations in Zone 5 decline to values comparable to Zone 1 and 3 concentrations.

Table 2-4. Spatial Extent of Zones Used in Non-Resuspending Dioxin Flux Analysis.

Zone	General Description	Distance Upstream from Lyman Mill Dam (ft)
1	Upstream area	0 → 1,500
2	Source area and upstream portion of Allendale Pond	1,500 → 4,300
3	Downstream portion of Allendale Pond	4,300 → 5,300
4	Upstream portion of Lyman Mill Pond	5,300 → 7,300
5	Downstream portion of Lyman Mill Pond	7,300 → 9,000

Table 2-5. Statistics for Dioxin Concentration in Five Zones (Oct-Nov 1999 Data).

Zone	No. Observations	Average (pg/L)	Standard Deviation (pg/L)	95% CI (pg/L)
1	3	27	7.1	9 → 45
2	8	1,160	3,130	0 → 3,800
3	5	28	9.9	16 → 40
4	9	105	99	29 → 180
5	5	22	14	5 → 39

Dioxin loads were calculated by multiplying the observed dioxin water-column concentration by the daily-average flow rate for the day of sample collection. The calculated water-column loads have a spatial pattern that is similar to the one observed for water-column concentrations (Figure 2-24). Higher loads occur in Zones 2 and 4, while lower loads are observed in Zones 1, 3 and 5. Dioxin loads range from about 2 to 870 mg/day during this low-flow period. Frequency distributions of dioxin loads in the five zones are shown on Figure 2-25; load statistics are listed in Table 2-6.

Table 2-6. Statistics for Dioxin Load in Five Zones (Oct-Nov 1999 Data).

Zone	No. Observations	Average (mg/day)	Standard Deviation (mg/day)	95% CI (mg/day)
1	3	4.6	1.2	1.6 → 7.6
2	8	115	310	0 → 380
3	5	6.0	2.2	3.3 → 8.7
4	9	17	18	3 → 31
5	5	4.2	2.5	1.1 → 7.3

Results of the water-column load analysis provide insights about dioxin loading to the water column during non-resuspending conditions in the study area. First, dioxin loads of approximately 110 and 11 mg/day, on average, are added to the water column in Zones 2 and 4, respectively. It assumed that the sediment bed is a source of the dioxin loading to the water column in Zones 2 and 4; mass transfer of pore water from the bed to water column (due to non-resuspension processes such as diffusion, bioturbation and groundwater advection) is probably the main source of dioxin. Another possible source of dioxin in Zone 2 is contaminated groundwater discharge to the river in the vicinity of the Brook Village parking lot, where the dioxin TEQ concentration in groundwater was 4,180 pg/L in 2002 (Battelle 2003). Second, transport processes within Allendale and Lyman Mill Ponds appear to remove the increased loads (in Zones 2 and 4) such that loads in the downstream portions of each pond return to background levels.

Background dioxin loads in the river appear to be approximately 4 mg/day. It is unclear what processes cause the removal of the loads added in Zones 2 and 4. Third, minimal increase in dioxin loading occurs between the upstream boundary of the study area and Lyman Mill Dam; minimal net export of dioxin from the two ponds occurs during low-flow, non-resuspending conditions. The October-November 1999 data set is limited, with only three to five samples in Zones 1, 3 and 5. Thus, uncertainty exists in the estimates of dioxin loads and the conclusions/insights developed from this analysis.

The validity of these hypotheses on low-flow dioxin loads was tested with additional data collected during December 2004. Water column samples were collected on December 9, 16 and 18 within Zones 1 (upstream of Allendale Pond), 3 (at Allendale Dam), and 5 (at Lyman Mill Dam). A total of three samples within each zone were collected, with flow rate in the river ranging from 106 to 130 cfs during sample collection. Note that one sample collected in Zone 1 had an anomalously high value (i.e., 220 pg/L) and it was excluded from the analysis because it is highly likely this data point is caused by sample contamination.

Statistics for dioxin concentrations and loads during the December 2004 period are presented in Tables 2-7 and 2-8. It is interesting to note that the average dioxin loads in Zones 1 and 3 during December 2004 are very similar to loads during the October-November 1999; average loads in Zones 1 and 3 are within 5 percent during the two periods. The average load in Zone 5 during December 2004 is about twice as large as the load during October-November 1999, but the two mean values are not statistically different at a 95% confidence level. Overall, the December 2004 results support the conclusions based on the October-November 1999 data.

Table 2-7. Statistics for Dioxin Concentration in Three Zones (December 2004 Data).

Zone	No. Observations	Average (pg/L)	Standard Deviation (pg/L)	95% CI (pg/L)
1	2	16	1.0	7 → 25
3	3	22	4.9	10 → 34
5	3	33	7.4	15 → 51

Table 2-8. Statistics for Dioxin Load in Three Zones (December 2004 Data).

Zone	No. Observations	Average (mg/day)	Standard Deviation (mg/day)	95% CI (mg/day)
1	2	4.5	0.8	0.0 → 12
3	3	6.3	1.5	2.5 → 10
5	3	9.5	1.4	5.9 → 13

3.0 MODEL-BASED STABILITY ANALYSES

The primary objective of the modeling analyses is to estimate the potential impacts of flood events on bed stability. This goal is accomplished by using a hydrodynamic model to predict current velocity and bottom shear stress in Allendale and Lyman Mill Ponds during flood events. Information from the hydrodynamic model is used to estimate areas of potential erosion in the ponds and approximate scour depths within those areas.

3.1 Hydrodynamic Model Development

The hydrodynamic model used in this study is an enhanced version of the Environmental Fluid Dynamics Code (EFDC). This model (EFDC) is an USEPA-approved model which QEA has modified so as to make the model easier to use; the QEA version of EFDC is non-proprietary. EFDC is a sophisticated three-dimensional, time-dependent, boundary-fitted hydrodynamic model capable of simulating density-driven circulation in rivers, reservoirs, lakes, estuaries and coastal waters. The model has been extensively tested and applied to a wide range of aquatic systems. For this study, the model was used in two-dimensional, vertically-averaged mode, which is a valid approximation for the shallow, non-stratified flow conditions that exist in the two ponds during flood conditions; a two-dimensional model produces results that are sufficiently accurate for this study.

3.1.1 Geometry and Bathymetry

The modeling domain extends from an upstream boundary at the Route 44 Bridge to a downstream boundary at Lyman Mill Dam. Flow is constrained within the normal shoreline, i.e., in-bank flow conditions, of the river and ponds; effects of floodplain flow during over-bank floods are neglected in all simulations. This approximation produces conservative results, i.e., predicted current velocities are higher by neglecting floodplain effects. Bathymetric model inputs were developed from water depth data collected during the October 2002 geophysical survey (Shields 2003). These data, which are limited to Allendale and Lyman Mill Ponds, were collected during low-flow conditions (i.e., river discharge less than 15 cfs, and average flow rate in the river is 74 cfs). Only water depths were measured during the geophysical survey, these measurements were not referenced to a specific vertical datum (e.g., NGVD 88). Bathymetric data are not available for the river channels upstream of the two ponds. As a first approximation, equilibrium water depths were assumed to be 1.2 and 0.72 m in the channels upstream of Allendale and Lyman Mill Ponds, respectively. These approximations are reasonable because the channels are not a focus of this study and uncertainty in channel bathymetry has minimal impact on model predictions in the ponds. The resulting bathymetric distributions for Allendale and Lyman Mill Ponds are presented on Figures 3-1 and 3-2, respectively.

Two numerical grids were generated to represent the study area: 1) Allendale Pond (extending from the Route 44 Bridge to Allendale Dam), and 2) Lyman Mill Pond (extending from Allendale Dam to Lyman Mill Dam). The grids were constructed using 5-meter square grid cells to delineate the geometry and bathymetry of each pond (Figures 3-1 and 3-2). A total of 2,201 and 4,157 grid cells were used for Allendale and Lyman Mill Ponds, respectively.

3.1.2 Boundary Conditions

Flow rate is specified at the upstream (inflow) boundary of the model. Discharge data collected at the USGS gaging station at Centredale (located near the Route 44 Bridge) were used to specify the inflow boundary condition. It is assumed that tributary inflow within the study area is small compared to flow in the river (particularly during flood conditions) and, thus, can be neglected. Estimation of the magnitude of discharge during flood events is discussed in Section 3.2.1.

Stage height (i.e., water surface elevation) as a function of flow rate at the dams is specified as the downstream boundary condition. Insufficient stage height data are available to develop a reliable rating curve, so a broad-crested weir formulation is used to estimate stage height at each dam (Roberson et al. 1998):

$$\eta = (Q / 3.3 L)^{0.67} \quad (3\text{-}1)$$

where η is depth of water over dam crest (ft), Q is flow rate (cfs) and L is length of dam crest (ft). Crest length of the Allendale and Lyman Mill Dams is 106 ft. The validity of Equation 3-1 for this application was assessed by comparing predicted and measured stage heights at the dams on October 26, 2005. This comparison indicated that Equation 3-1 adequately predicts stage height at the dam.

3.1.3 Model Calibration

The objective of calibrating the hydrodynamic model is to optimize the agreement between observed and predicted stage height and current velocity through adjustment of model parameters. Typically, the effective bottom roughness (Z_o) is the model parameter adjusted during hydrodynamic model calibration. This model parameter (Z_o) affects bottom shear stress and, hence, current velocity and stage height. Bottom shear stress (τ) is calculated using the quadratic stress formula (van Rijn 1993):

$$\tau = \rho_w C_f u^2 \quad (3\text{-}2)$$

where ρ_w is density of water, C_f is a bottom friction coefficient and u is depth-averaged velocity. The bottom friction coefficient depends on Z_o:

$$C_f = [2.5 \ln(0.5 h / Z_o)]^{-2} \quad (3\text{-}3)$$

where h is water depth.

A field survey was conducted in Allendale Pond and Lyman Mill Pond on October 26, 2005 to obtain current velocity and water depth data at six locations in each pond. Sampling locations shown on Figures 3-1 and 3-2 and listed in Table 3-1. Locations of the sampling points were determined using a Differential Global Positioning System (dGPS) device (Leica 420 with a "smart antenna") with sub-meter accuracy (Battelle 2005). Four sets of data were collected in Allendale Pond (Table 3-2) and three sets of measurements were obtained from Lyman Mill Pond (Table 3-3). Current velocity was measured at two points in the water column; at points located 20 and 80 percent of the water depth (i.e., near surface and near bottom, respectively). Flow rate in the river decreased from approximately 330 cfs when sampling started around 8 AM to about 300 cfs at 5 PM.

Table 3-1. Current Velocity Sampling Locations.

Pond Location	Sampling Location ID Number	Sampling Location: Longitude	Sampling Location: Latitude
Allendale	A-1	71° 28.903'	41° 51.101'
Allendale	A-2	71° 28.936'	41° 51.097'
Allendale	A-3	71° 29.008'	41° 51.138'
Allendale	A-4	71° 28.986'	41° 51.169'
Allendale	A-5	71° 29.082'	41° 51.163'
Allendale	A-6	71° 29.095'	41° 51.196'
Lyman Mill	LM-1	71° 28.617'	41° 50.389'
Lyman Mill	LM-2	71° 28.686'	41° 50.465'
Lyman Mill	LM-3	71° 28.737'	41° 50.528'
Lyman Mill	LM-4	71° 28.753'	41° 50.618'
Lyman Mill	LM-5	71° 28.752'	41° 50.668'
Lyman Mill	LM-6	71° 28.833'	41° 50.698'

Table 3-2. Current Velocity and Water Depth Measurements in Allendale Pond.

Sampling Location	Time (hour:minute)	Water Depth (ft)	Current Velocity at 80% Depth (near bottom) (ft/s)	Current Velocity at 20% Depth (near surface) (ft/s)
A-1	08:03	8.0	0.22	0.28
A-2	08:13	5.2	0.17	0.26
A-3	08:18	6.2	0.27	0.44
A-4	08:24	4.5	0.06	0.16
A-5	08:30	2.5	0.73	1.10
A-6	08:36	2.0	0.15	0.18
A-1	12:08	8.0	0.08	0.13
A-2	12:18	5.2	0.10	0.30
A-3	12:29	6.3	0.20	0.34
A-4	12:38	4.6	0.00	0.11
A-5	12:44	2.5	0.60	0.78
A-6	12:50	2.2	0.07	0.16
A-1	14:24	7.9	0.04	0.14
A-2	14:29	5.2	0.12	0.15
A-3	14:34	6.3	0.23	0.35
A-4	14:39	4.7	0.00	0.08
A-5	14:44	2.4	0.61	0.66
A-6	14:49	2.2	0.21	0.22
A-1	16:28	7.8	0.04	0.18
A-2	16:38	5.2	0.18	0.18
A-3	16:45	6.3	0.19	0.27
A-4	16:51	4.6	0.00	0.00
A-5	16:57	2.3	0.74	0.74
A-6	17:03	2.1	0.10	0.12

Table 3-3. Current Velocity and Water Depth Measurements in Lyman Mill Pond.

Sampling Location	Time (hour:minute)	Water Depth (ft)	Current Velocity at 80% Depth (near bottom) (ft/s)	Current Velocity at 20% Depth (near surface) (ft/s)
LM-1	13:18	7.3	0.00	0.10
LM-2	13:24	5.9	0.05	0.20
LM-3	13:30	6.8	0.20	0.48
LM-4	13:39	5.8	0.45	0.58
LM-5	13:45	5.0	0.69	0.75
LM-6	13:53	2.9	0.00	0.00
LM-1	15:03	7.3	0.00	0.00
LM-2	15:08	5.9	0.24	0.33
LM-3	15:13	6.8	0.33	0.41
LM-4	15:18	5.8	0.40	0.71
LM-5	15:23	5.0	0.42	0.72
LM-6	15:30	2.9	0.00	0.00
LM-1	16:09	7.3	0.00	0.00
LM-2	16:02	5.8	0.20	0.28
LM-3	15:56	6.8	0.33	0.44
LM-4	15:47	5.8	0.55	0.61
LM-5	15:38	5.0	0.36	0.70
LM-6	15:33	2.9	0.00	0.00

The hydrodynamic model was used to simulate circulation in Allendale and Lyman Mill Ponds on October 26, 2005, with time-variable inflow at the upstream boundary of the model specified using 15-min discharge data collected at the USGS gauging station. Model calibration was accomplished by adjusting the effective bottom roughness (Z_0) such that optimal agreement between observed and predicted current velocities was obtained. The model calibration process yielded a Z_0 value of 0.1 cm.

Comparisons of predicted and observed current velocity and water depth are shown on Figures 3-3 through 3-10. Current velocity data collected during the field study were measured at near bottom (80% depth) and near surface (20% depth) locations in the water column. These two measured values were used to estimate the depth-averaged velocity at each station, with this data-based value being compared to the depth-averaged velocity predicted by the model.

In Allendale Pond (Figures 3-3 through 3-6), predicted velocity and water depth at locations A-1 to A-4 are in reasonably good agreement with measured values. At locations A-1 and A-2, predicted velocities tend to pass through the center of the data, with maximum model-data differences of less that 0.1 ft/s. At location A-3, the model under-predicts velocity by about 0.1 ft/s. At location A-4, predicted current velocities are about 0.1 ft/s greater than measured values.

At location A-5, the model over-predicts water depth by about 4.5 ft and under-predicts current velocity by about 0.5-0.6 ft/s. This discrepancy is probably due to the bathymetry specified in the model near location A-5. The depth input to the model is 6.1 ft, which is inconsistent with the measured depth (2.5 ft) at that location during the current velocity survey. This inconsistency is caused by the interpolation process used to generate initial water depths at each grid cell in the numerical grid. At location A-6, the predicted water depth is in agreement with the observed depth, but the predicted velocity is about 0.5-0.6

ft/s greater than the observed velocity. It is possible that the inconsistencies in observed and predicted velocities at locations A-5 and A-6 are due to uncertainties in the geometry and bathymetry of inlet region of Allendale Pond.

In Lyman Mill Pond (Figures 3-7 through 3-10), predicted values of velocity and water depth generally agree with the data. Overall, the model under-predicts water depth at all six locations, with the difference between predicted and observed water depths ranging from less than 0.5 ft to 1-2 ft. At locations LM-2, LM-4 and LM-5, predicted current velocities tend to pass through the range of measured values, with maximum discrepancies of less than 0.2 ft/s. At location LM-1, the model over-predicts velocity by 0.2 ft/s or less; however, measured velocities at this location are very low. At location LM-3, predicted velocities are about 0.20-0.25 ft/s greater than observed values. At location LM-6, the measured velocity is zero and the predicted velocity is about 0.6 ft/s, while measured and predicted water depths are in agreement at this location.

Overall, the model is able to predict current velocity and water depth in both ponds with adequate accuracy. These results indicate that: 1) model inputs adequately represent geometry and bathymetry of the study area, with the possible exception of the inlet region of Allendale Pond; 2) boundary conditions are specified correctly; and 3) a bottom roughness of 0.1 cm is an appropriate value for both ponds. Even though discrepancies exist between predicted and observed current velocities, the overall accuracy of the model is deemed to be sufficient to meet the objectives of this study. The reliability of the model is adequate for developing a CSM and various conclusions about sediment transport for the study area.

3.2 Flood Flow Simulations

The hydrodynamic model was used to evaluate the potential impacts of flood events on bed stability in Allendale and Lyman Mill Ponds. Five floods were simulated, corresponding to return periods of 5, 10, 25, 50 and 100 years.

3.2.1 Estimates of Flood Flow Rates

Historical flow rate data collected at the USGS gaging station at Centredale were used by USACE personnel to conduct a flood frequency analysis (M. Corcoran, personal communication, June 3, 2004). The results of this analysis are used in this study to define flow rates for floods with the following return periods: 5, 10, 25, 50 and 100 years. A summary of the flow rates associated with each flood return period is provided in Table 3-4.

Table 3-4. Flow Rates for Flood Event Simulations.

Flood Return Period (years)	Flow Rate (cfs)
5	894
10	1,111
25	1,398
50	1,621
100	1,850

3.2.2 Methods for Estimating Potential Bed Scour

The hydrodynamic model is used to evaluate the potential impacts of the range of floods estimated above on bed stability. Impacts of floods with 5-, 10-, 25-, 50- and 100-year return periods are investigated. For each flood simulation, two methods are used to analyze the potential impacts of floods on bed scour: 1)

comparison of bottom shear stress and current velocity to critical values of those parameters; and 2) estimation of scour depth.

Predicted current velocity is used to calculate bottom shear stress (τ), using Equations 3-2 and 3-3, which is compared to a critical shear stress for erosion (τ_{cr}). Areas where the bottom shear stress is greater than the critical value (i.e., $\tau > \tau_{cr}$) correspond to areas that are subject to scour during a flood. Critical shear stress for cohesive sediment is variable and depends on the site-specific erosion properties of surficial sediments. Shaker studies of the resuspension properties of cohesive sediments in the Fox, Saginaw and Buffalo Rivers suggested an appropriate value for τ_{cr} of 0.1 Pa (Lick et al. 1995). A Sedflume study conducted in the Grand River yielded estimates of τ_{cr} ranging from approximately 0.1 to 1.6 Pa (Jepsen et al. 2001). Another Sedflume study examined Boston Harbor sediments, with values between approximately 0.1 and 5 Pa (Roberts et al. 2001). Generally, the higher critical shear stresses reported in the two Sedflume studies are for deeper sediment; surficial sediment typically has critical shear stresses in the lower portion of the range. Because uncertainty exists in the value of τ_{cr}, lower- and upper-bound estimates of 0.1 and 0.5 Pa, respectively, are used in this study. Areas of potential bed scour are determined using upper ($\tau_{cr.up} = 0.5$ Pa) and lower ($\tau_{cr.low} = 0.1$ Pa) bounds of critical shear stress. Note that the lower-bound critical shear stress produces the most conservative results. Areas where the bottom shear stress is less than the critical shear stress for erosion are conducive to deposition.

The critical velocity criterion (i.e., $u > u_{cr}$) is used to estimate where potential-measurable-erosion may occur, meaning about 0.1 to 1 cm of bed scour or more. For this study, the 2 ft/s threshold value is used to estimate areas of potential-measurable-erosion in the two ponds. The 2 ft/s scour threshold is taken from two different sources: 1) *Hydraulic Design of Flood Control Channels* (USACE 1991) suggests that a maximum permissible mean channel velocity of 2 ft/s should be used as a guide in designing non-scouring flood control channels comprised of fine sands or sandy silts; and 2) results of flume studies presented in Graf (1971) indicate that significant scour of pure clayey soil and mixtures of pure clayey soil and sand does not occur until velocities of about 2 ft/s are encountered. This approach was successfully applied to a bed stability study on the Grasse River (New York) (Alcoa 2002). Note that a depth-averaged current speed of 2 ft/s corresponds to a bottom shear stress value of about 1.5 Pa (assuming a bottom friction factor of 0.004).

The second method uses predicted bottom shear stress to estimate scour depth in the two ponds. This approach will apply the Lick equation (Ziegler 2002):

$$\varepsilon = A\,(\tau/\tau_{cr} - 1)^n, \qquad \tau > \tau_{cr} \qquad (3\text{-}4)$$

where ε is resuspension potential (i.e., mass eroded per unit area); τ is bottom shear stress; τ_{cr} is critical bottom shear stress, assumed to be 0.1 Pa for this analysis (Ziegler 2002); A is site-specific constant; and n is site-specific exponent.

A field study was conducted during December 2004 to obtain site-specific data on the resuspension properties of sediment in Allendale and Lyman Mill Ponds. Sediment cores were collected from 10 locations each in Allendale and Lyman Mill Ponds between December 13 and 16 (Table 3-5, Figures 3-11 and 3-12). Locations of the sampling points were determined using a hand-held GPS device, with a horizontal accuracy of 2-3 m (QEA 2004b). The cores were tested in a device called a "shaker". A description of the field study and shaker testing procedure is presented in QEA (2004b).

Table 3-5. Shaker Core Locations and Descriptions.

Pond Location	Core ID Number	Core Location: Longitude	Core Location: Latitude	Physical Description of Core
Allendale	A-S1	71° 28.930'	41° 51.080'	1 in organic surface layer on top of silty sediment
Allendale	A-S2	71° 28.895'	41° 51.080'	6 in silt layer on top of sand and small pebbles
Allendale	A-S3	71° 28.934'	41° 51.112'	1-2 in of mucky organics on top of 3-4 in of sand on top of silt and dark brown clay
Allendale	A-S4	71° 28.972'	41° 51.126'	2 in fine organics and vegetation on top of 7 in of sand with small pebbles on top of fine silt
Allendale	A-S5	71° 28.956'	41° 51.155'	2 in organics on top of silt
Allendale	A-S6	71° 29.007'	41° 51.159'	2 in organics on top of wood chips and fine sediment
Allendale	A-S7	71° 29.063'	41° 51.154'	1 in organics on top of silty sand
Allendale	A-S8	71° 29.065'	41° 51.188'	3 in organics (with vegetation and sticks) on top of silt and sand
Allendale	A-S9	71° 29.109'	41° 51.218'	1 in organics on top of silt/sand
Allendale	A-S10	71° 29.119'	41° 51.266'	1 in organics and vegetation on top of 6 in coarse sand on top of silt/sand
Lyman Mill	LM-S1	71° 28.703'	41° 50.396'	Organics and silt throughout core
Lyman Mill	LM-S2	71° 28.605'	41° 50.397'	Organics on top of silt
Lyman Mill	LM-S3	71° 28.695'	41° 50.454'	Organics and silt
Lyman Mill	LM-S4	71° 28.669'	41° 50.478'	Organics and silt
Lyman Mill	LM-S5	71° 28.704'	41° 50.500'	Organics and silt
Lyman Mill	LM-S6	71° 28.738'	41° 50.534'	Organics and silt
Lyman Mill	LM-S7	71° 28.754'	41° 50.580'	Organics and silty sand, very mucky
Lyman Mill	LM-S8	71° 28.750'	41° 50.638'	Organics and silt
Lyman Mill	LM-S9	71° 28.781'	41° 50.693'	Organics and silt
Lyman Mill	LM-S10	71° 28.816'	41° 50.706'	Organics and silt, some wood chips

Data collected from the shaker tests is used to determine the resuspension potential (ε) at three applied shear stresses: 0.3, 0.5 and 0.9 Pa (Table 3-6). These data indicate that, generally, the resuspension potential of sediment in Allendale Pond is lower than the resuspension potential in Lyman Mill Pond, for a particular shear stress (Figures 3-13 and 3-14). The data also indicate that resuspension potential increases with increasing shear stress, which is consistent with Equation 3-4.

The site-specific parameters in Equation 3-4 (i.e., A and n) for Allendale and Lyman Mill Ponds are estimated by conducting a log-linear regression analysis of the resuspension potential data. The relationships between resuspension potential and shear stress in Allendale and Lyman Mill Ponds are illustrated on Figures 3-15 and 3-16, respectively. These figures indicate that variability exists in the data, but a reasonable log-linear correlation between resuspension potential and shear stress exists in both ponds. The range of variability in the resuspension potential data shown on Figures 3-15 and 3-16 approximately spans an order-of-magnitude. This amount of variability in resuspension potential is typical of river systems. Even though significant variability exists in the data, the average parameter

values for each pond resulting from the log-linear regression analysis provides a reasonable approximation for site-specific conditions. Values of the site-specific parameters (A and n) resulting from this analysis are listed in Table 3-7, with these values representing spatial averages for each pond.

Table 3-6. Measured Resuspension Potential in Allendale and Lyman Mill Ponds.

Pond Location	Core ID Number	Resuspension Potential: 0.3 Pa (mg/cm^2)	Resuspension Potential: 0.5 Pa (mg/cm^2)	Resuspension Potential: 0.9 Pa (mg/cm^2)
Allendale	A-S1	7.7	18	75
Allendale	A-S2	20	37	59
Allendale	A-S3	14	48	115
Allendale	A-S4	16	22	100
Allendale	A-S5	46	95	286
Allendale	A-S6	43	90	184
Allendale	A-S7	15	54	230
Allendale	A-S8	11	27	198
Allendale	A-S9	31	84	311
Allendale	A-S10	2.8	7.9	41
Lyman Mill	LM-S1	182	257	426
Lyman Mill	LM-S2	134	224	349
Lyman Mill	LM-S3	66	82	210
Lyman Mill	LM-S4	60	151	288
Lyman Mill	LM-S5	107	192	294
Lyman Mill	LM-S6	86	149	322
Lyman Mill	LM-S7	104	192	380
Lyman Mill	LM-S8	43	79	283
Lyman Mill	LM-S9	21	48	129
Lyman Mill	LM-S10	45	104	154

Table 3-7. Resuspension Parameters Used in Scour Depth Analysis.

Pond	Eq. (3-4) Parameter: A (mg/cm^2)	Eq. (3-4) Parameter: n
Allendale	5.1	1.5
Lyman Mill	37	0.94

Scour depth is calculated using:

$$T = \varepsilon / (1000\ \rho) \qquad (3\text{-}5)$$

where T is scour depth (cm), ε is resuspension potential (mg/cm^2) and ρ is dry density of sediment (g/cm^3). As discussed in Section 2.1, 95% CI for dry density in Allendale and Lyman Mill Ponds are 0.63 to 0.89 g/cm^3 and 0.47 to 0.71 g/cm^3, respectively.

The analyses discussed above apply to cohesive sediment beds (i.e., muddy sediment), but not to non-cohesive (sandy) beds. To estimate portions of the sediment bed in Allendale and Lyman Mill Ponds that are cohesive and non-cohesive, a probing survey was conducted during January 2005. Manual probing of

the sediment bed was done to qualitatively estimate bed type at various locations in both ponds. The sediment was separated into four bed types: 1) organic silt, clay, peat; 2) clay; 3) sand; and 4) gravel. The results of the probing study are presented on Figures 3-17 and 3-18. These data indicate that sediment bed in both ponds is primarily composed of cohesive sediment, with some areas of non-cohesive sediment. Development of a credible sediment bed map, which delineates cohesive and non-cohesive areas and is used to define bed type for each grid cell in the model, is difficult with the available data. Thus, it assumed that the entire bed is cohesive in these simulations.

3.2.3 Allendale Pond Results

The spatial distribution of current velocity for the 100-year flood in Allendale Pond is shown on Figure 3-19. Similar velocity patterns are predicted for the 5-, 10-, 25, and 50-year floods except that current velocity magnitude decreases with decreasing flow rate. Relatively high velocities occur in the upstream (inlet) portion of the pond due to shallower depths and smaller cross-sectional area. Generally, higher velocities are found in the deeper central area of the pond.

Areas in the pond where bottom shear stress exceeds the upper- and lower-bound estimates of τ_{cr} (i.e., 0.1 and 0.5 Pa) for the five floods are presented on Figures 3-20 and 3-21. Areas of potential scour (i.e., $\tau > \tau_{cr}$) increase with increasing flow rate. Potential scour areas for each flood in Allendale Pond are tabulated in Table 3-8. Current velocities exceeding the critical velocity criterion for significant scour (i.e., 2 ft/s) are predicted in the areas shown on Figures 3-22 and 3-23. These areas are quantified and listed in Table 3-9. Note that the total area of Allendale Pond is 4.49 hectares. The portion of Allendale Pond with shear stress greater than 0.1 and 0.5 Pa ranges from 28 to 62 and 5 to 15 percent, respectively, over the range of flow discharges. While erosion may occur in these areas, between 1 and 5 percent of the pond will experience potential-measurable-erosion (i.e., velocities greater than 2 ft/s) for 5-year to 100-year floods; these elevated velocities occur near the river inlet in the upstream portion of the pond.

Table 3-8. Potential Scour Areas in Allendale Pond.

Flood Return Period (years)	Area with $\tau > 0.1$ Pa (hectares)	% of Pond Area with $\tau > 0.1$ Pa	Area with $\tau > 0.5$ Pa (hectares)	% of Pond Area with $\tau > 0.5$ Pa
5	1.24	28	0.21	5
10	1.84	41	0.27	6
25	2.39	53	0.41	9
50	2.62	58	0.50	11
100	2.77	62	0.66	15

Table 3-9. Areas of Potential-Measurable-Erosion in Allendale Pond.

Flood Return Period (years)	Area with u > 2 ft/s (hectares)	% of Pond Area with u > 2 ft/s
5	0.05	1
10	0.09	2
25	0.16	3
50	0.19	4
100	0.23	5

Scour depths in Allendale Pond are estimated using Equations (3-4) and (3-5) with these average parameter values: $A = 5.1$ mg/cm^2, $n = 1.5$ and $\rho = 0.76$ g/cm^3. Spatial distributions of predicted scour depths for the five floods are illustrated on Figures 3-24 and 3-25. Scour impacts are quantified by

examining two metrics: 1) area with scour depths > 1 cm and 2) mass of eroded sediment (see Table 3-10). For convenience, the volume of eroded sediment is included in Table 3-10; it is based on the predicted eroded mass and assumes a dry density of 0.76 g/cm^3 (see Section 2.1.1). A flood event will cause 1 cm or more of erosion in less than approximately 2 percent of the pond area for all floods with return periods of 100 years or less. Mass of eroded sediment is predicted to be about 30 metric tons or less for this range of floods; most of the erosion occurs in the region where velocities exceed 2 ft/s.

Table 3-10. Impacts of Bed Scour in Allendale Pond.

Flood Return Period (years)	Area with Scour > 1 cm (hectares)	% of Pond Area with Scour > 1 cm	Mass of Eroded Sediment (metric tons)	Volume of Eroded Sediment (yd^3)
5	0.02	<1	5	9
10	0.04	1	10	17
25	0.05	1	17	29
50	0.06	1	23	40
100	0.09	2	31	53

3.2.4 Lyman Mill Pond Results

Predicted velocities for the 100-year flood in Lyman Mill Pond are shown on Figures 3-26 and 3-27. Current patterns for the four floods with lower flow rates are similar to the 100-year flood results. Relatively high velocities occur in the northern portion of the pond due to shallower depths and smaller cross-sectional area, with recirculation zones (which may be conducive to deposition) occurring along the western shoreline. Current velocities tend to decrease in the southern portion of the pond due to deeper water and larger cross-sectional area.

Areas in the pond where bottom shear stress exceeds the upper- and lower-bound estimates of τ_{cr} for the five floods are presented on Figures 3-28 and 3-29 and tabulated in Table 3-11. Current velocities exceeding the critical velocity criterion for potential-measurable-erosion (i.e., 2 ft/s) are predicted in the areas shown on Figures 3-30 and 3-31. These areas are quantified and listed in Table 3-12. Total area of Lyman Mill Pond is 9.08 hectares. The area of potential scour is larger in Lyman Mill Pond than in Allendale Pond, with potential-measurable-erosion (i.e., velocities greater than 2 ft/s) occurring over 2 to 12 percent of Lyman Mill Pond for floods with return periods between 5 and 100 years.

Table 3-11. Potential Scour Areas in Lyman Mill Pond.

Flood Return Period (years)	Area with $\tau > 0.1$ Pa (hectares)	% of Pond Area with $\tau > 0.1$ Pa	Area with $\tau > 0.5$ Pa (hectares)	% of Pond Area with $\tau > 0.5$ Pa
5	3.68	42	1.09	12
10	4.16	47	1.67	19
25	4.65	53	2.19	25
50	4.88	55	2.49	28
100	5.05	57	2.66	30

Table 3-12. Areas of Potential-Measurable-Erosion in Lyman Mill Pond.

Flood Return Period (years)	Area with u > 2 ft/s (hectares)	% of Pond Area with u > 2 ft/s
5	0.14	2
10	0.27	3
25	0.42	5
50	0.68	8
100	1.05	12

Lyman Mill Pond scour depths are estimated using these average parameter values: A = 37 mg/cm^2, n = 0.94, and ρ = 0.59 g/cm^3. Spatial distributions of predicted scour depths for the five floods are illustrated on Figures 3-32 and 3-33. Scour impacts are quantified by examining two metrics: 1) area with scour depths > 1 cm and 2) mass of eroded sediment (see Table 3-13). For convenience, the volume of eroded sediment is included in Table 3-13; it is based on the predicted eroded mass and assumes a dry density of 0.56 g/cm^3 (see Section 2.1.2). Scour depths greater than 1 cm are predicted to occur in 5 percent or less of Lyman Mill Pond for floods with return periods between 5 and 100 years. For the five floods simulated, approximately four times more bed area has scour depths greater than 1 cm in Lyman Mill Pond than the scour area predicted in Allendale Pond (see Tables 3-10 and 3-13). Similarly, mass of eroded sediment is about five to six times greater in Lyman Mill Pond than in Allendale Pond for all flow rates, with the eroded mass ranging from 42 to 139 metric tons for 5-year to 100-year floods.

Table 3-13. Impacts of Bed Scour in Lyman Mill Pond.

Flood Return Period (years)	Area with Scour > 1 cm (hectares)	% of Pond Area with Scour > 1 cm	Mass of Eroded Sediment (metric tons)	Volume of Eroded Sediment (yd^3)
5	0.04	<1	42	93
10	0.16	2	62	137
25	0.28	3	91	202
50	0.35	4	115	255
100	0.41	5	139	308

3.3 Sensitivity Analysis

The model results presented in Section 3.2 were developed using 'best' estimates of key model parameters. Uncertainty exists in model predictions, and the data used to develop and calibrate the model. An effort is made in this section to quantify this uncertainty by investigating the sensitivity of model results to variations in key parameters. The parameters that are varied between upper- and lower-bound estimates are: 1) effective bottom roughness (Z_o); and 2) dry density. The range of Z_o used in the sensitivity analysis is base case Z_o (lower-bound) and 10 Z_o (upper-bound). Even though the base case Z_o was determined through model calibration, uncertainty exists in Z_o because the hydrodynamic model is not very sensitive to Z_o for the specified range (i.e., 0.1 to 1.0 cm). Bounding estimates of dry density are based on the 95% CI values for each pond: 0.63 to 0.89 g/cm^3 (Allendale Pond) and 0.47 to 0.71 g/cm^3 (Lyman Mill Pond). The sensitivity analyses are conducted using the 100-year flood flow rate; sensitivity results are compared to results from the 'base case' simulation, which is the 100-year flood using the model parameter values discussed in Sections 3.1 and 3.2.

3.3.1 Sensitivity Analysis: Bottom Roughness

Increasing bottom roughness (Z_o) by a factor of ten causes an increase in the area of potentially significant scour and the mass of eroded sediment. In Allendale Pond, the portion of the pond with scour greater than 1 cm increased from 2 to 4 percent, while the mass of eroded sediment increased by about a factor of three (Table 3-14). Similar increases occurred in Lyman Mill Pond, with >1 cm scour area increasing from 5 to 19 percent of the pond area and erosional mass increasing by about a factor of two (Table 3-15).

Table 3-14. Sensitivity to Bottom Roughness Variation: Allendale Pond, 100-Year Flood.

Value of Z_o With Respect to Base Case	% of Pond Area with u > 2 ft/s	% of Pond Area with Scour > 1 cm	Mass of Eroded Sediment (metric tons)
Base Case (Z_o = 0.1 cm)	5	2	31
10 Z_o (Z_o = 1.0 cm)	4	4	99

Table 3-15. Sensitivity to Bottom Roughness Variation: Lyman Mill Pond, 100-Year Flood.

Value of Z_o With Respect to Base Case	% of Pond Area with u > 2 ft/s	% of Pond Area with Scour > 1 cm	Mass of Eroded Sediment (metric tons)
Base Case (Z_o = 0.1 cm)	12	5	139
10 Z_o (Z_o = 1.0 cm)	8	19	246

3.3.2 Sensitivity Analysis: Dry Density

Uncertainty in dry density affects predicted scour depth, see Equation (3-8). For Allendale Pond, bed area with scour greater than 1 cm varies by about 1 percent, with respect to the base case, with the specified variation in dry density. In Lyman Mill Pond, the variation in scour depth area (> 1 cm) is about 2 percent.

3.4 Summary of Model Results

The potential impacts of flood events on bed stability in the two ponds were evaluated using a hydrodynamic model as discussed in the preceding sections. Primary results of the modeling are:

- In Allendale Pond, scour greater than approximately 1 cm will occur over less than 2 percent of the bed area in the pond during a flood event. Scour depths greater than approximately 1 cm will generally occur in the northern portion of the pond, near the upstream inlet.

- Bed erosion greater than approximately 1 cm will occur over a larger area in Lyman Mill Pond than in Allendale Pond, with up to 5 percent of the Lyman Mill Pond bed having erosion greater than approximately 1 cm. Bed scour generally occurs in the northern portion of Lyman Mill Pond, with maximum erosion near the upstream inlet.

- The most useful model metrics for evaluating potential impacts on bed stability are areas with u > 2 ft/s (depth-averaged velocity) and scour depth > 1 cm. Comparison of bottom shear stress to critical shear stress values is less useful because of the nonlinear relationship between scour depth (or resuspension potential) and shear stress for cohesive sediment. Generally, minimal erosion of a cohesive bed occurs for applied shear stress near the critical value; in contrast to

non-cohesive sediment, where significant erosion can happen once the critical shear stress is exceeded.

- Absolute magnitude of model predictions is more uncertain than relative magnitude. For example, the model predicts that 31 and 139 metric tons of sediment are eroded during a 100-year flood in Allendale and Lyman Mill Ponds, respectively. The qualitative difference between the two predictions (i.e., about four to five time more erosion occurs in Lyman Mill Pond than in Allendale Pond) is more accurate and reliable than the absolute values of the scour predictions.

- The sensitivity analysis indicates that, generally, uncertainty associated with the quantitative modeling results ranges between a factor of two and ten.

Comparison of potential impacts of flood events on bed scour between the two ponds provides additional insights concerning bed stability in the study area. Generally, a larger area of the sediment bed is impacted by a flood event in Lyman Mill Pond than in Allendale Pond (Figure 3-34). About five times more bed area in Lyman Mill Pond will experience bed scour greater than approximately 1 cm during a flood than in the upstream pond. Similarly, the mass of eroded sediment is greater in Lyman Mill Pond, with about five times more sediment being scoured during a 100-year flood in the downstream pond than in Allendale Pond (Figure 3-35).

3.5 Model Limitations

The modeling analysis provides useful information for evaluating bed stability in the two ponds. Limitations exist in the model, however, primarily due to uncertainties in specifying model parameters and inputs. Specific model limitations are:

- The assumption that the sediment bed in each pond is composed of cohesive sediment. This assumption is necessary because available bed-type data are insufficient for developing a reliable bed map. Even though assuming that the bed is entirely cohesive is a reasonable first-approximation, model results may be impacted. For example, non-cohesive sediment exists in the inlet areas of the ponds, where the model presently predicts maximum erosion depths, due to higher velocities routinely occurring in those areas. The erosion properties of cohesive and non-cohesive sediments are significantly different and, hence, model predictions may change if bed type is switched to non-cohesive in a particular area.

- Other potential limitations include: neglecting effects of floodplains during overbank flow conditions; and neglecting impact of vegetation on hydrodynamic drag. Neglecting floodplain and vegetation effects tends to produce conservative results; predicted current velocity and bottom shear stress are maximized when the effects of floodplains and vegetation are not incorporated into the model.

- The approach in this study uses a hydrodynamic model to make estimates of potential bed scour during flood events in Allendale and Lyman Mill Ponds. The model results cannot be used to infer the fate of eroded sediment during a flood. That type of analysis requires the development and application of a sediment transport model, which was not incorporated into this study.

This page intentionally left blank

4.0 CONCEPTUAL SITE MODEL FOR SEDIMENT TRANSPORT

Results of the data-based analyses in Section 2 may be used to develop a CSM for sediment transport. A CSM is an important component of a sediment stability analysis because consistency must be maintained between the CSM and the results of quantitative and qualitative sediment stability analyses. A sediment transport CSM is a detailed component of the overall CSM that is typically developed for risk assessment at a contaminated sediment site. The sediment transport CSM is a qualitative description of the processes (e.g., deposition and erosion) and system characteristics (e.g., upstream and tributary sediment loads, spatial distribution of bed properties) that control sediment dynamics within the study area.

Based on the data-based analyses presented earlier in the report, the following CSM for sediment transport is proposed:

- The surficial layer of the sediment bed in each pond, i.e., approximately upper 1-2 ft, is generally composed of cohesive sediment. Relatively small areas of non-cohesive sediment exist in each pond, typically in locations where higher current velocities exist.

- The composition of surficial sediment is finer in the downstream pond (Lyman Mill Pond) due to selective deposition of coarser sediment in the upstream pond (Allendale Pond).

- The two ponds, which are dammed and serve as run-of-the-river impoundments, are net depositional environments for most flow rates. Significant erosion during a high-flow event is expected to occur over small areas within each pond.

- The river channel upstream of each pond is composed of coarse, non-cohesive sediment and is typically non-depositional. The river channels serve as conduits for suspended sediment into and between the ponds.

The model-based analyses presented in Section 3 are consistent with the proposed CSM. The impacts of flood events on bed scour are predicted to be restricted to a relatively small portion (i.e., less than approximately 2 to 5 percent of pond area with scour greater than 1 cm for Allendale and Lyman Mill Ponds, respectively) of the sediment bed in each pond. The modeling results suggest that deposition occurs over large portions of Allendale and Lyman Mill Ponds during high-flow events; deposition rates during a flood will be spatially variable within each pond due to variations in sediment load and bottom shear stress. In addition, sediment eroded in the upstream portions of each pond during a flood will be transported downstream by river currents. A portion of the eroded sediment will be re-deposited within the pond; current velocity and bottom shear stress tend to decrease in the downstream portions of each pond, making those areas conducive to re-deposition of eroded material from upstream locations.

This page intentionally left blank.

5.0 CONCLUSIONS RELATED TO BED STABILITY

The data- and model-based analyses conducted during this study provide information that may be used to develop conclusions regarding bed stability within Allendale and Lyman Mill Ponds. These conclusions, along with the supporting data and analysis results, may prove to be helpful when considering potential remedial alternatives for the two ponds. Specific conclusions based on the results of the analyses are:

- A representative average sedimentation rate for Allendale Pond varies from 0.5 to 0.8 cm/yr, which corresponds to a range for depositional mass in the pond of 170 to 270 metric tons/yr (assuming a dry density of 0.76 g/cm^3 and an area of 4.49 hectares).

- A representative depth range for the 1940 time horizon in the sediment bed of Allendale Pond is between 1 and 2 feet. An estimate of the 1940-TH could not be made for Lyman Mill Pond due to insufficient data.

- Minimal net export of dioxin from the two ponds occurs during low-flow, non-resuspending conditions; the water-column load of dioxin entering the study area (i.e., background load) is approximately equal to the load over Lyman Mill Dam during low-flow periods.

- In Allendale Pond, significant scour (i.e., scour depth greater than 1 cm) will occur over 2 percent or less of the bed area in the pond during a flood event. Significant erosion, i.e., greater than approximately 1 cm, will generally occur in the northern portion of the pond, near the upstream inlet.

- Significant scour will occur over a larger area in Lyman Mill Pond than in Allendale Pond, with up to 5 percent of the Lyman Mill Pond bed having erosion greater than approximately 1 cm. Bed scour generally occurs in the northern portion of Lyman Mill Pond, with maximum erosion near the upstream inlet.

- Generally, uncertainty associated with the quantitative modeling results ranges between a factor of two and ten.

The validity of these conclusions is dependent on the uncertainty in the data and model. Attempts were made to incorporate the effects of uncertainty in the data-based analyses, which are discussed in Section 2. Uncertainty in the data-based analyses is reflected in the conclusions through use of ranges of results, rather than specific numbers. Uncertainty in the model-based conclusions is primarily due to spatial and temporal variability in model parameters.

This page intentionally left blank.

6.0 REFERENCES

Alcoa, 2002. *Analysis of Alternatives Report. Grasse River Study Area. Massena, New York.* Alcoa report. June 12, 2002.

Allen, J.R.L., Rae, J.E., Longworth, G., Hasler, S.E., and Ivanovich, M., 1993. A comparison of the ^{210}Pb dating technique with three other independent dating methods in an oxic estuarine salt-marsh sequence. *Estuaries*, 16(3B):670-677.

Battelle, 2003. Data Summary Report, Interim Data Collection, Remedial Investigation and Feasibility Study, Centredale Manor Restoration Project Superfund Site, North Providence, Rhode Island. Prepared for U.S. Army Corps of Engineers, New England District. June 2003.

Battelle, 2005. Final Work Plan. Task RI-10B – Sediment Stability Evaluation Phase Two. Current Velocity/Stage Height Data Collection Activities. Centredale Manor Restoration Project Superfund Site. Prepared for U.S. Army Corps of Engineers, New England District. March 2005.

Corcoran, M., 2004. *Geomorphic Assessment of the Woonasquatucket River, RI.* USGS report, Engineer Research and Development Center, Vicksburg, MS.

Graf, W.H. 1971. *Hydraulics and Sediment Transport.* McGraw-Hill, Inc., New York, NY. 513 p.

Jepsen, R., Roberts, J., Langford, R. and Gailani, J., 2001. *Rio Grande Erosion Potential Demonstration, Report for the National Border Technology Partnership Program.* Sandia National Laboratories report SAND2001-3611.

Lick, W., Xu, Y.J., and McNeil, J., 1995. Resuspension properties of sediments from the Fox, Sagninaw and Buffalo Rivers. *J. Great Lakes Res.*, 21(2):257-274.

Olsen, C.R., Simpson H.J., Bopp R.F., Williams S.C., Peng T.H. and Deck B.L., 1978. Geochemical analysis of the sediments and sedimentation of the Hudson River Estuary. *J Sed Petrol* 48:401-418.

Orson R.A., Simpson R.L. and Good E.E., 1990. Rates of sediment accumulation in a tidal freshwater marsh. J. Sediment Petrology. *J Sed Petrol* 19:849-869.

Quantitative Environmental Analysis, 2004a. Final Work Plan, Centredale Manor Sediment Stability Study. Prepared for USACE, New England District, June 2004.

Quantitative Environmental Analysis, 2004b. Final Work Plan, Shaker Study in Allendale and Lyman Mill Ponds, Centredale Manor Restoration Project Superfund Site. Prepared for USACE, New England District, December 2004.

Quantitative Environmental Analysis, 2004c. Final Technical Memorandum. Sediment Stability Study. Centredale Manor Restoration Project Superfund Site. Prepared for USACE, New England District, November 2004.

Robbins, J.A., 1978. Geochemical and geophysical applications of radioactive lead isotopes. In: Nriagu JO, ed, *Biogeochemistry of lead.* Elsevier, Amsterdam, pp 285-393.

Roberson, J.A., Cassidy, J.J. and Chaudhry, M.H., 1998. *Hydraulic Engineering.* John Wiley & Sons, New York, 204 p.

Roberts, J., Jepsen, R., Bryan, C. and Chapin, M., 2001. *Boston Harbor Sediment Study*. Sandia National Laboratories, report SAND2001-2226.

Shields, G., 2003. Waterborne geophysical surveys and sediment coring, Centredale Manor site, Work Assignment R1A00270 – trip report. Lockheed Martin Technology Services, October 21, 2003.

Simpson, H.J., Olsen C.R., Trier R.M. and Williams S.C., 1976. Manmade radionuclides and sedimentation in the Hudson River Estuary. *Science* 194:179-183.

TTNUS, Inc., 2000. *Final Technical Memorandum, Volume I Text, Woonasquatucket River Sediment Investigation, Centredale Manor Restoration Project Site, North Providence, Rhode Island.* Prepared for U.S. Environmental Protection Agency, Region 1. June 2000.

U.S. Army Corps of Engineers (USACE), 1991. *Hydraulic Design of Flood Control Channels*. EM-1110-2-1601. Vicksburg, MS.

U.S. Geological Survey (USGS), 1996. *Water Resources Data, Massachusetts and Rhode Island, Water Year 1996*. USGS water-data report MA-RI-96-1.

Van Rijn, L.C., 1993. *Principles of Sediment Transport in Rivers, Estuaries and Coastal Seas*. Aqua Publications, Amsterdam.

Ziegler, C.K., 2002. Evaluating sediment stability at sites with historic contamination. *Environmental Management*, 29(3):409-427.

Ziegler, C.K. and Nisbet, B.S., 1994. Fine-grained sediment transport in Pawtuxet River, Rhode Island. *ASCE J. Hydr. Engr.*, 121(11):773-781.

APPENDIX A

FIGURES

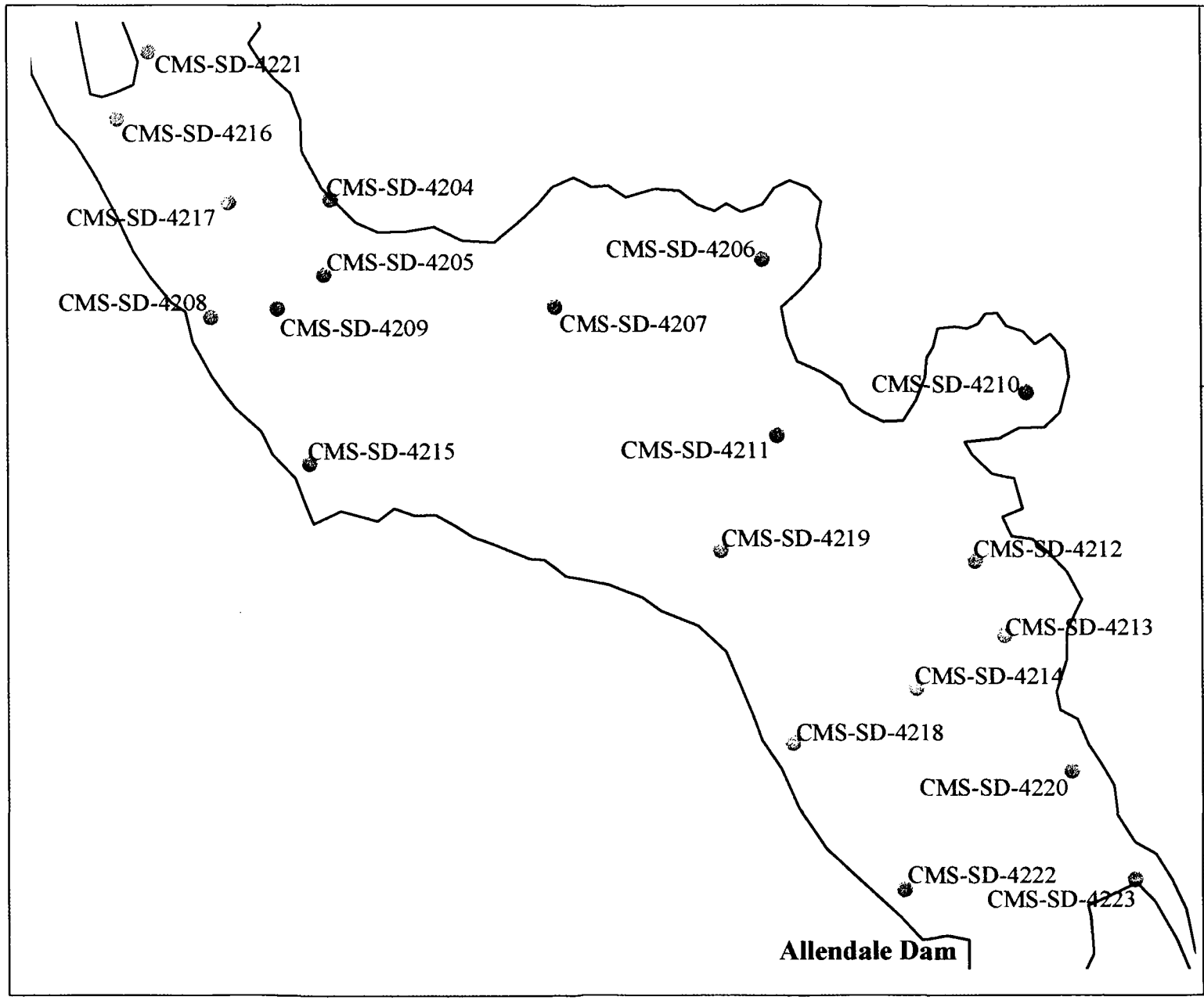

Locator Map

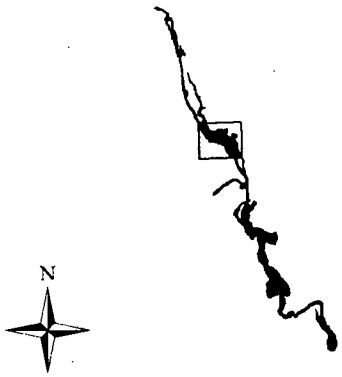

Legend

1997 Shoreline

May 2003 Core Locations *

* Location based on GPS measurement

Figure 2-1. Locations of cores collected in Allendale Pond during May 2003.

QEA
Quantitative Environmental Analysis, LLC

BATcen:120 **February 2006**

CO- C:\BATman\Maps\ArcGIS\May2003r\batcen_allendale_may03_loc.mxd

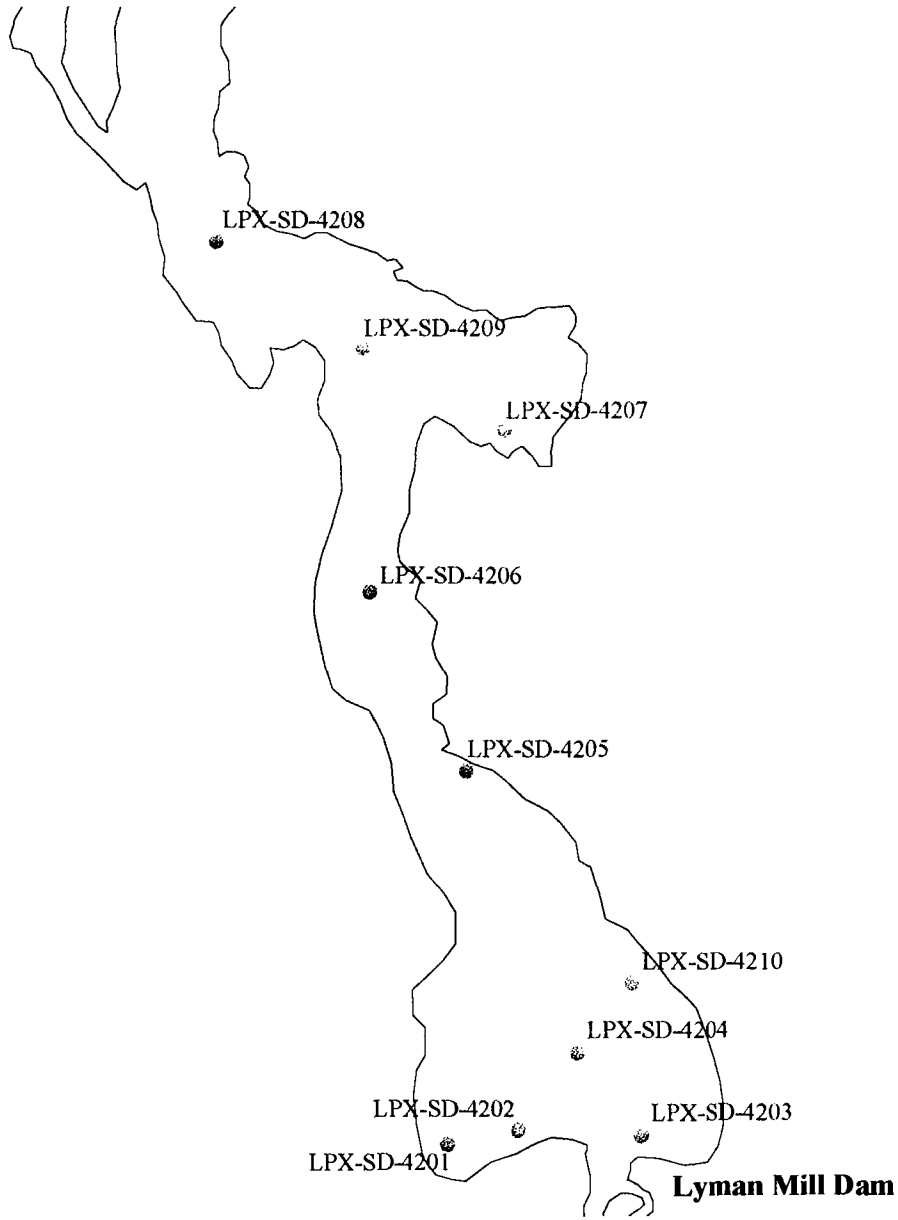

Locator Map

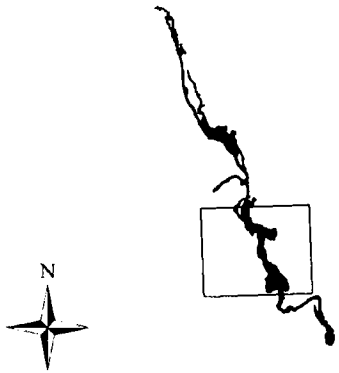

Legend

1997 Shoreline

May 2003 Core Locations *

* Location based on GPS measurement

Figure 2-2. Locations of cores collected in Lyman Mill Pond during May 2003.

QEA
Quantitative Environmental Analysis, LLC

BATcen:120 **February 2006**

CO- C:\BATman\Maps\ArcGIS\May2003\batcen_lyman_may03_loc_fixed _core_labels.mxd

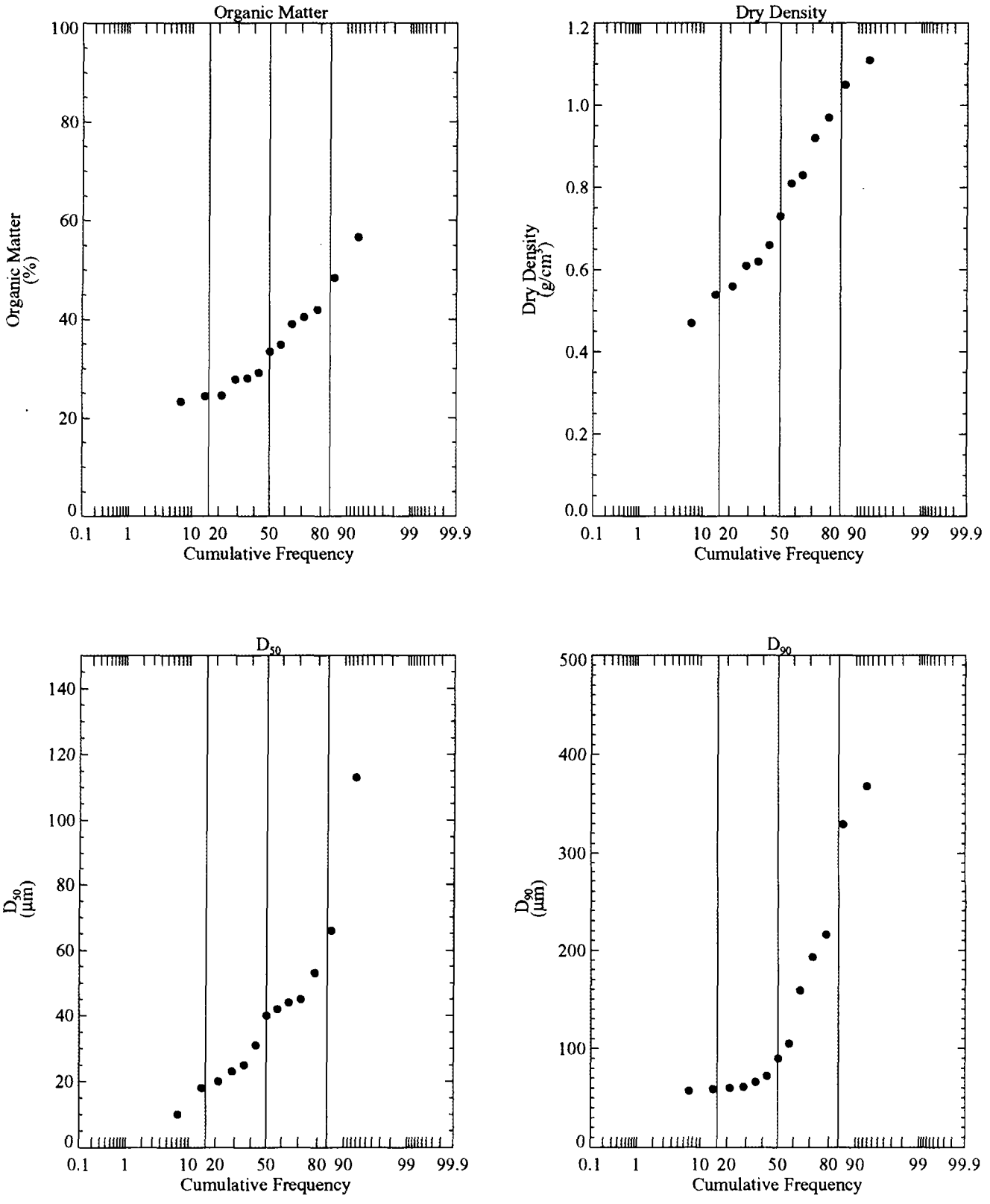

Figure 2-3. Frequency distributions of bulk bed properties in Allendale Pond (May 2003 data).

cfo - C:\BATman\Analysis\Sediment_Investigations\May2003\plot_bedproperties_040823.pro
Thu Aug 26 15:18:29 2004

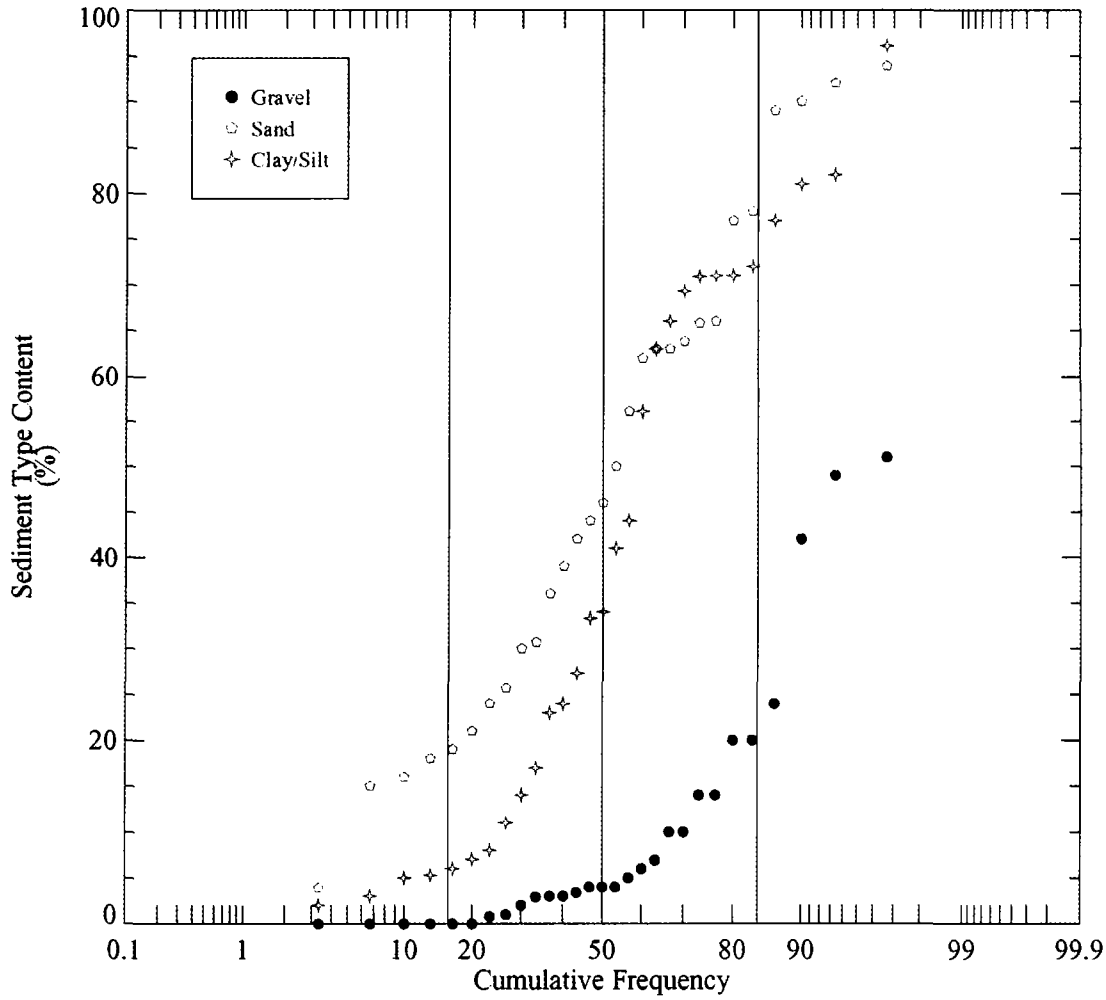

Figure 2-4. Frequency distributions of clay/silt, sand and gravel content in Allendale Pond sediment (May 2003 data).

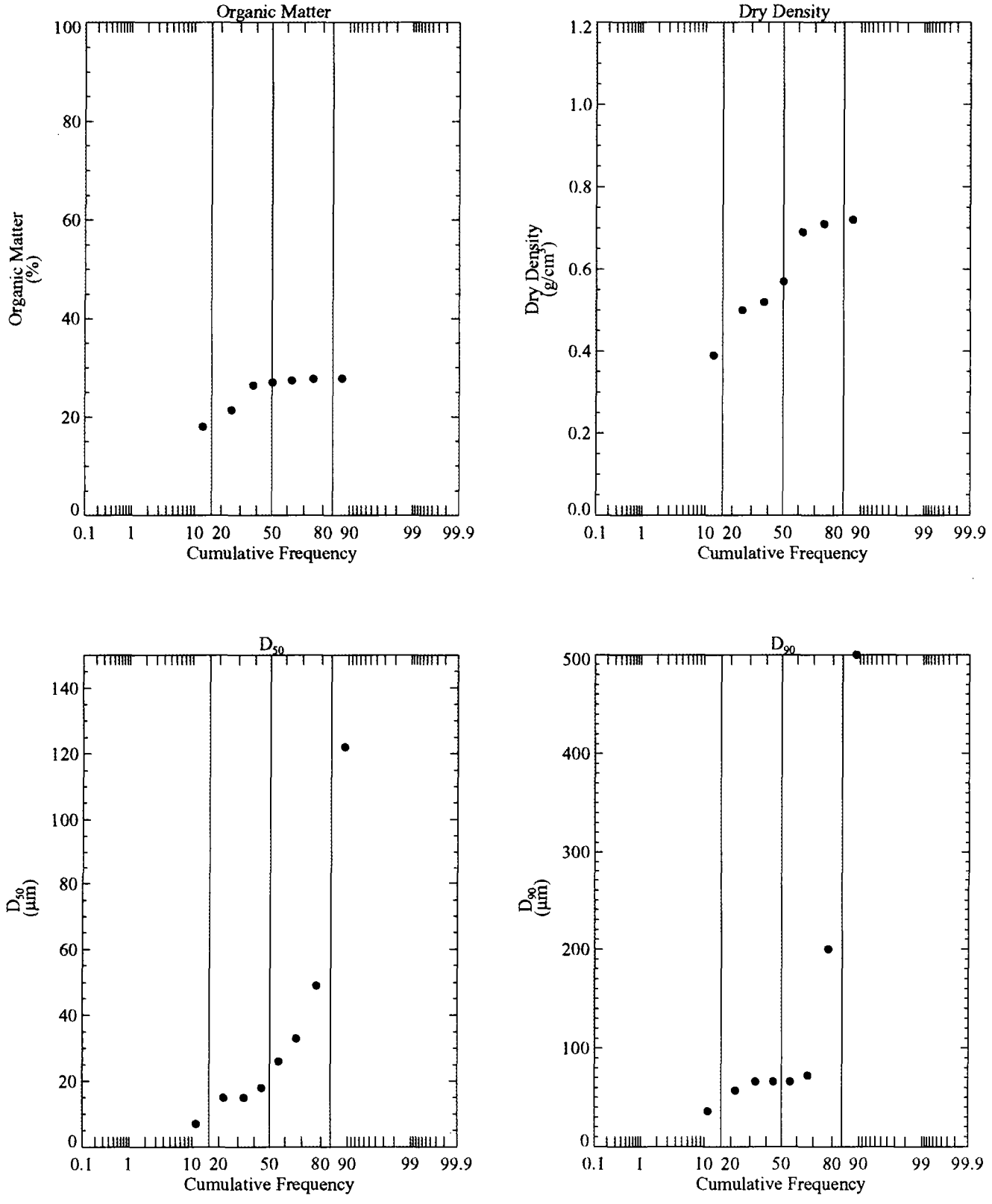

Figure 2-5. Frequency distributions of bulk bed properties in Lyman Mill Pond (May 2003 data).

cfo - C:\BATman\Analysis\Sediment_Investigations\May2003\plot_bedproperties_040823.pro
Thu Aug 26 15:18:29 2004

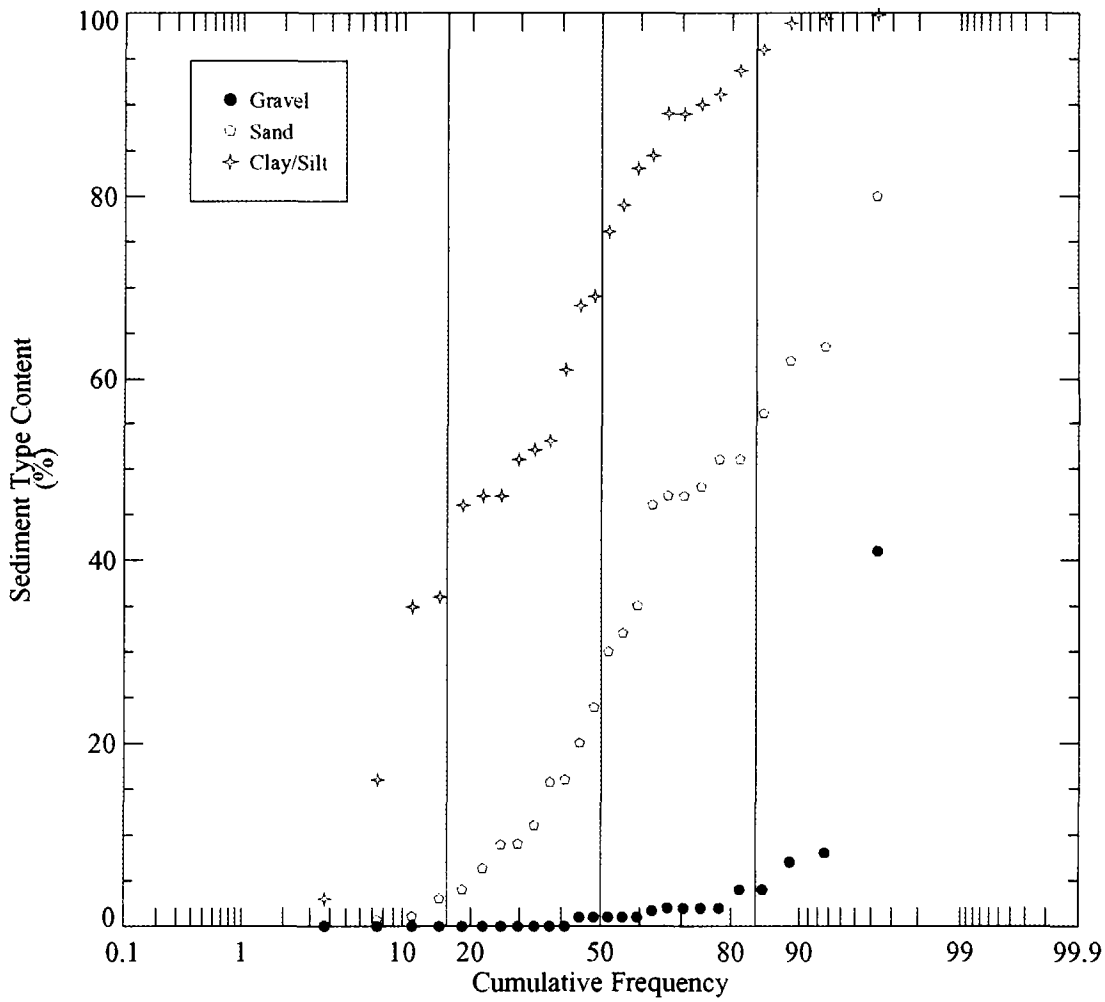

Figure 2-6. Frequency distributions of clay/silt, sand and gravel content in Lyman Mill Pond sediment (May 2003 data).

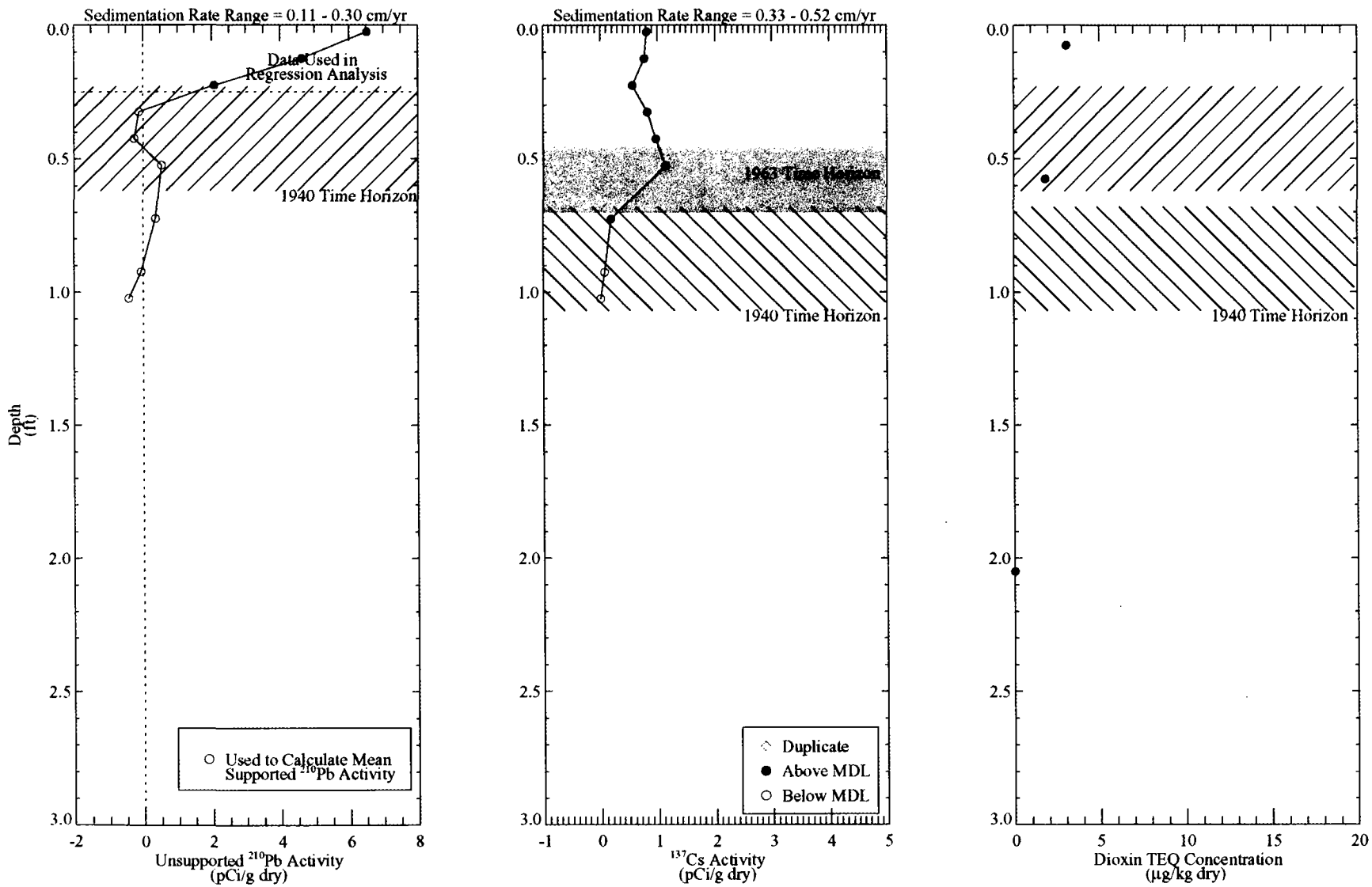

Figure 2-7. Vertical profiles of Pb-210 activity, Cs-137 activity and dioxin TEQ concentration for core CMS-SD-4204 in Allendale Pond (May 2003 data).

cfo - C:\BATman\Analysis\Sedimentation_rates\plot_pb_cs_profiles_3panel_040721.pro
Thu Aug 26 16:02:04 2004

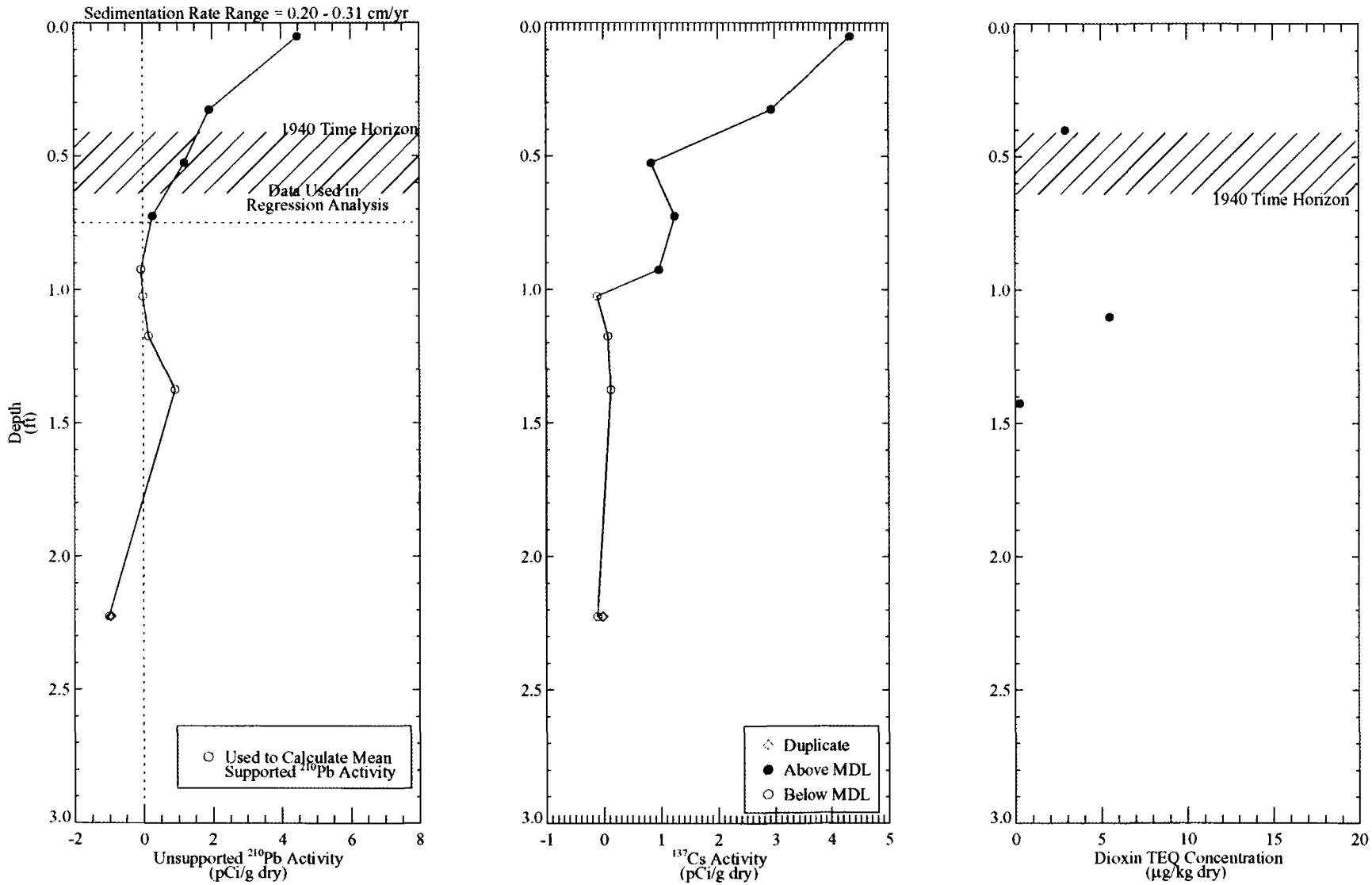

Figure 2-8. Vertical profiles of Pb-210 activity, Cs-137 activity and dioxin TEQ concentration for core CMS-SD-4206 in Allendale Pond (May 2003 data).

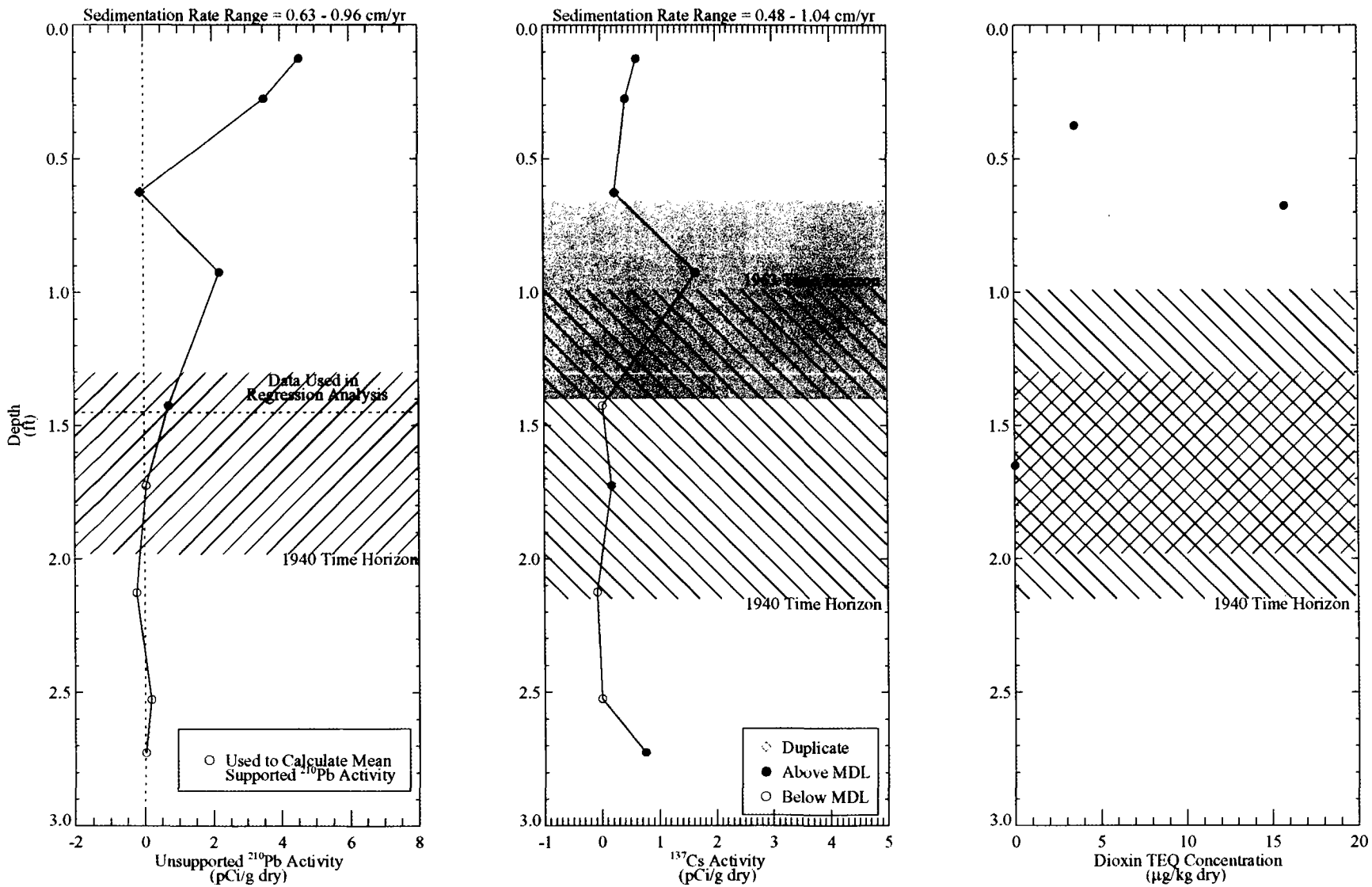

Figure 2-9. Vertical profiles of Pb-210 activity, Cs-137 activity and dioxin TEQ concentration for core CMS-SD-4209 in Allendale Pond (May 2003 data).

cfo - C:\BATman\Analysis\Sedimentation_rates\plot_pb_cs_profiles_3panel_040721.pro
Thu Aug 26 16:02:04 2004

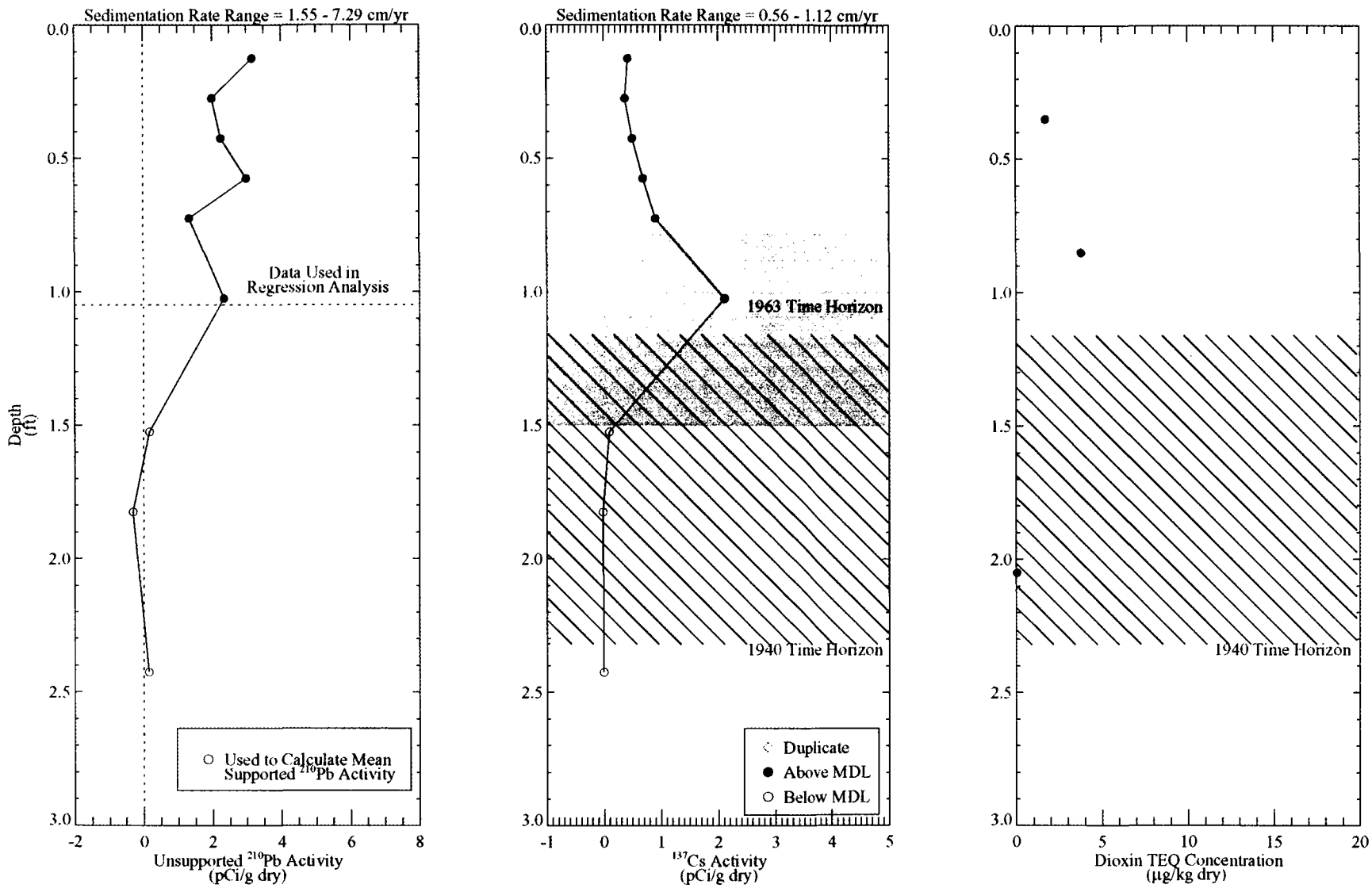

Figure 2-10. Vertical profiles of Pb-210 activity, Cs-137 activity and dioxin TEQ concentration for core CMS-SD-4210 in Allendale Pond (May 2003 data).

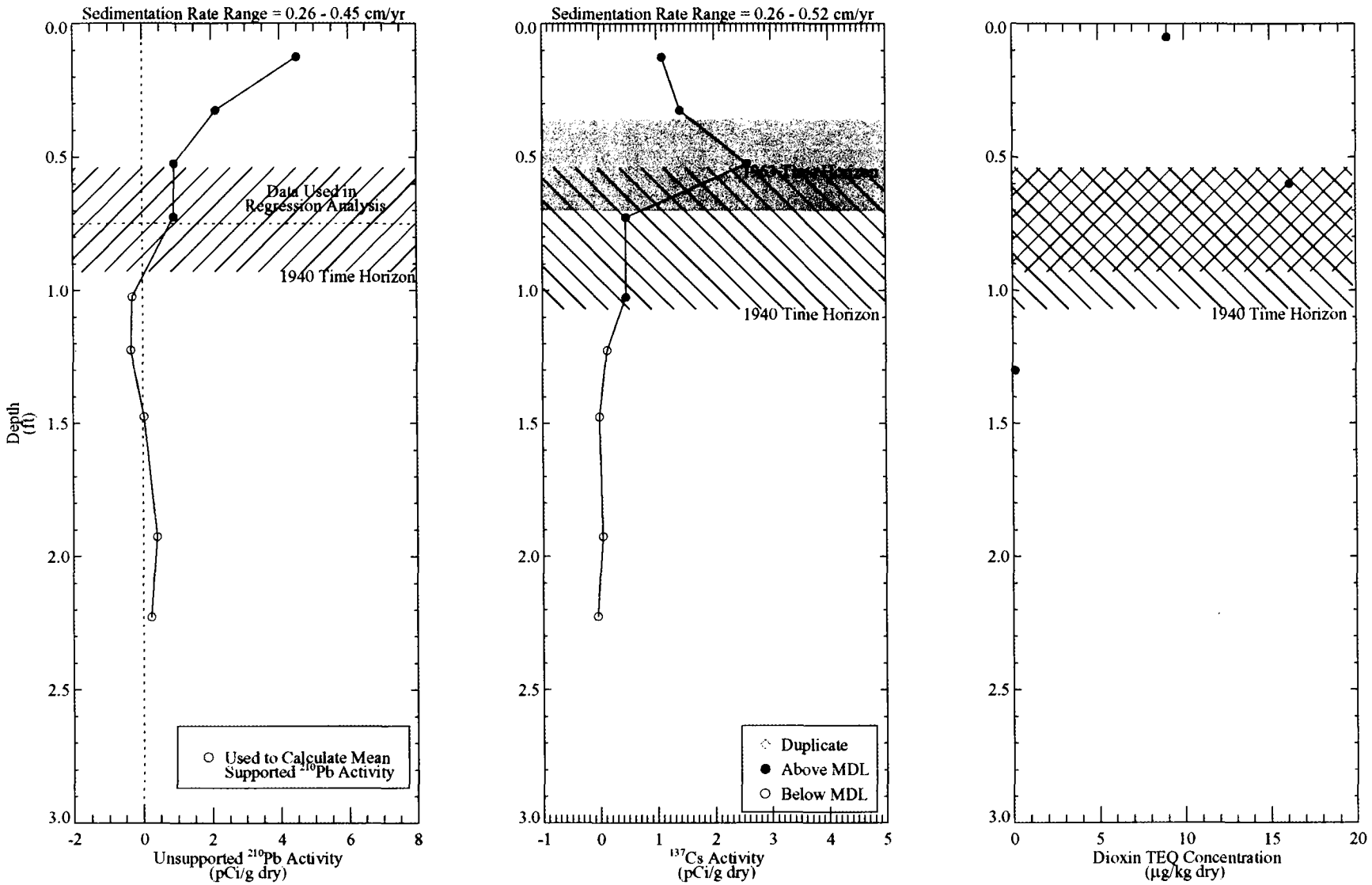

Figure 2-11. Vertical profiles of Pb-210 activity, Cs-137 activity and dioxin TEQ concentration for core CMS-SD-4212 in Allendale Pond (May 2003 data).

cfo - C:\BATman\Analysis\Sedimentation_rates\plot_pb_cs_profiles_3panel_040721.pro
Thu Aug 26 16:02:04 2004

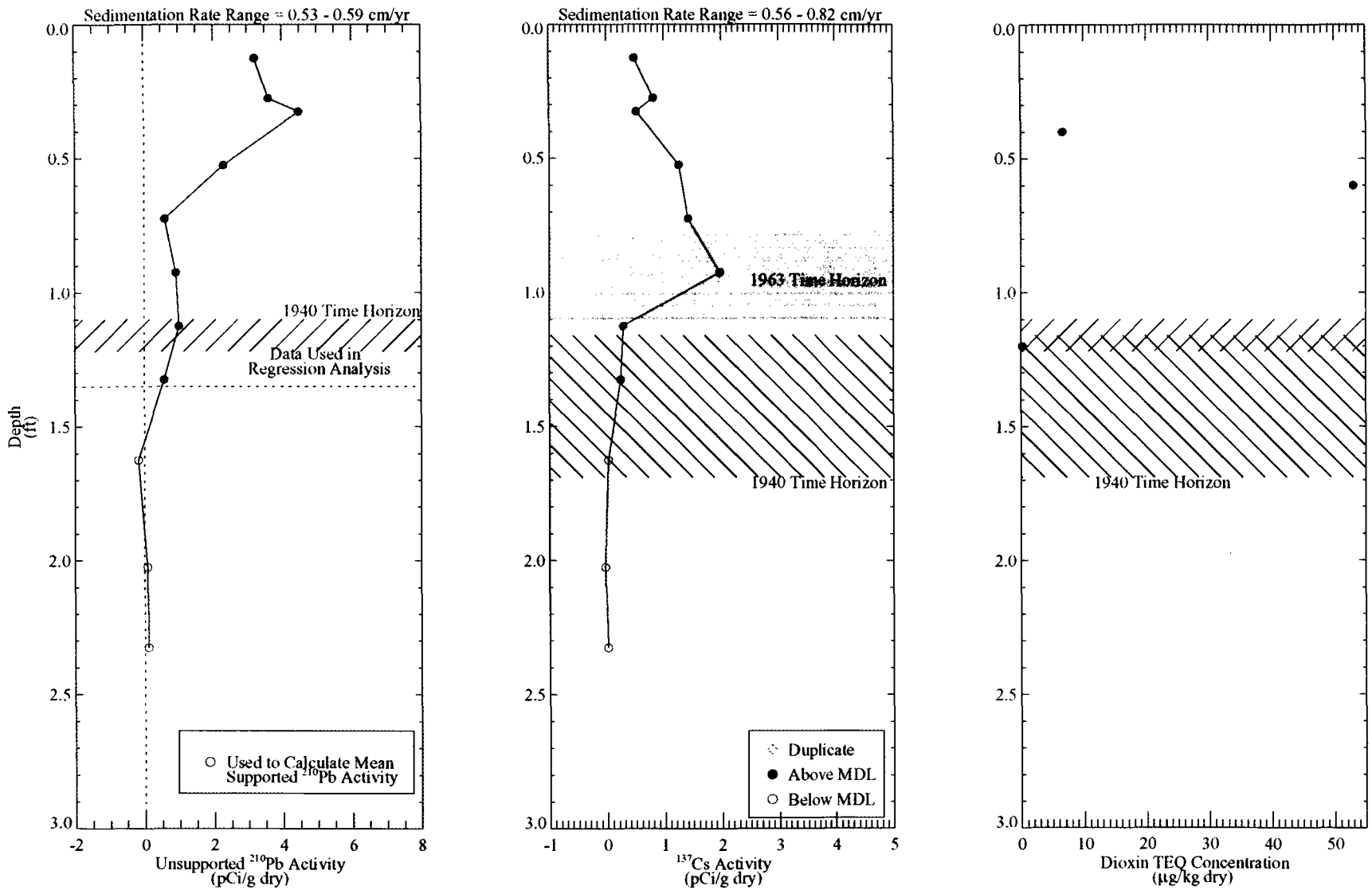

Figure 2-12. Vertical profiles of Pb-210 activity, Cs-137 activity and dioxin TEQ concentration for core CMS-SD-4213 in Allendale Pond (May 2003 data).

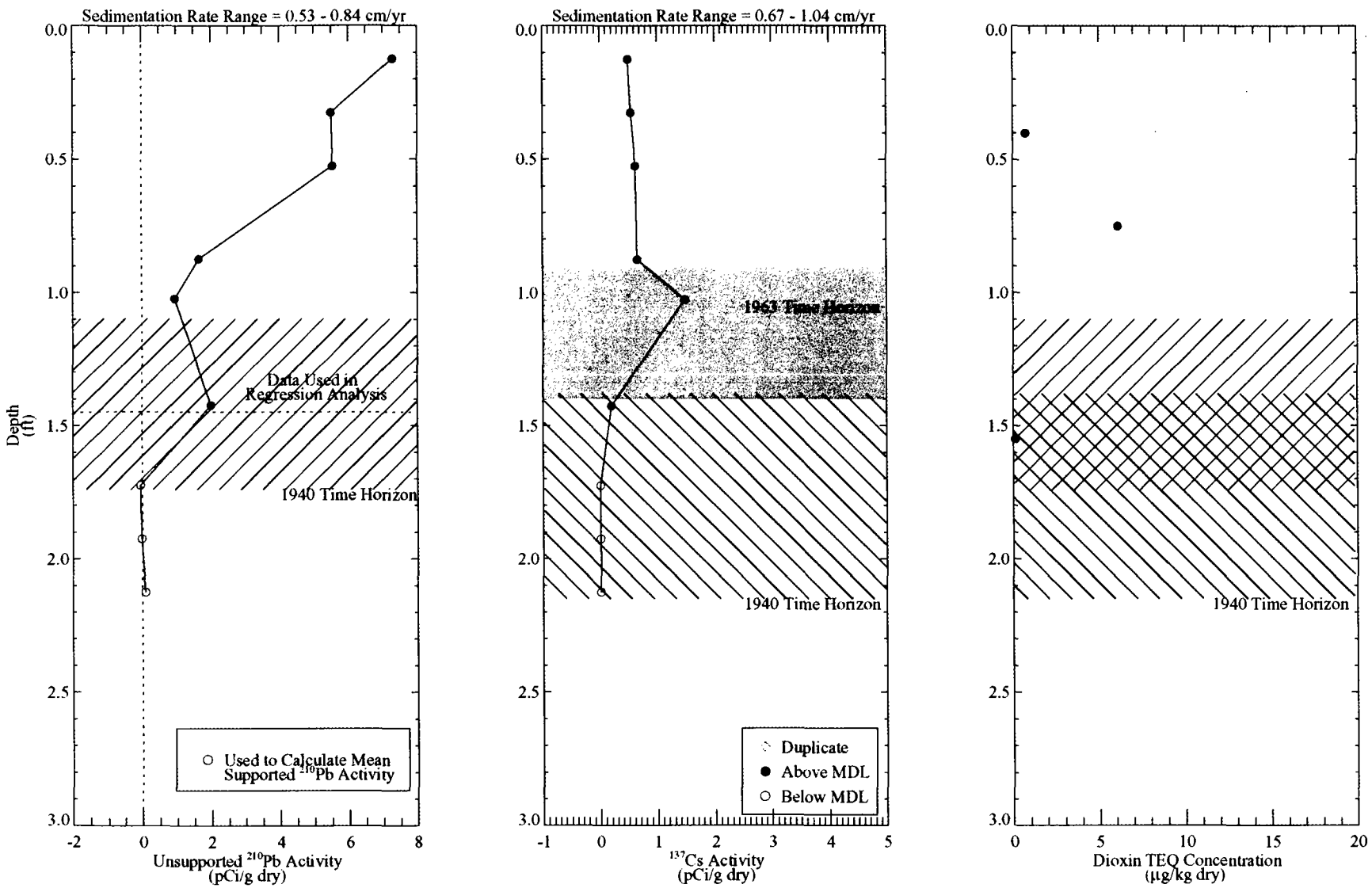

Figure 2-13. Vertical profiles of Pb-210 activity, Cs-137 activity and dioxin TEQ concentration for core CMS-SD-4218 in Allendale Pond (May 2003 data).

cfo - C:\BATman\Analysis\Sedimentation_rates\plot_pb_cs_profiles_3panel_040721.pro
Thu Aug 26 16:02:04 2004

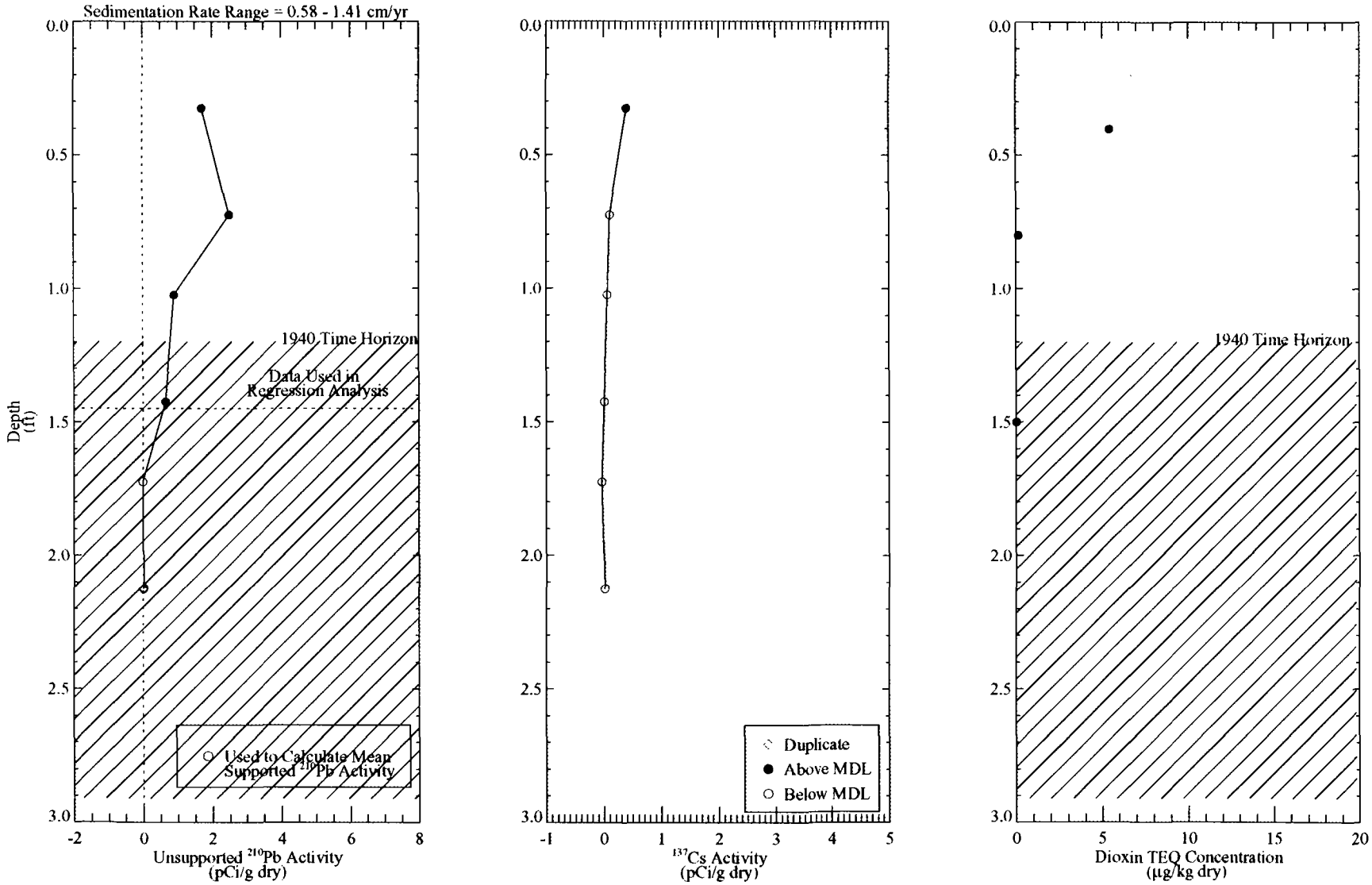

Figure 2-14. Vertical profiles of Pb-210 activity, Cs-137 activity and dioxin TEQ concentration for core CMS-SD-4219 in Allendale Pond (May 2003 data).

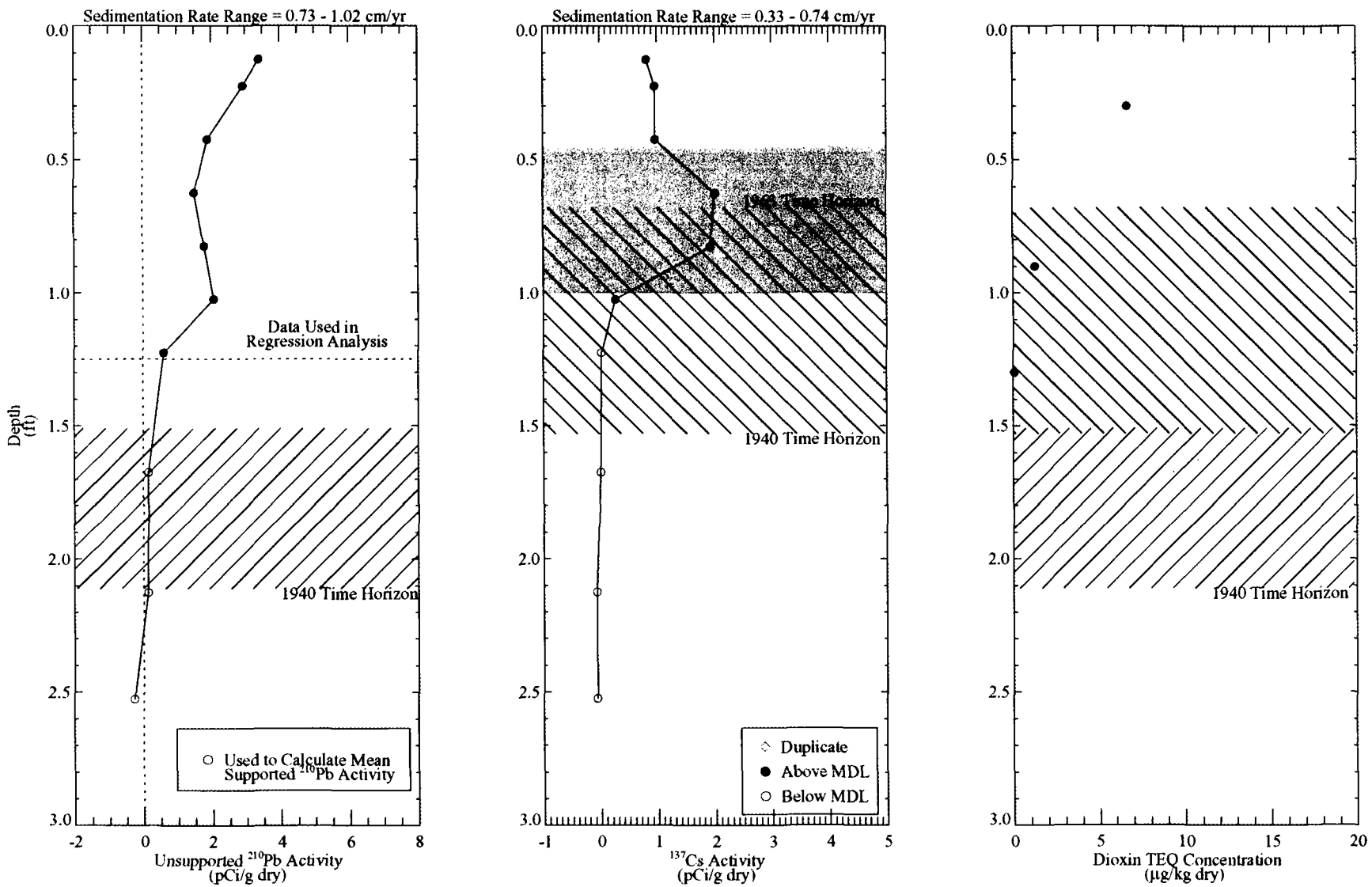

Figure 2-15. Vertical profiles of Pb-210 activity, Cs-137 activity and dioxin TEQ concentration for core CMS-SD-4222 in Allendale Pond (May 2003 data).

cfo - C:\BATman\Analysis\Sedimentation_rates\plot_pb_cs_profiles_3panel_040721.pro
Thu Aug 26 16:02:04 2004

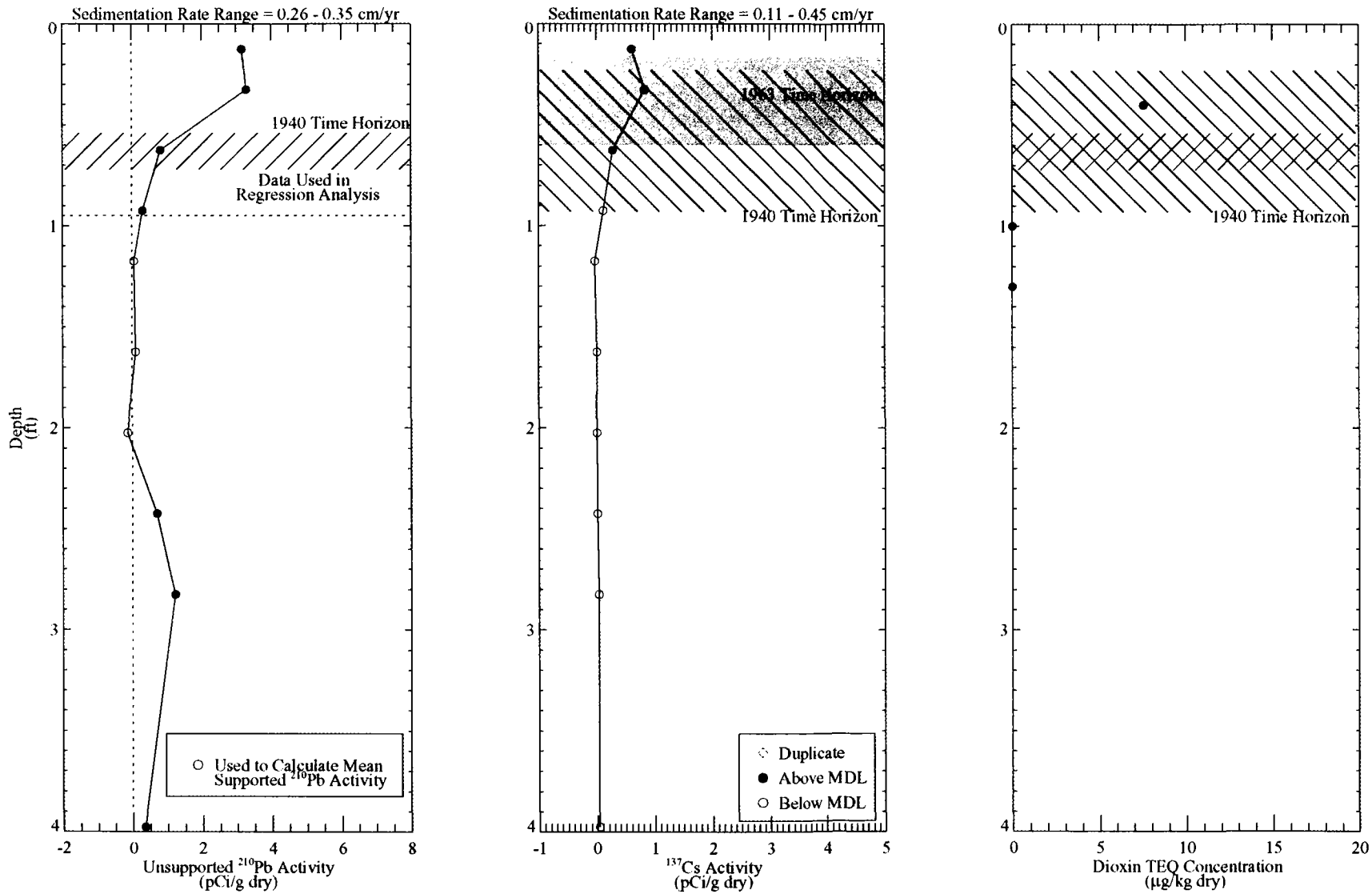

Figure 2-16. Vertical profiles of Pb-210 activity, Cs-137 activity and dioxin TEQ concentration for core LPX-SD-4201 in Lyman Mill Pond (May 2003 data).

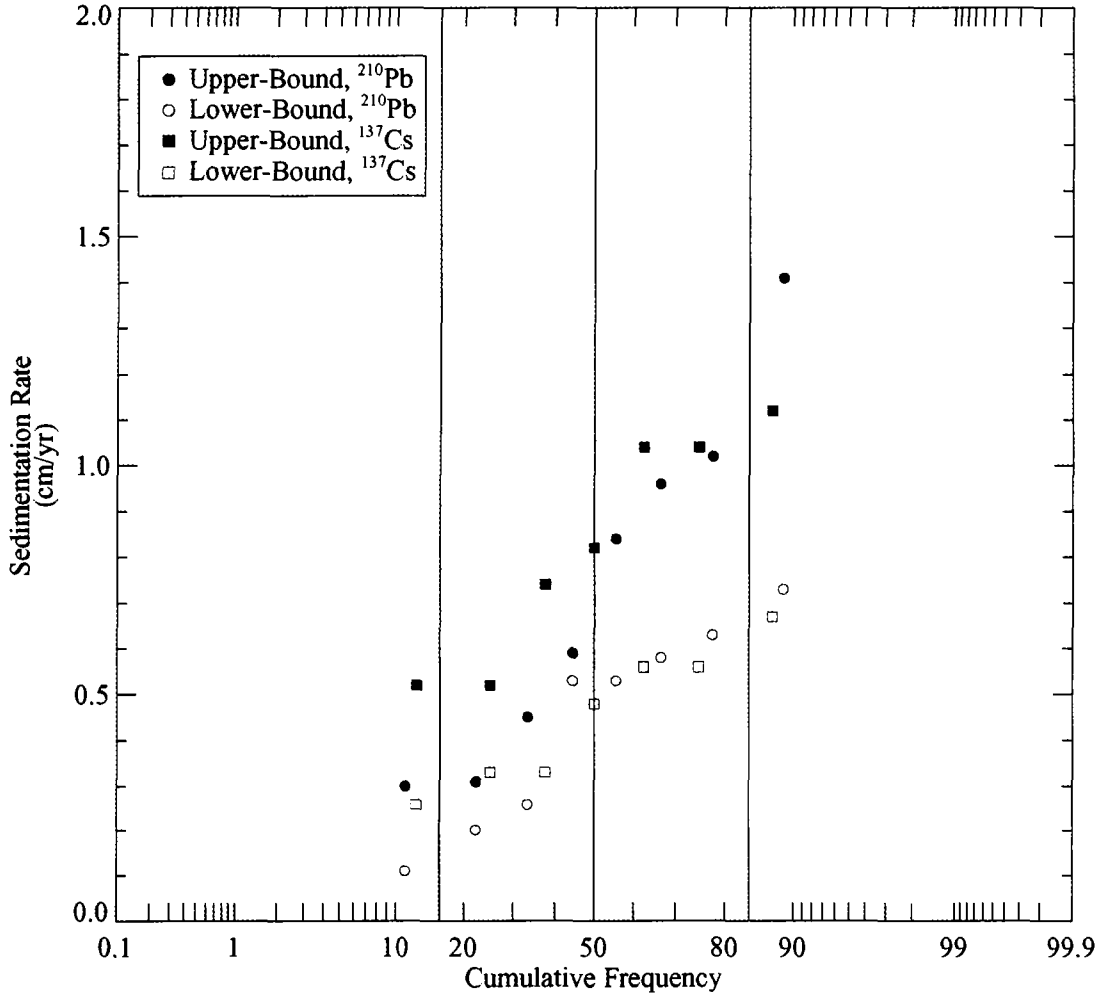

Figure 2-17. Frequency distributions of upper- and lower-bound estimates of Allendale Pond sedimentation rates based on analysis of Pb-210 and Cs-137 activity data.

cfo - C:\BATman\Analysis\Sedimentation_rates\probplot_pb_cs_sedrate_bounds_040823.pro
Thu Aug 26 15:20:44 2004

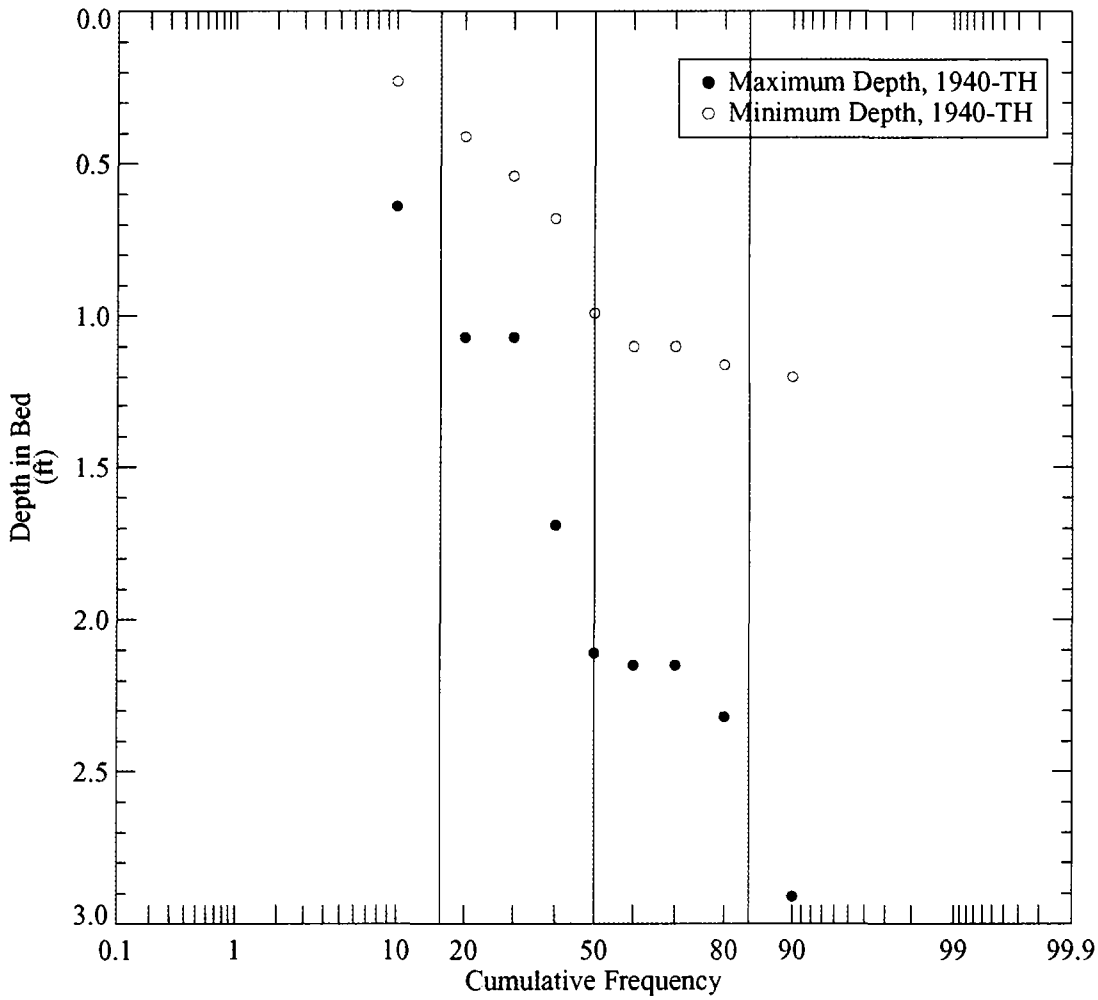

Figure 2-18. Frequency distributions of minimum and maximum depths of 1940-TH in Allendale Pond sediment cores.

cfo - C:\BATman\Analysis\Sedimentation_rates\probplot_pb_cs_sedrate_bounds_040823.pro
Thu Aug 26 15:20:44 2004

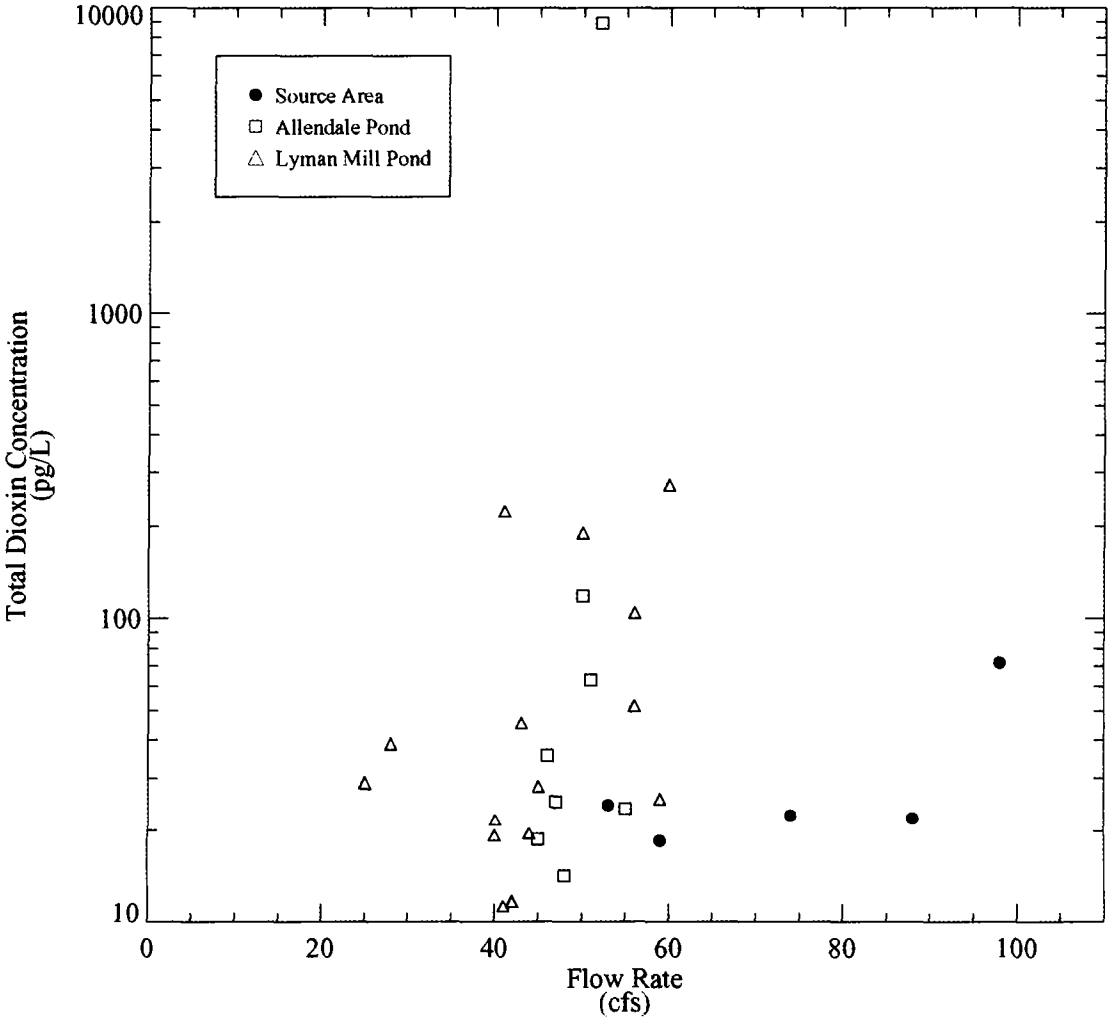

Figure 2-19. Correlation between total dioxin water-column concentration and flow rate during October-November 1999 sampling period.

cfo - C:\BATman\Analysis\WQ_spatial\wq_spatial_040820.pro
Fri Aug 27 08:38:38 2004

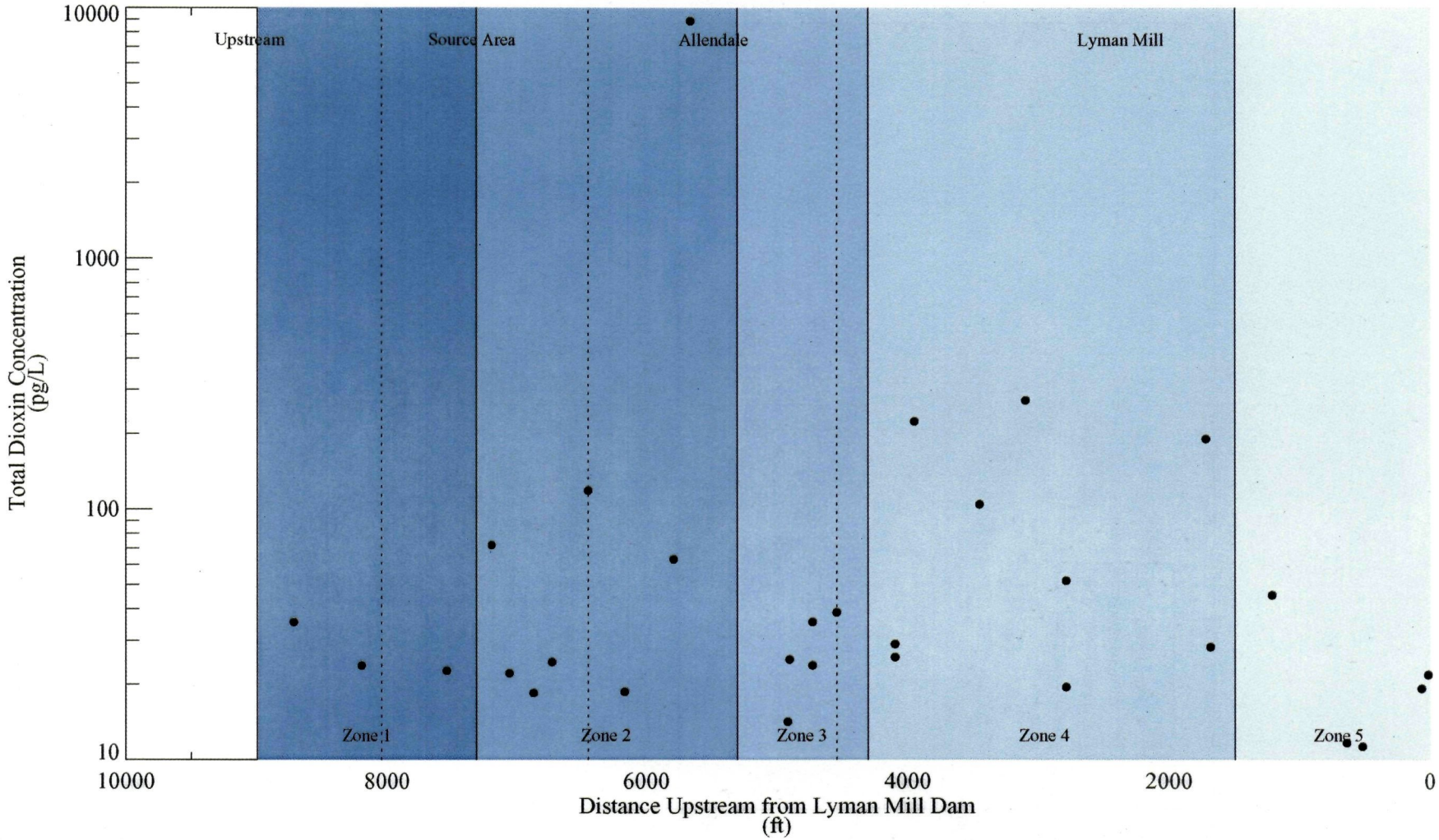

Figure 2-20. Spatial distribution of total dioxin water-column concentration during October-November 1999 sampling period.

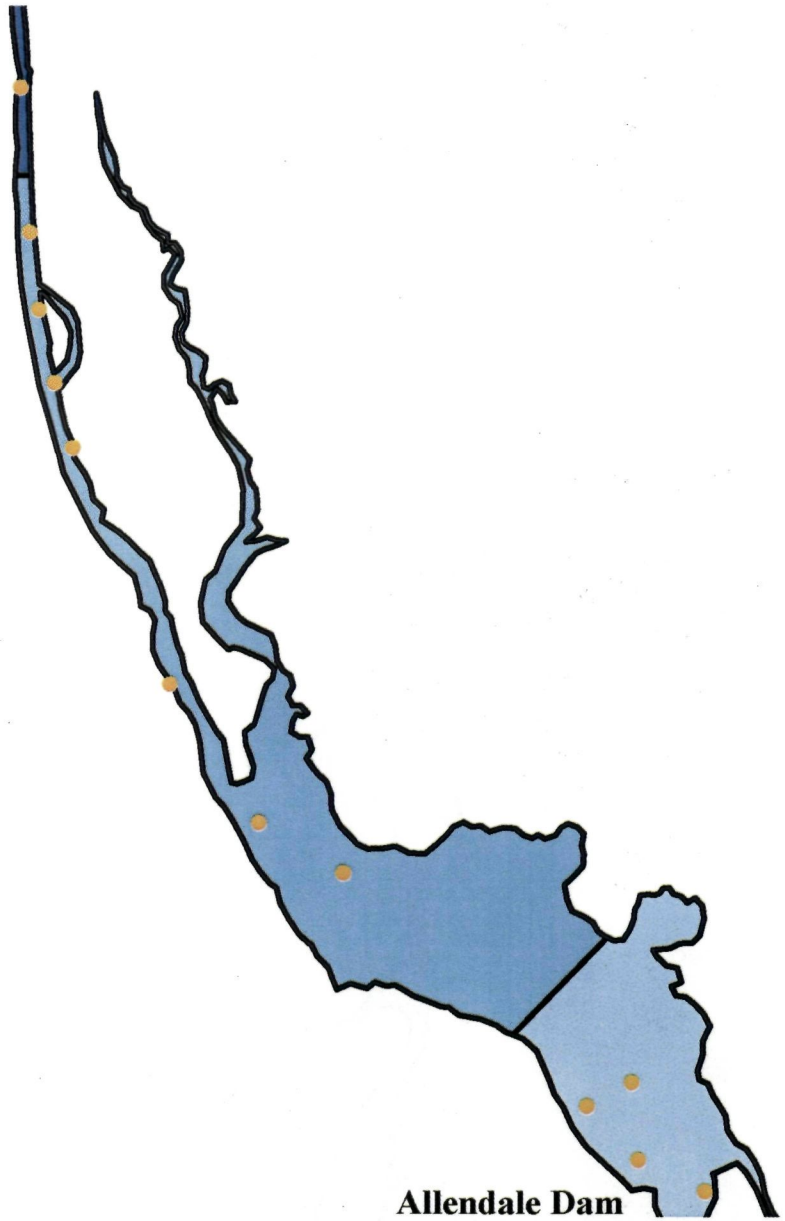

Locator Map

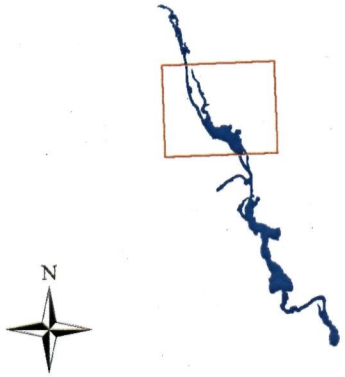

Legend

1997 Shoreline

1999 WQ Sampling Locations

Zones

1

2

3

4

5

Figure 2-21. Definitions of zones used in analysis of dioxin water-column data collected during 1999: Allendale Pond.

QEA Quantitative Environmental Analysis, LLC

BATcen:120 **February 2006**

CO- C:\BATman\Maps\ArcGIS\zones\batcen_allendale_zones_20060207.mxd

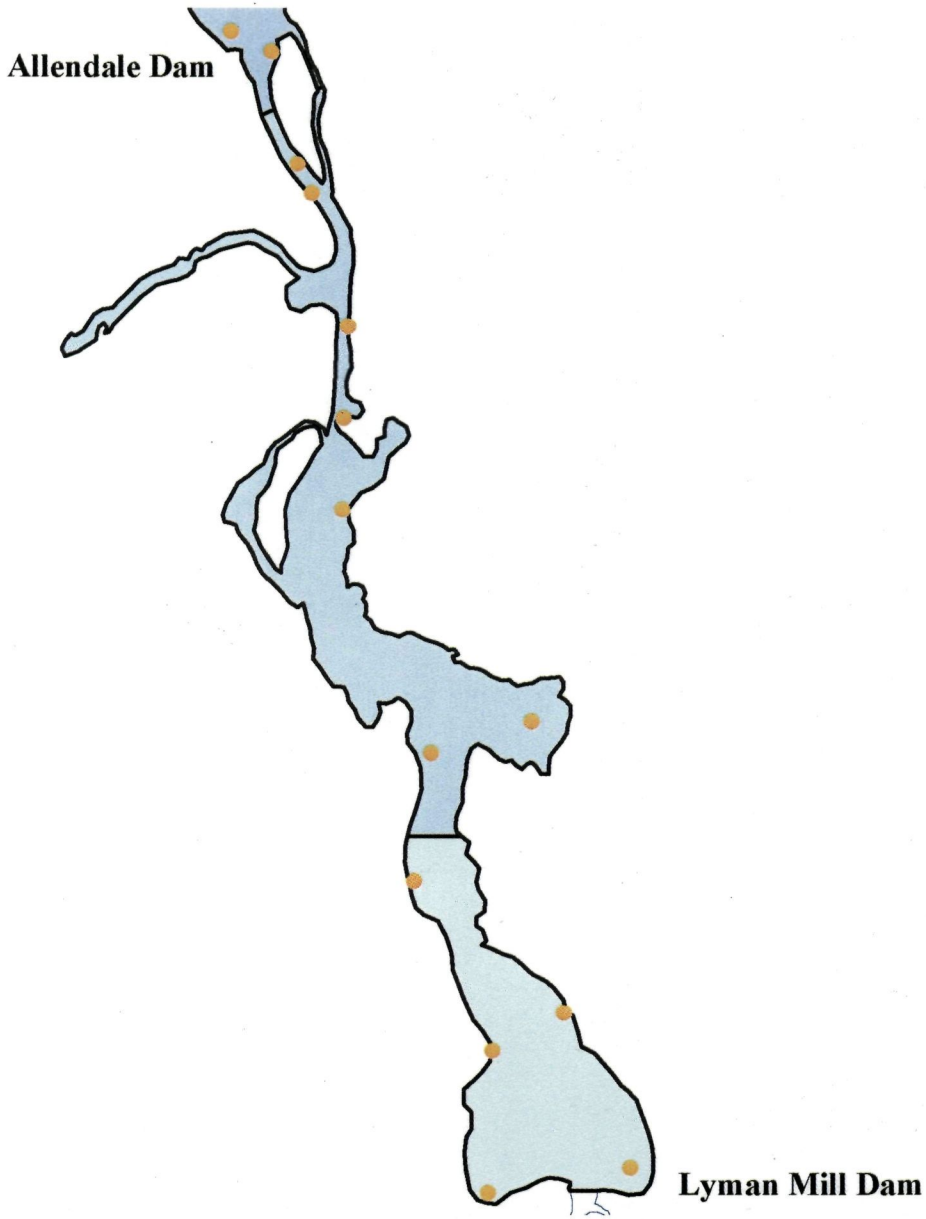

Locator Map

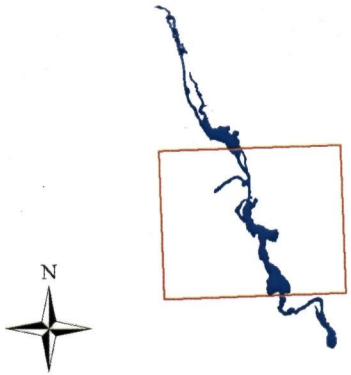

Legend

1997 Shoreline

1999 WQ Sampling Locations

Zones

1
2
3
4
5

Figure 2-22. Definitions of zones used in analysis of dioxin water-column data collected during 1999: Lyman Mill Pond.

QEA
Quantitative Environmental Analysis, LLC

BATcen:120 **February 2006**

CO- C:\BATman\Maps\ArcGIS\zones\tcen_lyman_zones_20060207.mxd

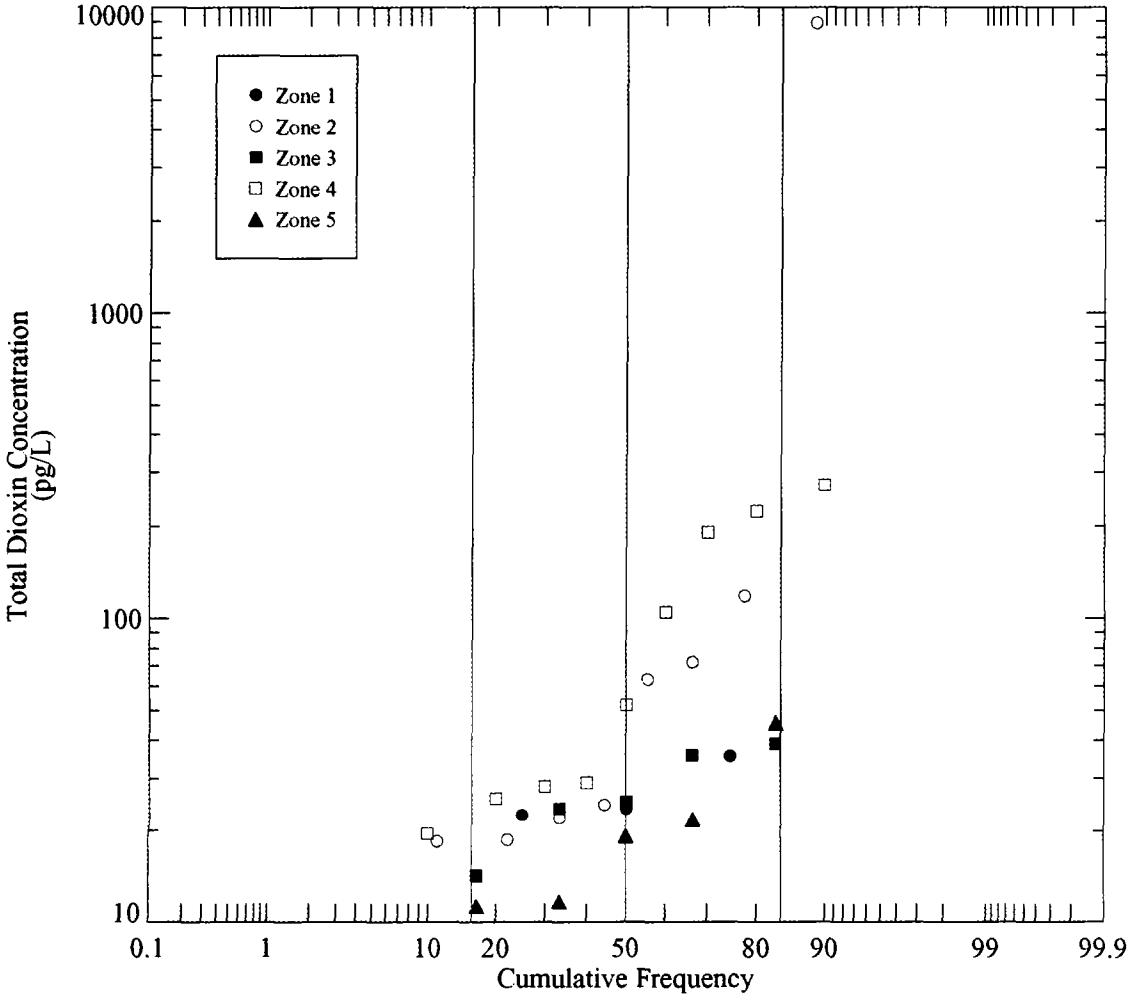

Figure 2-23. Frequency distributions of total dioxin water-column concentration in Zones 1, 2, 3, 4 and 5 during October-November 1999 sampling period.

cfo - C:\BATman\Analysis\WQ_spatial\wq_spatial_040820.pro
Fri Aug 27 08:38:51 2004

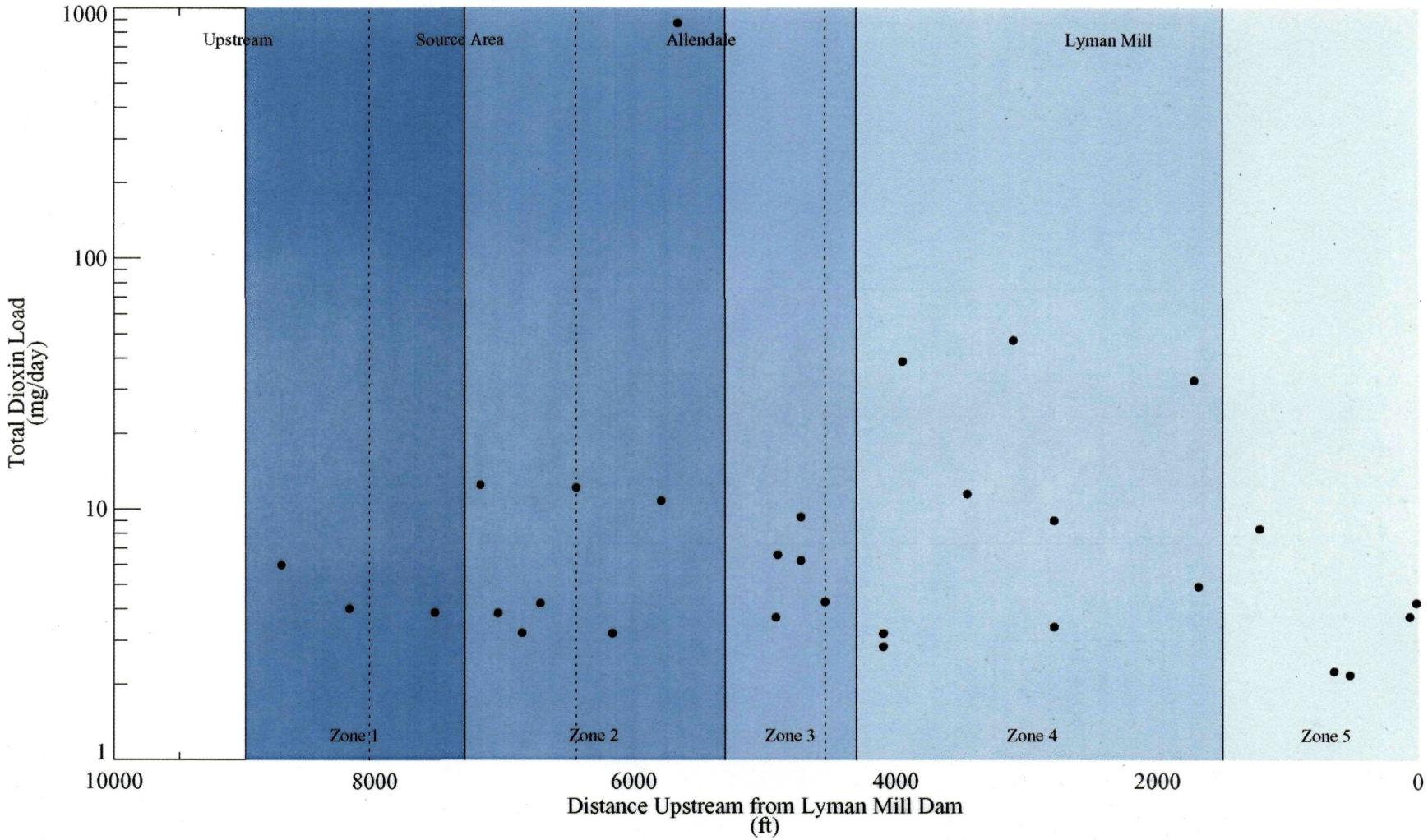

Figure 2-24. Spatial distribution of total dioxin water-column load during October-November 1999 sampling period.

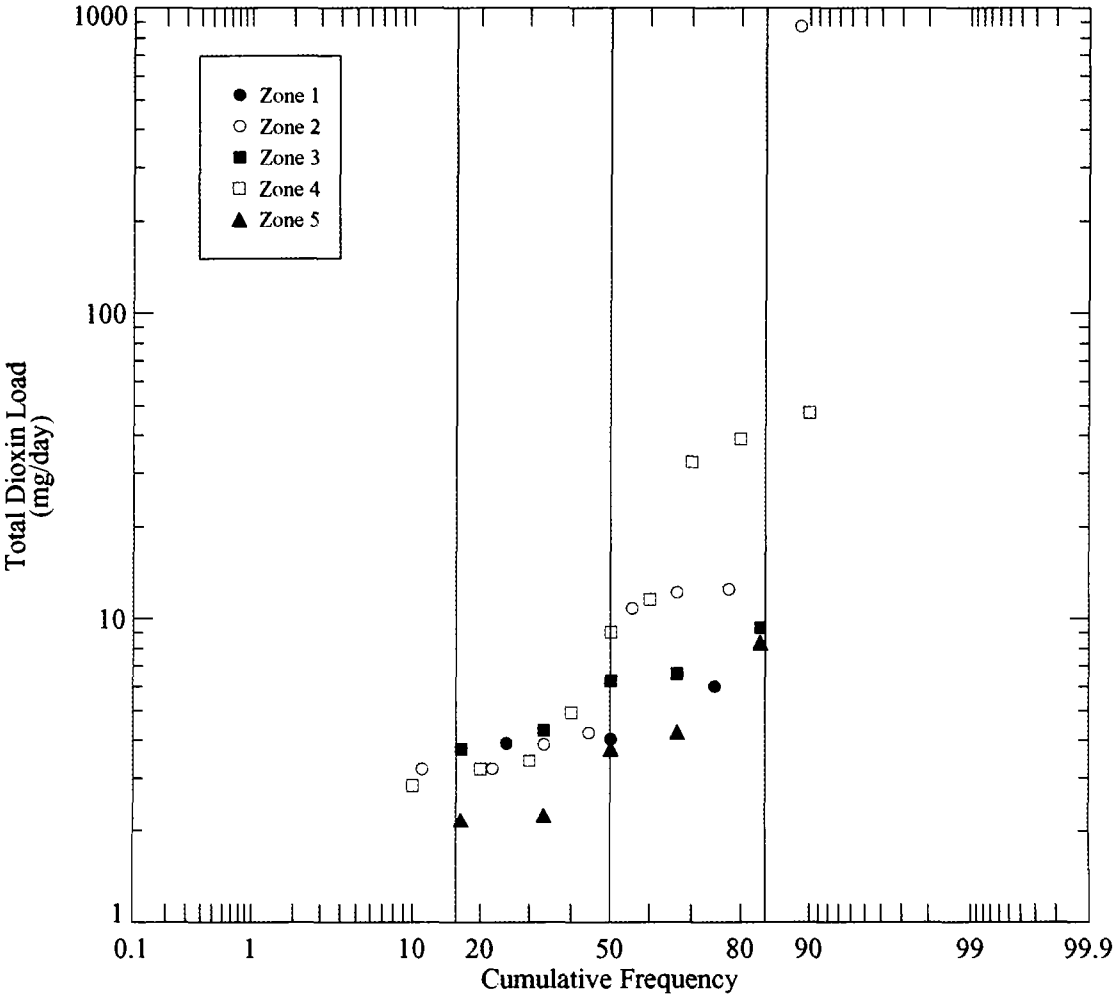

Figure 2-25. Frequency distributions of total dioxin water-column load in Zones 1, 2, 3, 4 and 5 during October-November 1999 sampling period.

cfo - C:\BATman\Analysis\WQ_spatial\wq_spatial_040820.pro
Fri Aug 27 08:38:51 2004

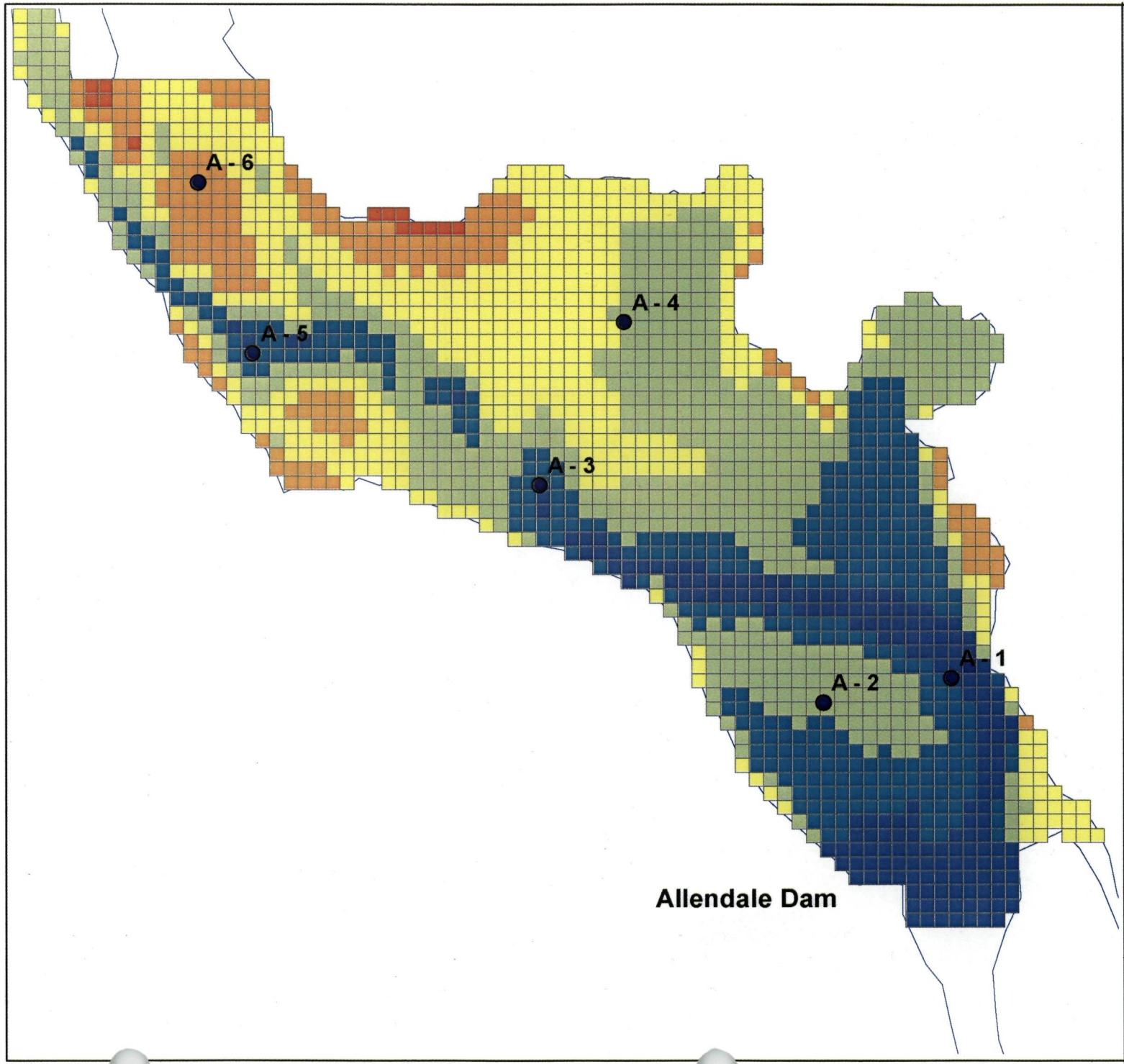

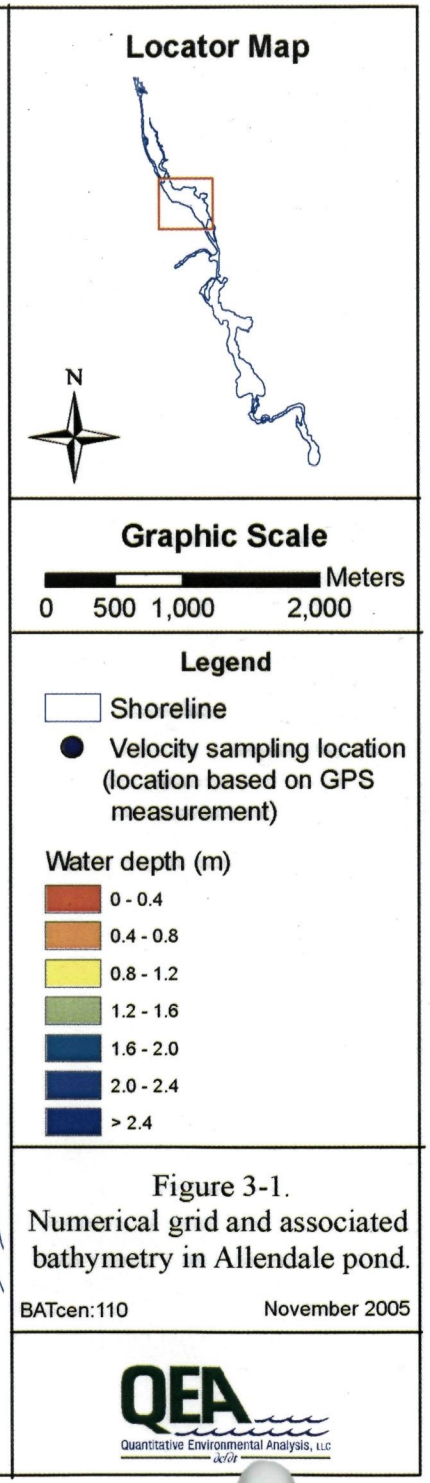

Figure 3-1.
Numerical grid and associated bathymetry in Allendale pond.

BATcen:110 November 2005

QEA
Quantitative Environmental Analysis, LLC

FC - \\Fanghui\d_dri en\Analysis\GISplot\Finalplot\Fig3-1_051121.mxd

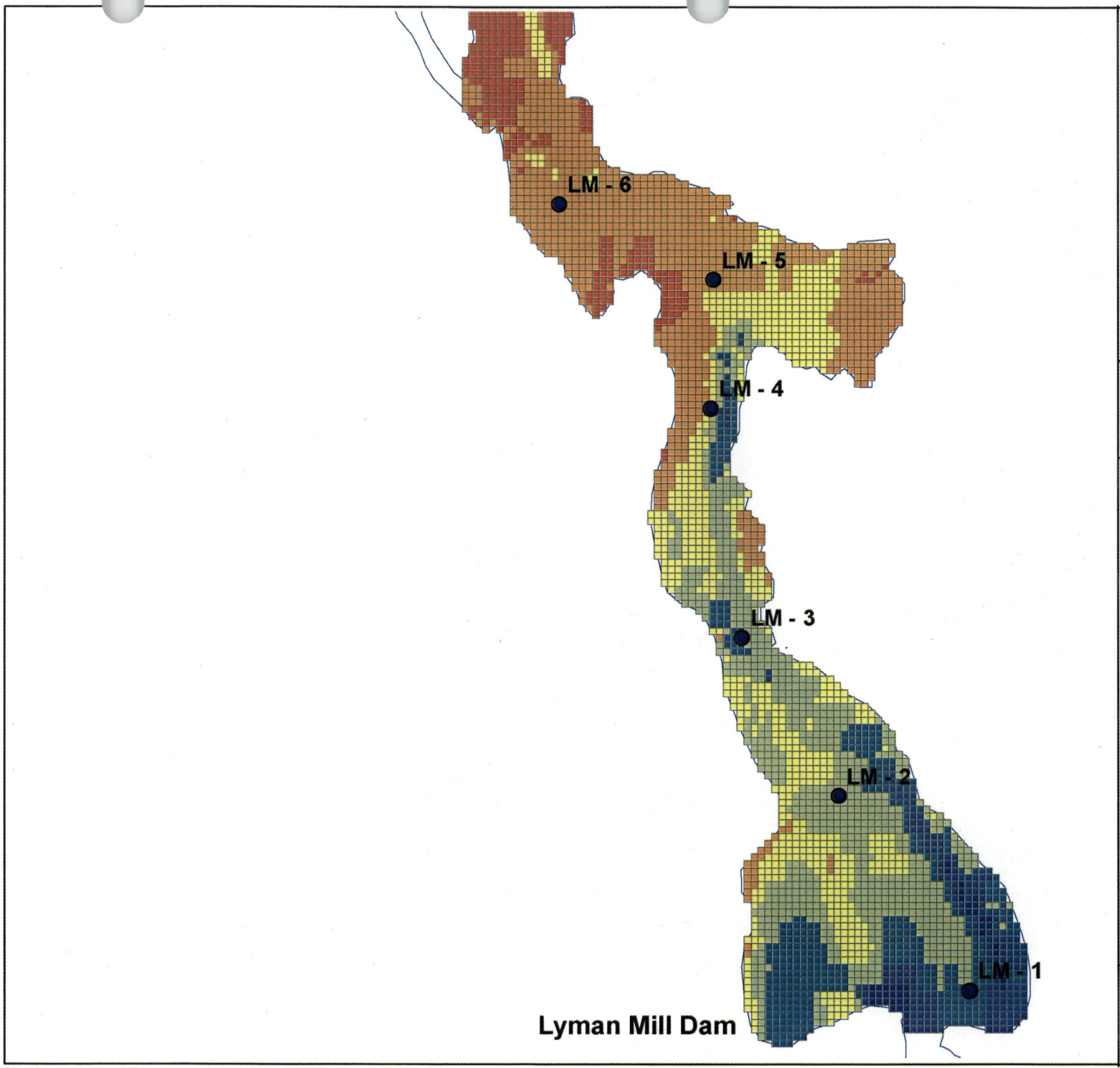

Locator Map

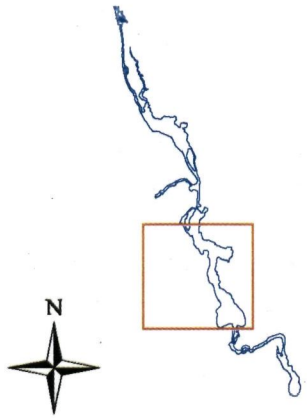

Graphic Scale

Meters

0 500 1,000 2,000

Legend

Shoreline

Velocity sampling location (location based on GPS measurement)

Water Depth (m)

- 0 - 0.4
- 0.4 - 0.8
- 0.8 - 1.2
- 1.2 - 1.6
- 1.6 - 2.0
- 2.0 - 2.4
- > 2.4

Figure 3-2.
Numerical grid and associated bathymetry in Lyman Mill Pond.

BATcen:110 November 2005

QEA
Quantitative Environmental Analysis, LLC

FC - \\Fanghui\d_drive\BATcen\Analysis\GISplot\Finalplot\Fig3-2.mxd

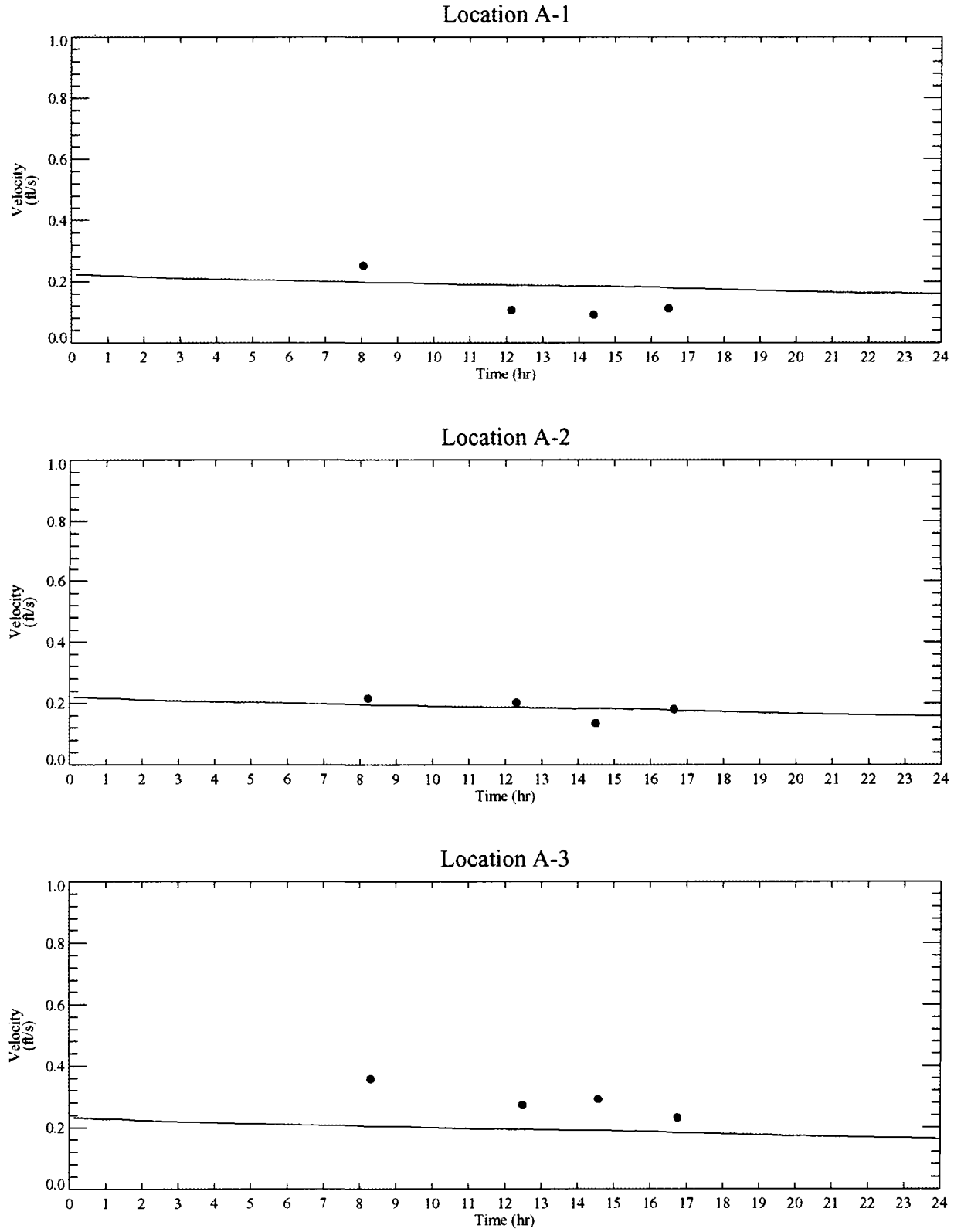

Figure 3-3. Comparison of predicted (line) and observed (symbol) current velocities at locations A-1 to A-3 in Allendale Pond on October 26, 2005.

fc - D:\BATcen\Analysis\ModelOutput\batcen_plot_vel_al.pro
Mon Nov 21 08:48:17 2005

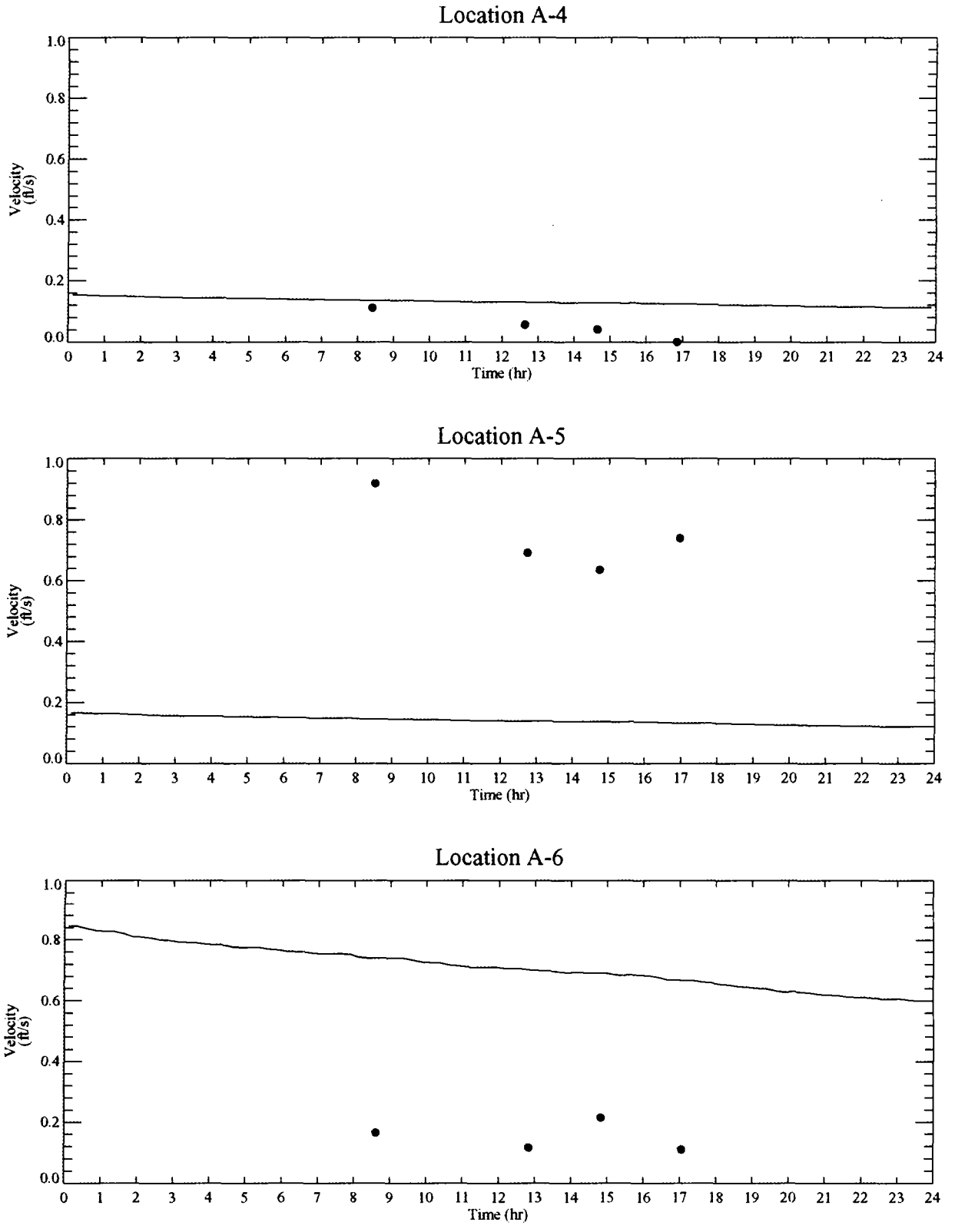

Figure 3-4. Comparison of predicted (line) and observed (symbol) current velocities at locations A-4 to A-6 in Allendale Pond on October 26, 2005.

fc - D:\BATcen\Analysis\ModelOutput\batcen_plot_vel_al.pro
Mon Nov 21 08:48:17 2005

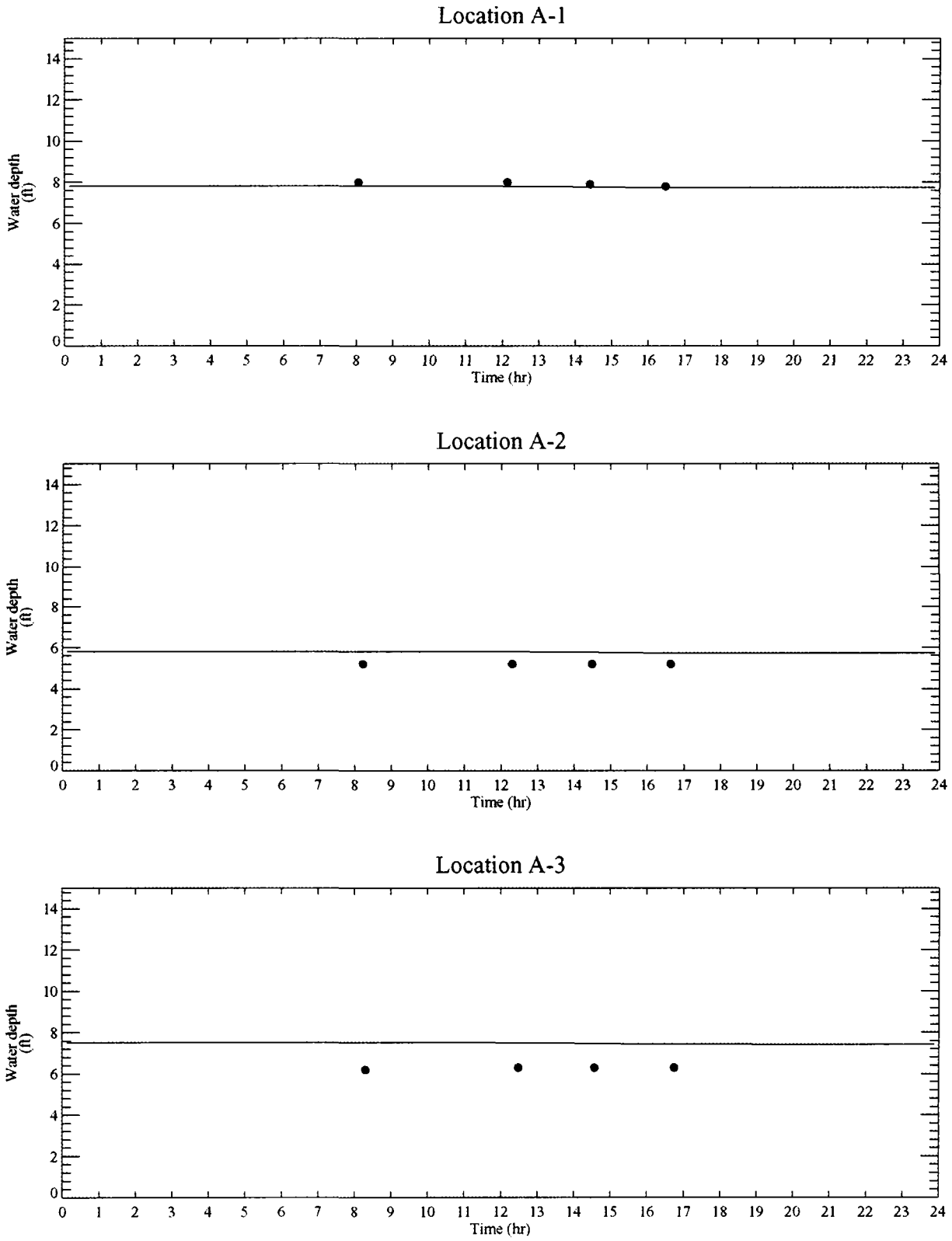

Figure 3-5. Comparison of predicted (line) and observed (symbol) water depth at locations A-1 to A-3 in Allendale Pond on October 26, 2005.

fc - D:\BATcen\Analysis\ModelOutput\batcen_plot_depth_al.pro
Tue Mar 07 16:31:40 2006

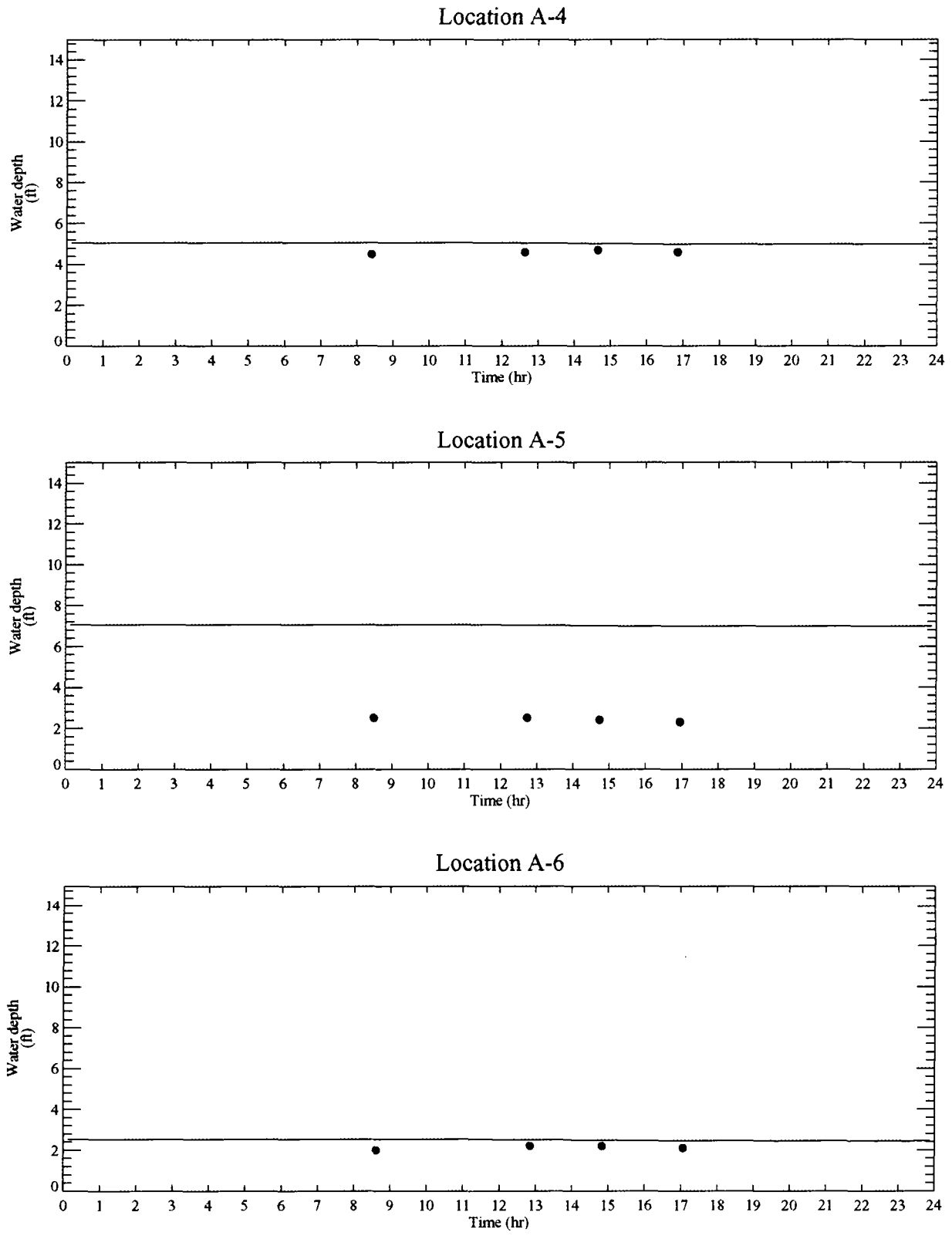

Figure 3-6. Comparison of predicted (line) and observed (symbol) water depth at locations A-4 to A-6 in Allendale Pond on October 26, 2005.

fc - D:\BATcen\Analysis\ModelOutput\batcen_plot_depth_al.pro
Tue Mar 07 16:31:40 2006

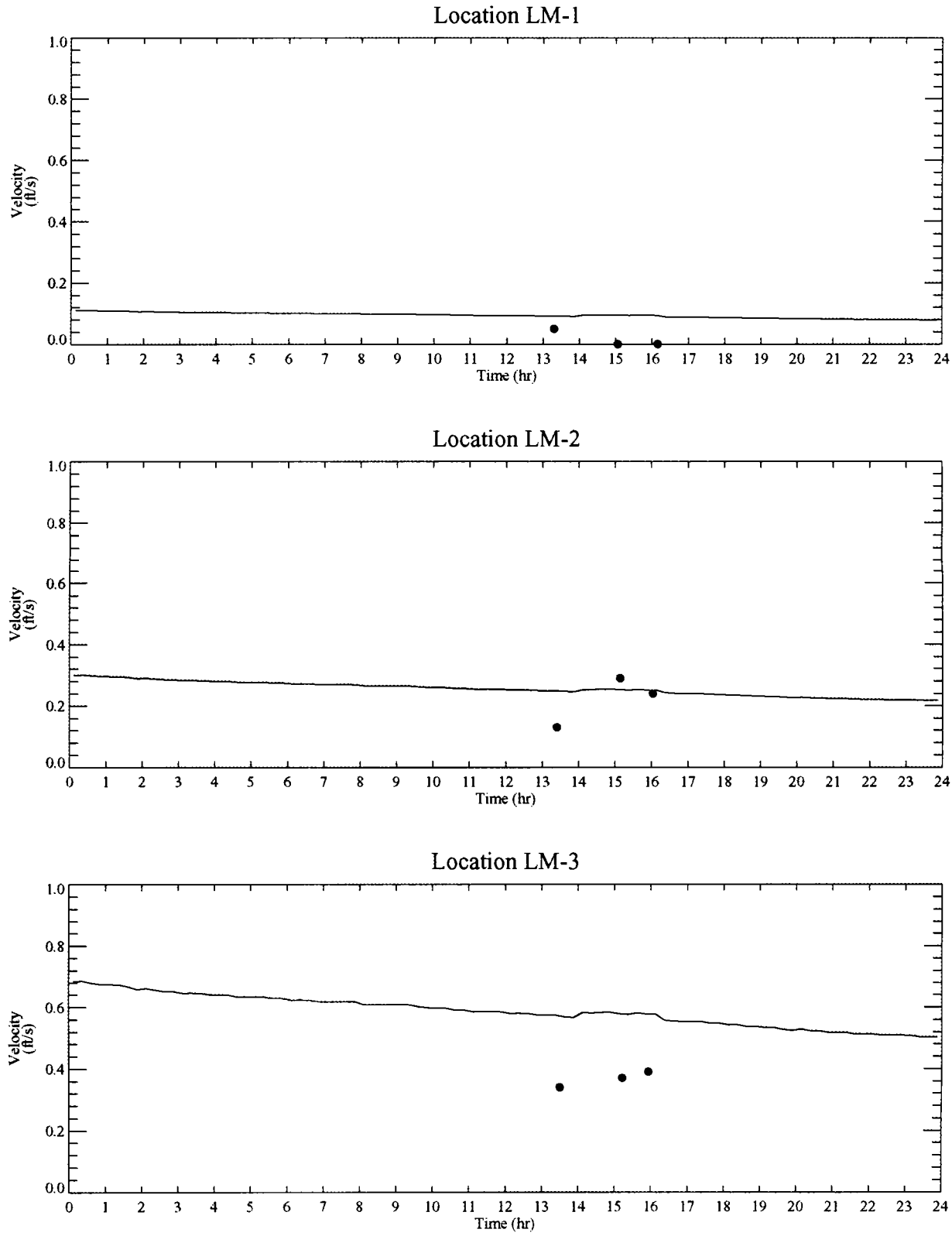

Figure 3-7. Comparison of predicted (line) and observed (symbol) current velocities at locations LM-1 to LM-3 in Lyman Mill Pond on October 26, 2005.

fc - D:\BATcen\Analysis\ModelOutput\batcen_plot_vel_lyman.pro
Mon Nov 21 08:55:26 2005

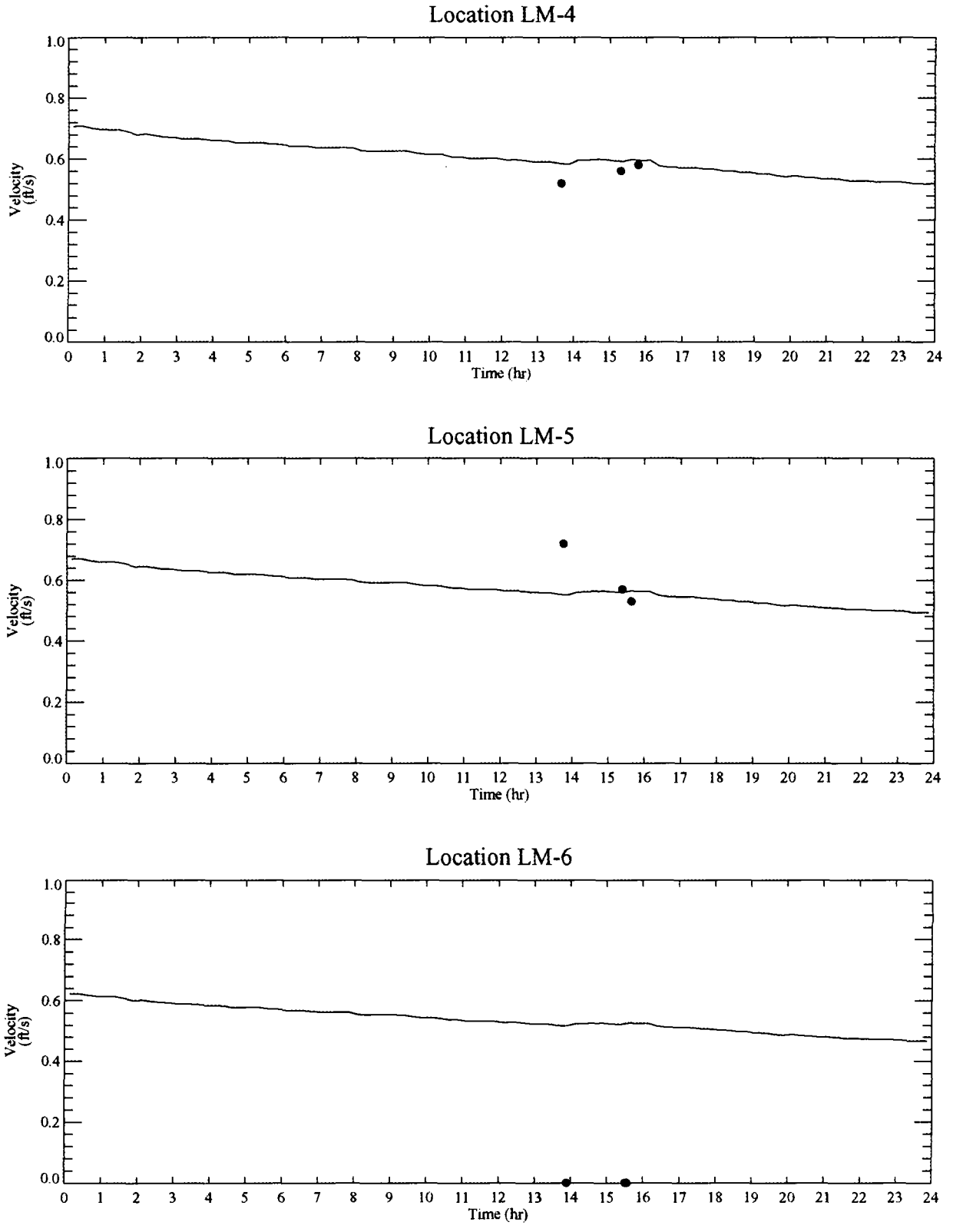

Figure 3-8. Comparison of predicted (line) and observed (symbol) current velocities at locations LM-4 to LM-6 in Lyman Mill Pond on October 26, 2005.

fc - D:\BATcen\Analysis\ModelOutput\batcen_plot_vel_lyman.pro
Mon Nov 21 08:55:26 2005

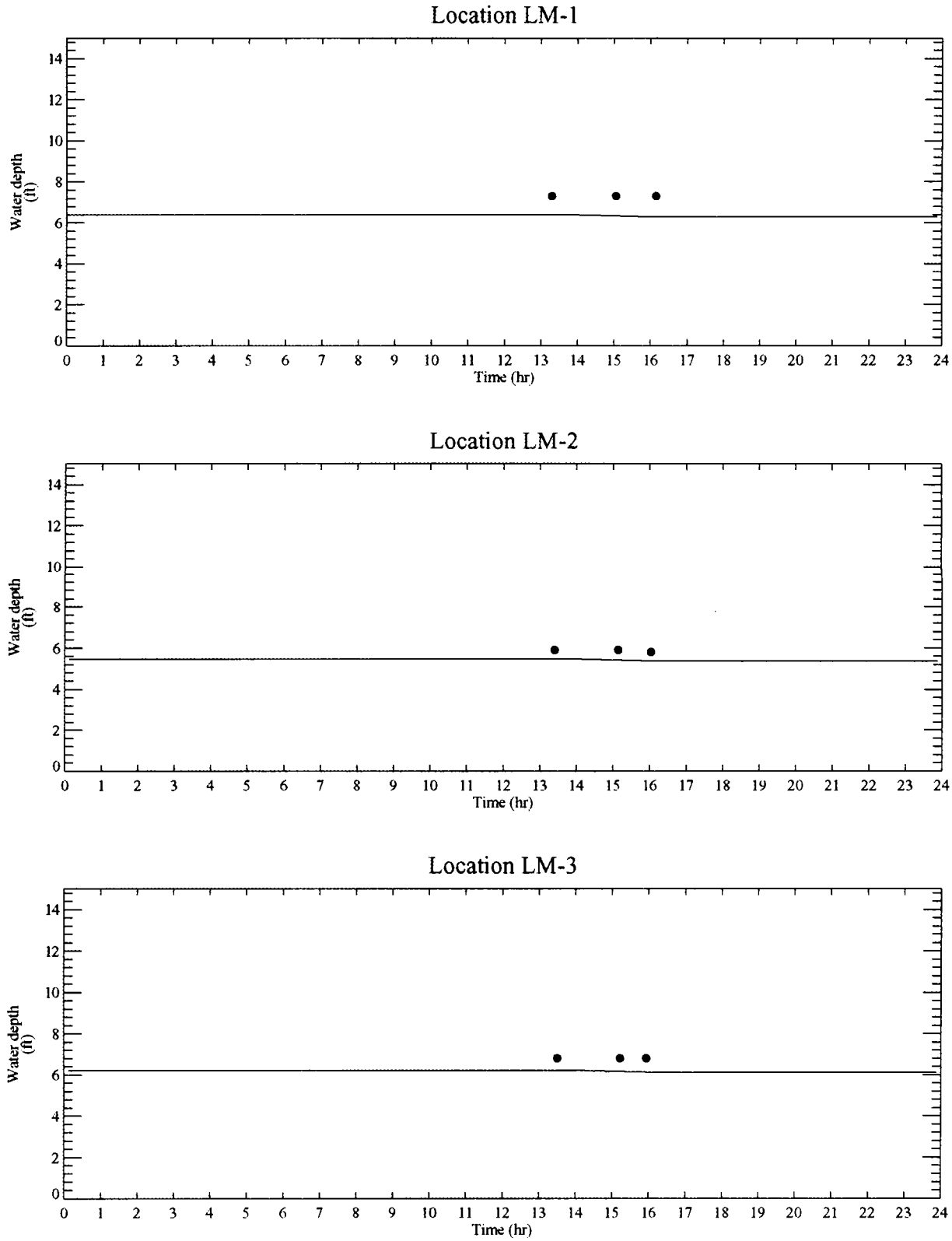

Figure 3-9. Comparison of predicted (line) and observed (symbol) water depth at locations LM-1 to LM-3 in Lyman Mill Pond on October 26, 2005.

fc - D:\BATcen\Analysis\ModelOutput\batcen_plot_depth_ly.pro
Mon Nov 21 08:58:42 2005

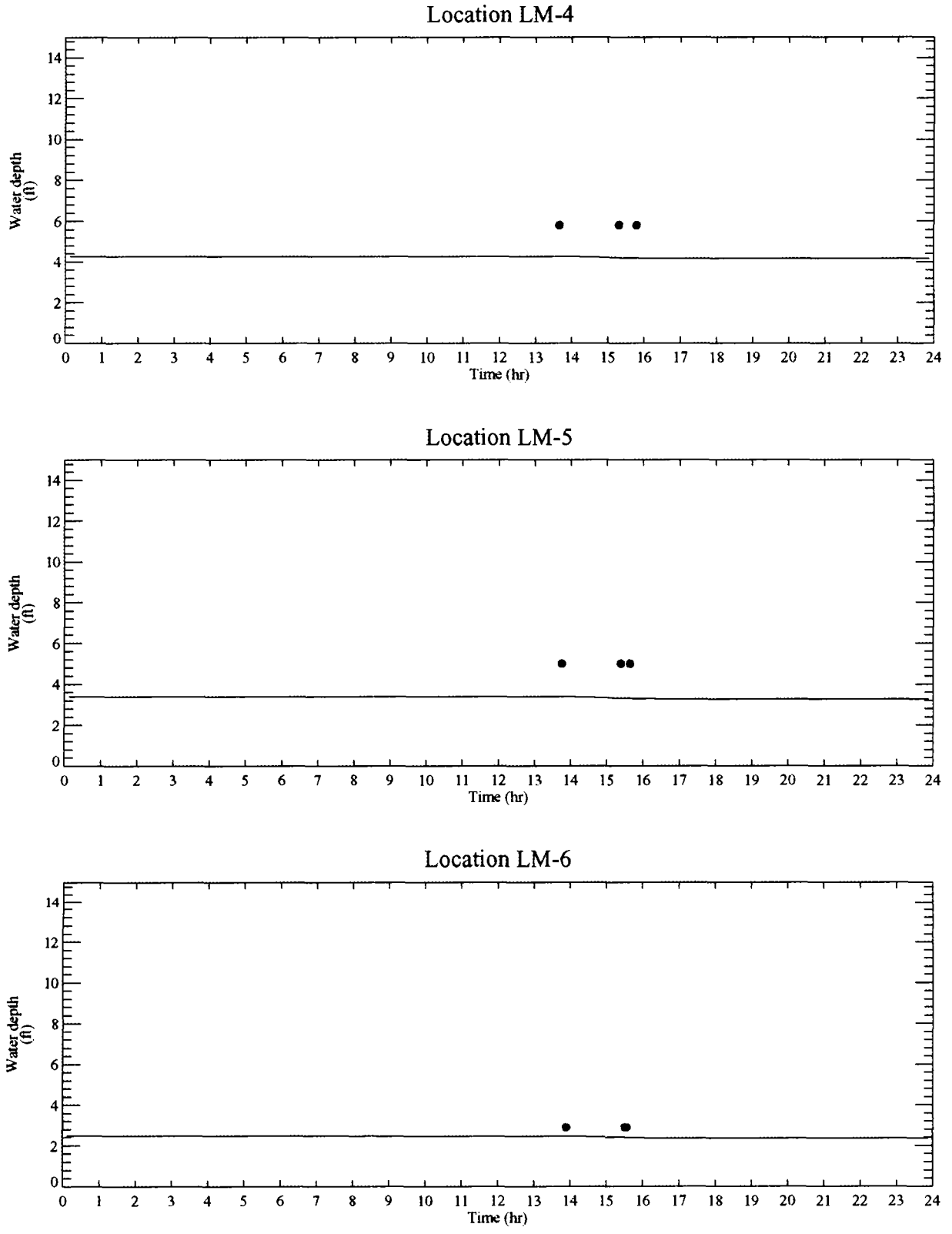

Figure 3-10. Comparison of predicted (line) and observed (symbol) water depth at locations LM-4 to LM-6 in Lyman Mill Pond on October 26, 2005.

fc - D:\BATcen\Analysis\ModelOutput\batcen_plot_depth_ly.pro
Mon Nov 21 08:58:42 2005

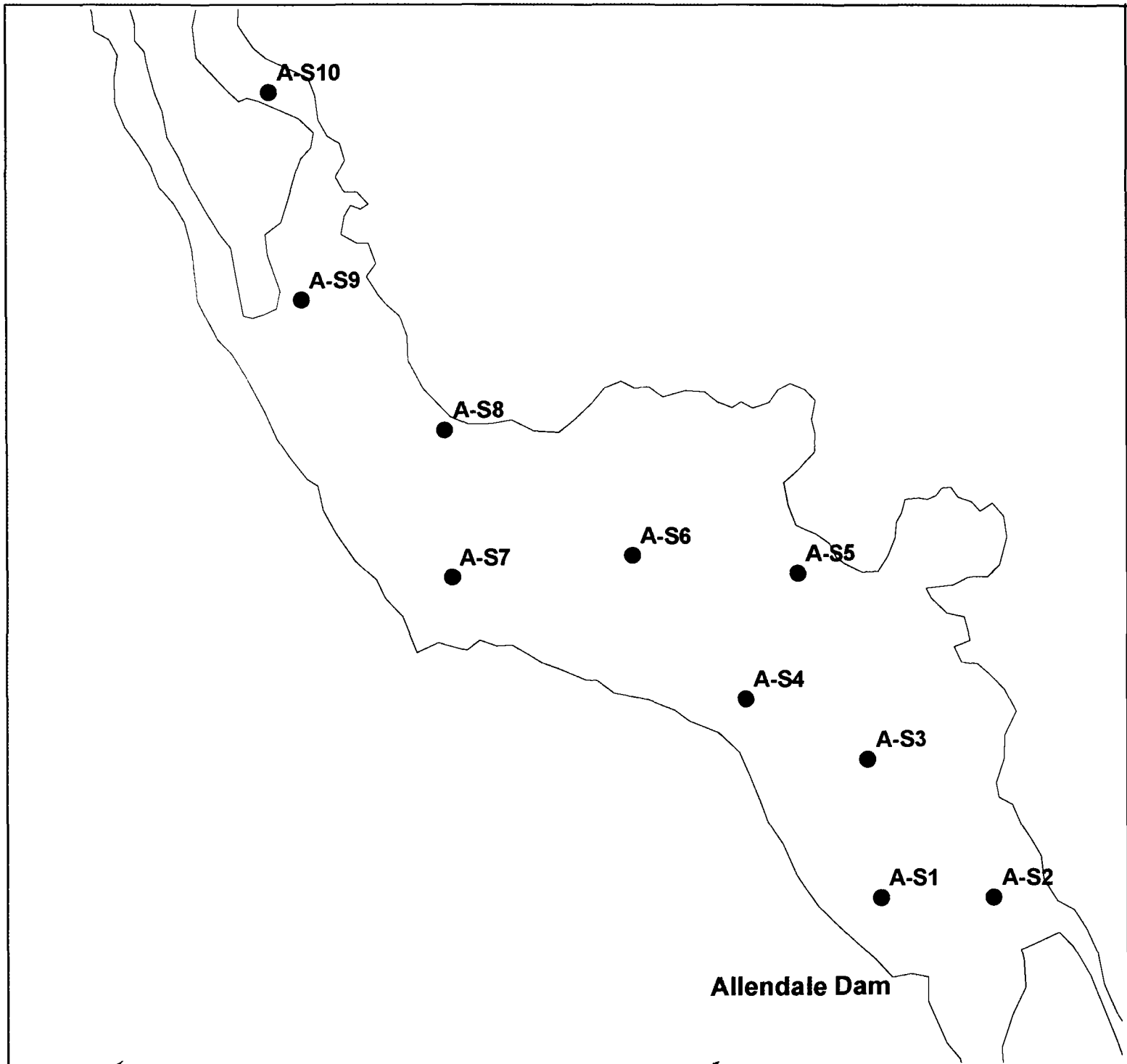

Locator Map

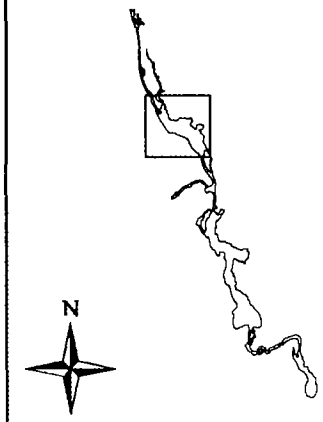

Graphic Scale

Meters

0 500 1,000 2,000

Legend

Shoreline

Shaker Core Locations (location based on GPS measurement)

Figure 3-11.
Locations of cores collected in Allendale Pond during shaker study.

BATcen:110 November 2005

QEA
Quantitative Environmental Analysis, LLC

FC - \\Fanghui\d_dr ...n\Analysis\GISplot\Finalplot\Fig3-11_051121.mxd

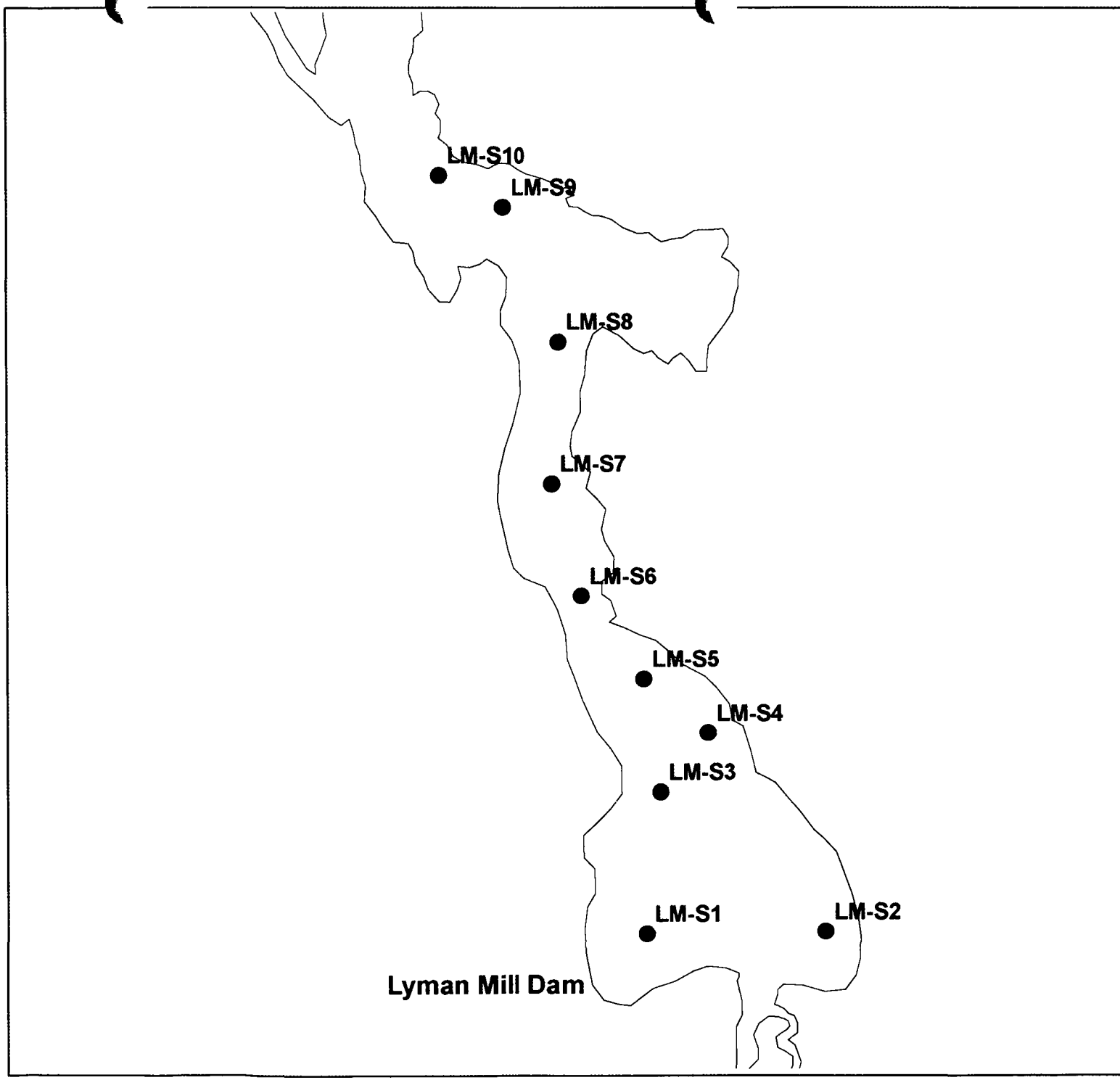

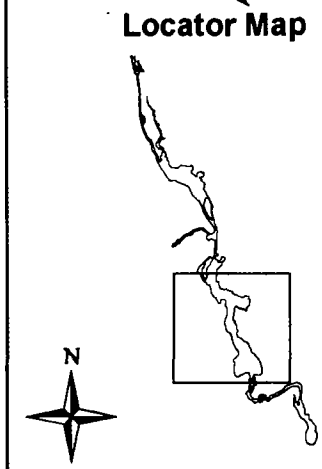

Graphic Scale

Meters

0 500 1,000 2,000

Legend

- Shoreline
- Shaker Core Locations (location based on GPS measurement)

Figure 3-12.
Locations of cores collected in Lyman Mill Pond during shaker study.

BATcen:110 November 2005

QEA Quantitative Environmental Analysis, LLC

FC - \\Fanghui\d_drive\BATcen\Analysis\GISplot\Finalplot\Fig3-12_051121.mxd

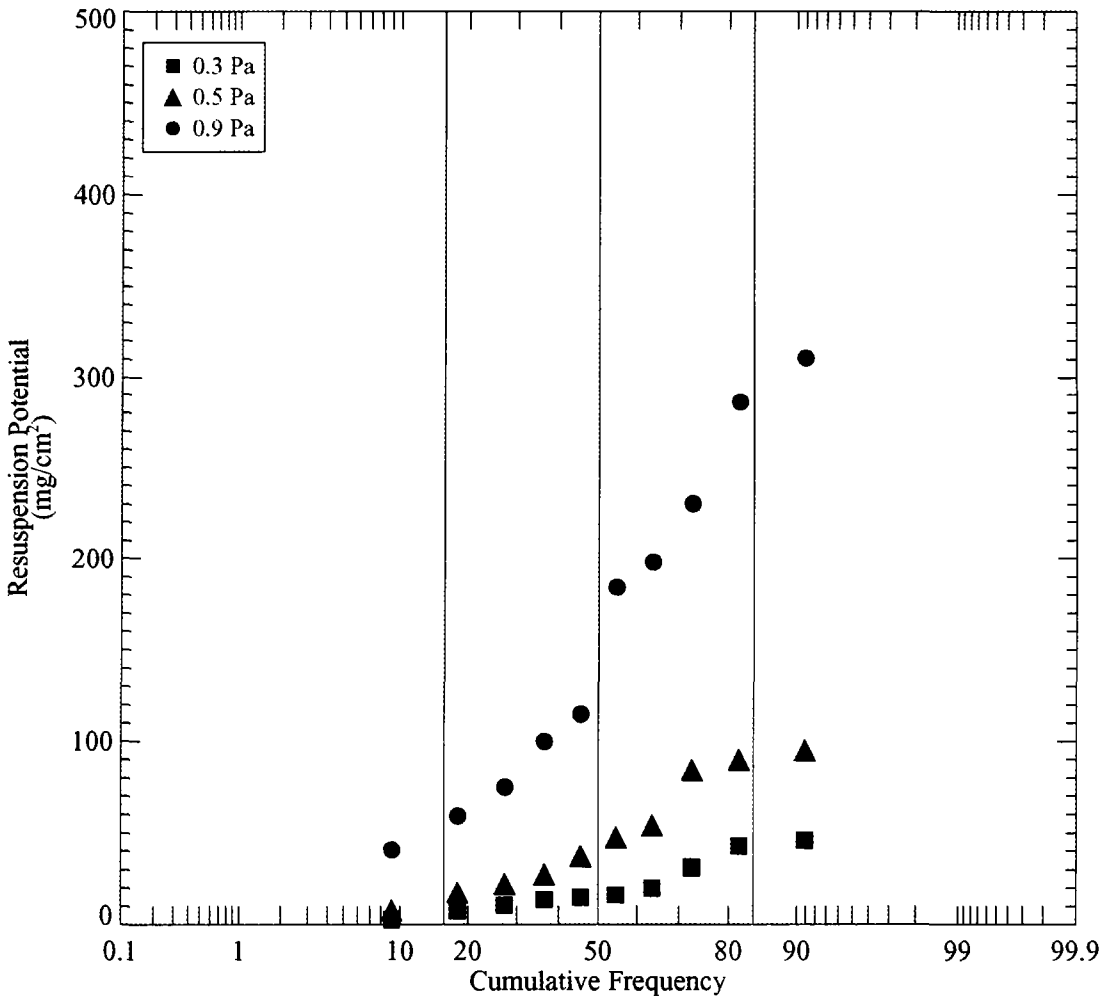

Figure 3-13. Frequency distributions of Allendale Pond resuspension potential measured at shear stresses of 0.3, 0.5 and 0.9 Pa.

Data Source: Allendale Pond Shaker Study

FC - D:\BATcen\Analysis\SHAKER_DATA_2004\Analysis\Shaker_study_dec_04\Prob_plot_resuspension_potential.pro
Tue Mar 07 16:28:35 2006

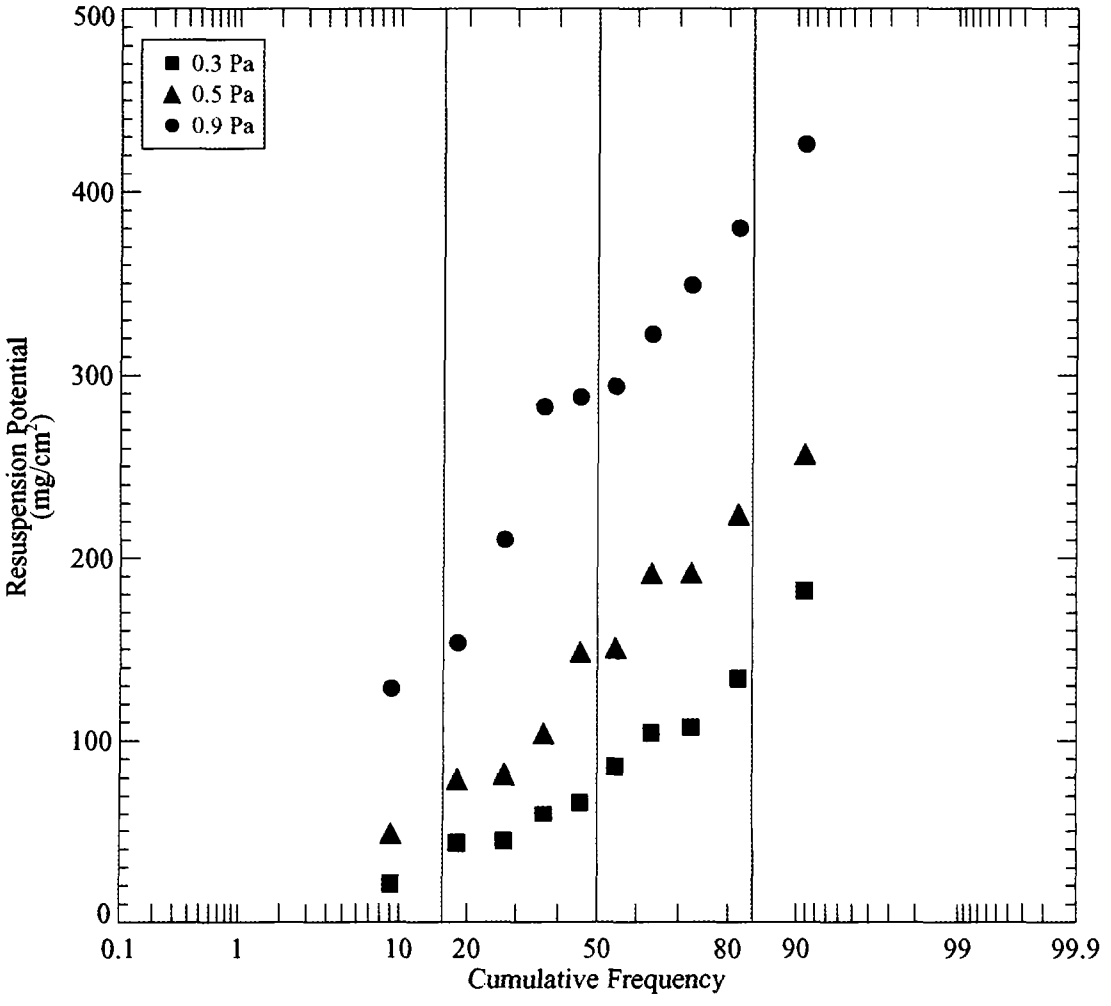

Figure 3-14. Frequency distributions of Lyman Mill Pond resuspension potential measured at shear stresses of 0.3, 0.5 and 0.9 Pa.

Data Source: Lyman Mill Pond Shaker Study

FC - D:\BATcen\Analysis\SHAKER_DATA_2004\Analysis\Shaker_study_dec_04\Prob_plot_resuspension_potential.pro
Tue Mar 07 16:28:35 2006

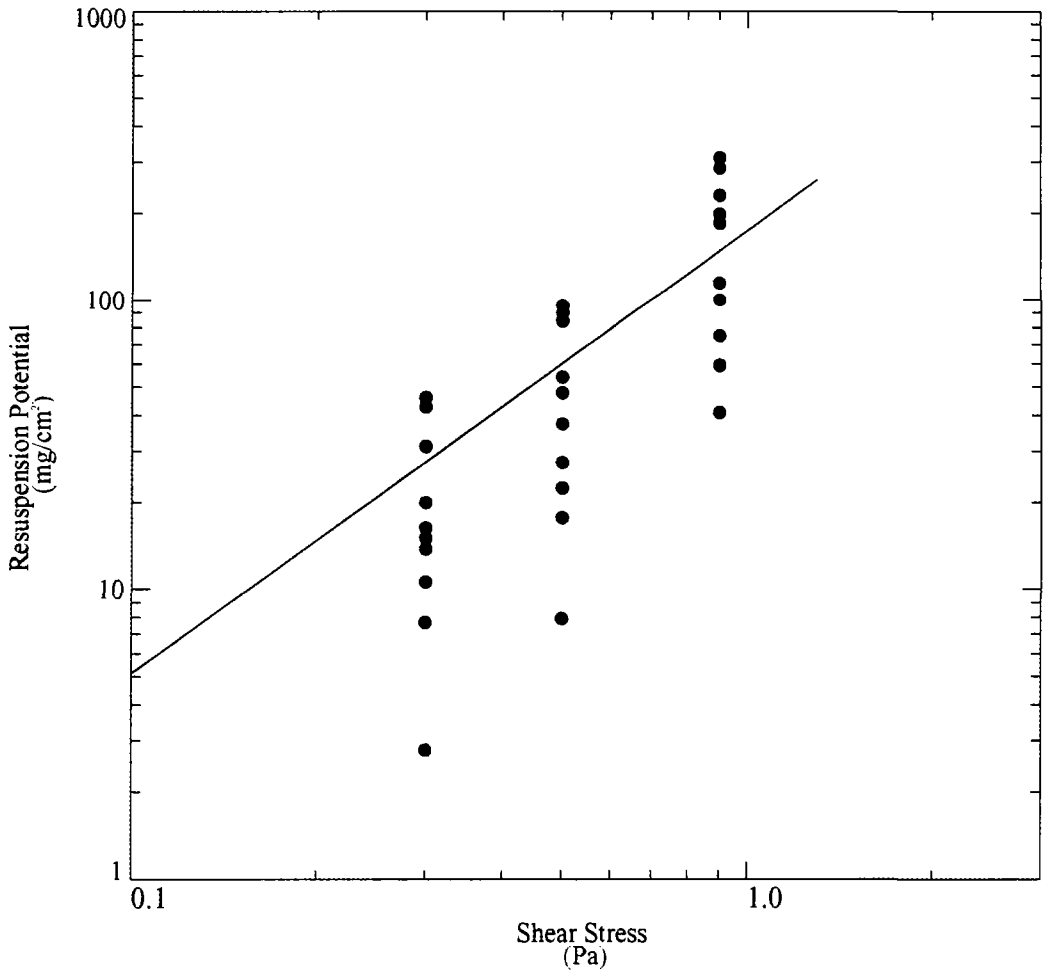

Figure 3-15. Relationship between resuspension potential and shear stress in Allendale Pond. Closed symbols represent data. Solid line is based on log-linear regression through data.

Data Source: Allendale Pond Shaker Study

FC - Z:\BATcen\Analysis\SHAKER_DATA_2004\Analysis\Shaker_study_dec_04\resuspension_potential_v_shear_stress.pro
Mon Nov 21 09:42:11 2005

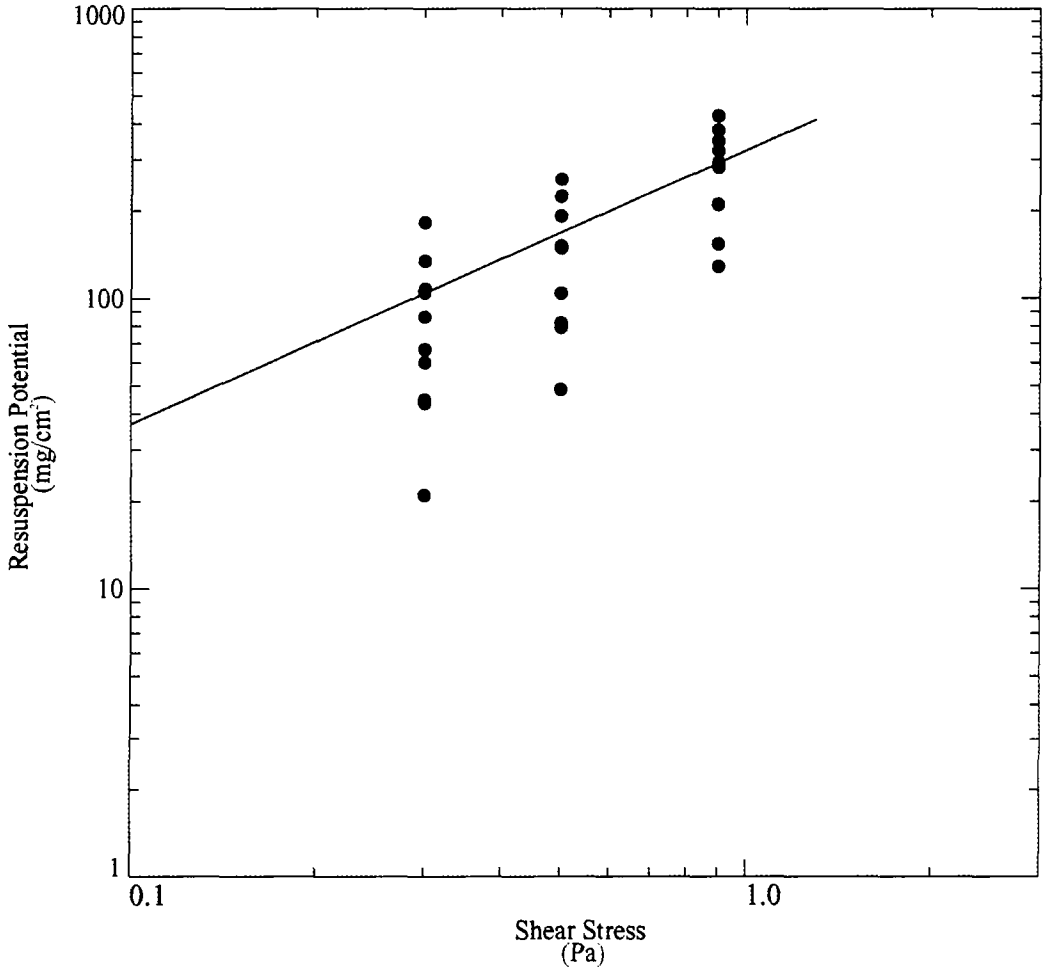

Figure 3-16. Relationship between resuspension potential and shear stress in Lyman Mill Pond. Closed symbols represent data. Solid line is based on log-linear regression through data.

Data Source: Lyman Mill Pond Shaker Study

FC - Z:\BATcen\Analysis\SHAKER_DATA_2004\Analysis\Shaker_study_dec_04\resuspension_potential_v_shear_stress.pro
Mon Nov 21 09:42:11 2005

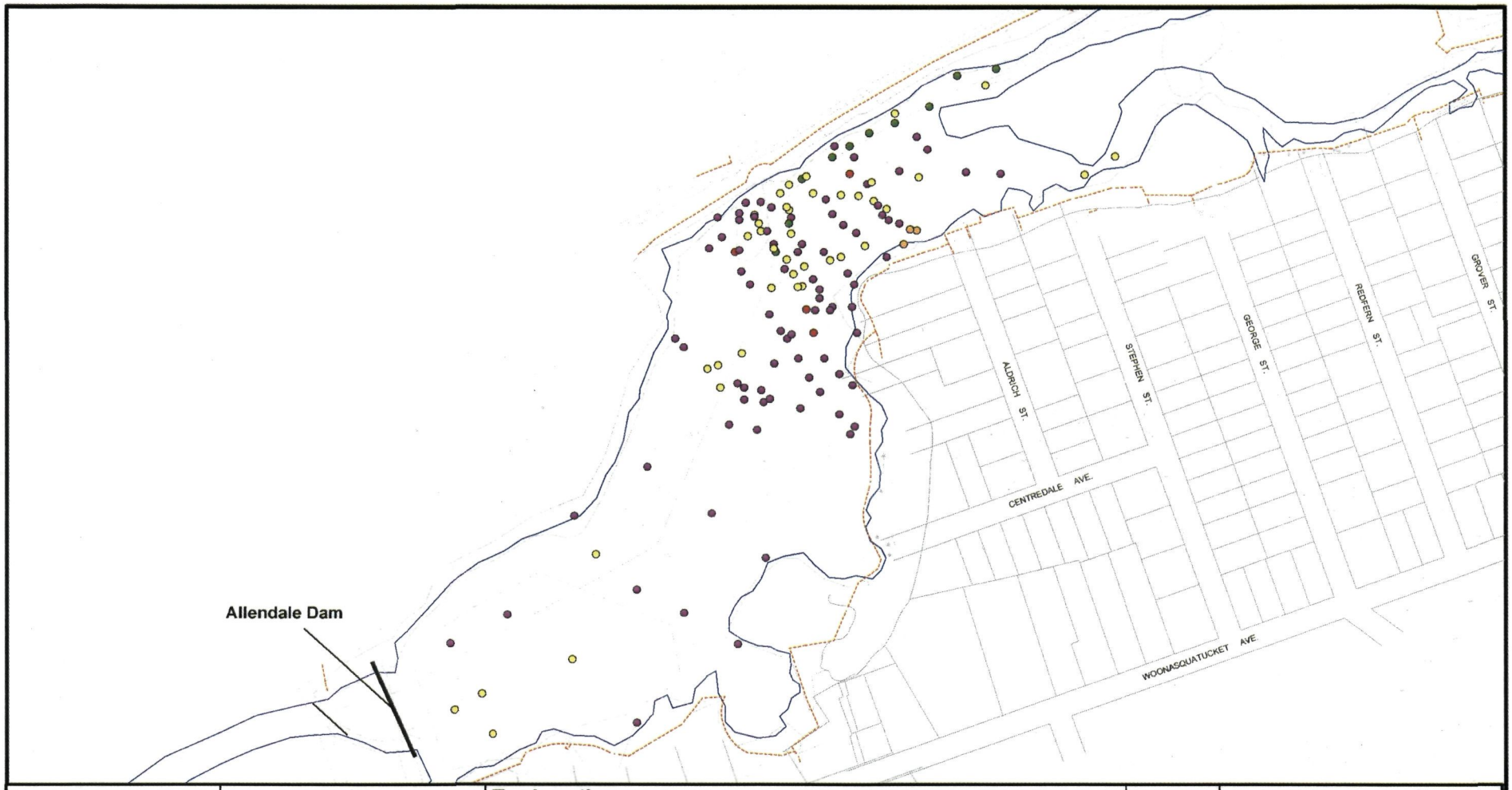

Battelle

0 100 200 400
Feet

Figure 3-17. Sediment types in Allendale Pond. (location based on GPS measurement)

Explanation:

- Fence
- Roads
- Roads
- 1997 River Channel

Sediment Type

- Gravel
- Sand
- Silt
- Clay
- Organic silt, clay, peat

N

Date: 2/2/05

Document: AD_sed_type*.mxd

Drawn By: Jim Hicks (Battelle)

Checked by: Patty White (Battelle)

Projection: Rhode Island State Plane (NAD 83 Feet)

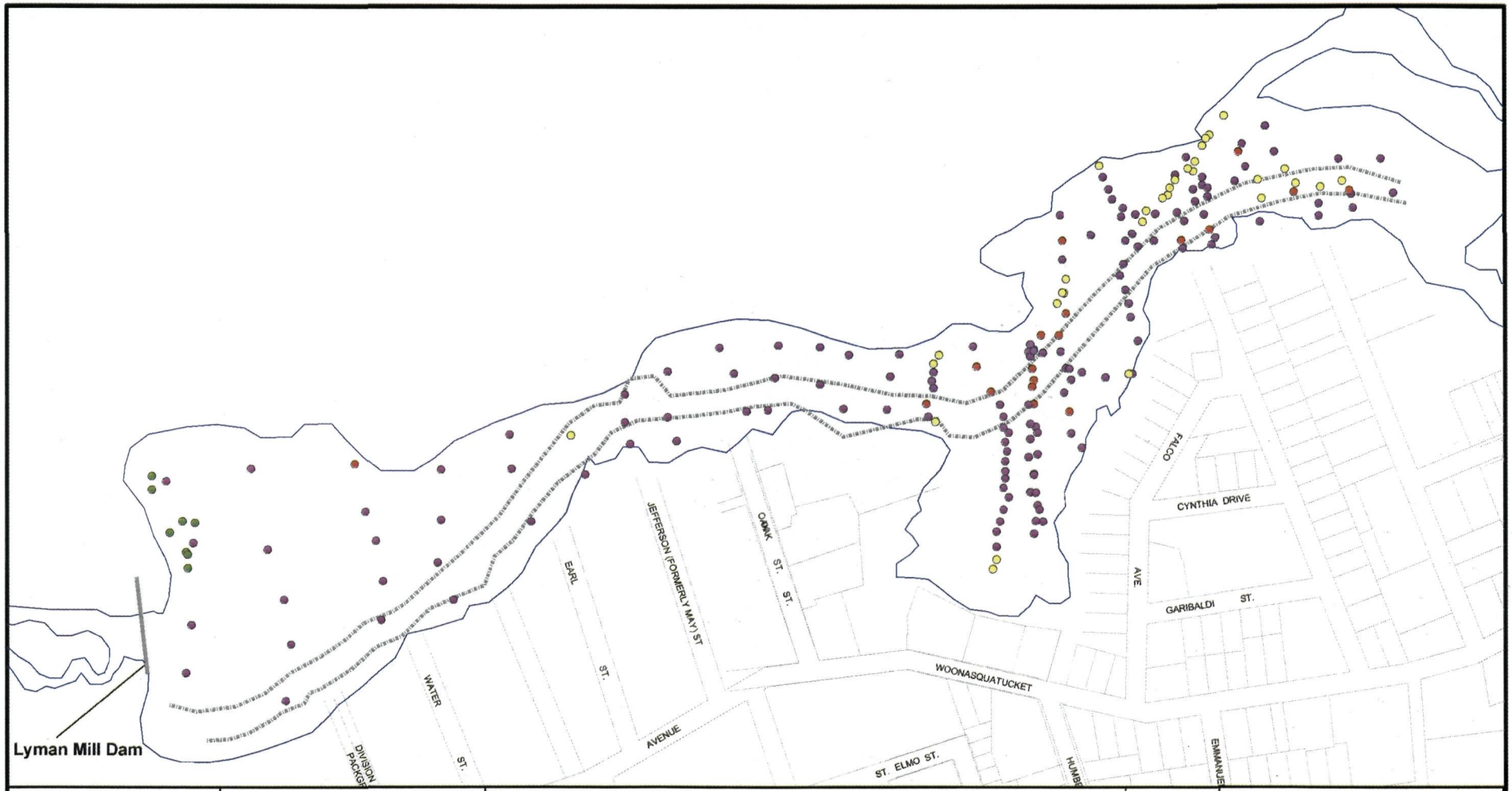

Battelle

0 100 200 400
Feet

Figure 3-18. Sediment types in Lyman Mill Pond. (location based on GPS measurement)

Explanation:

1997 River Channel
Recent Flow (Scour) Channel
Roads

Sediment Type
- Gravel
- Sand
- Clay
- Organic silt, clay, peat

N

Date: 2/2/05

Document: LM_sed_type*.mxd
Drawn By: Jim Hicks (Battelle)
Checked by: Patty White (Battelle)
Projection: Rhode Island State Plane (NAD 83 Feet)

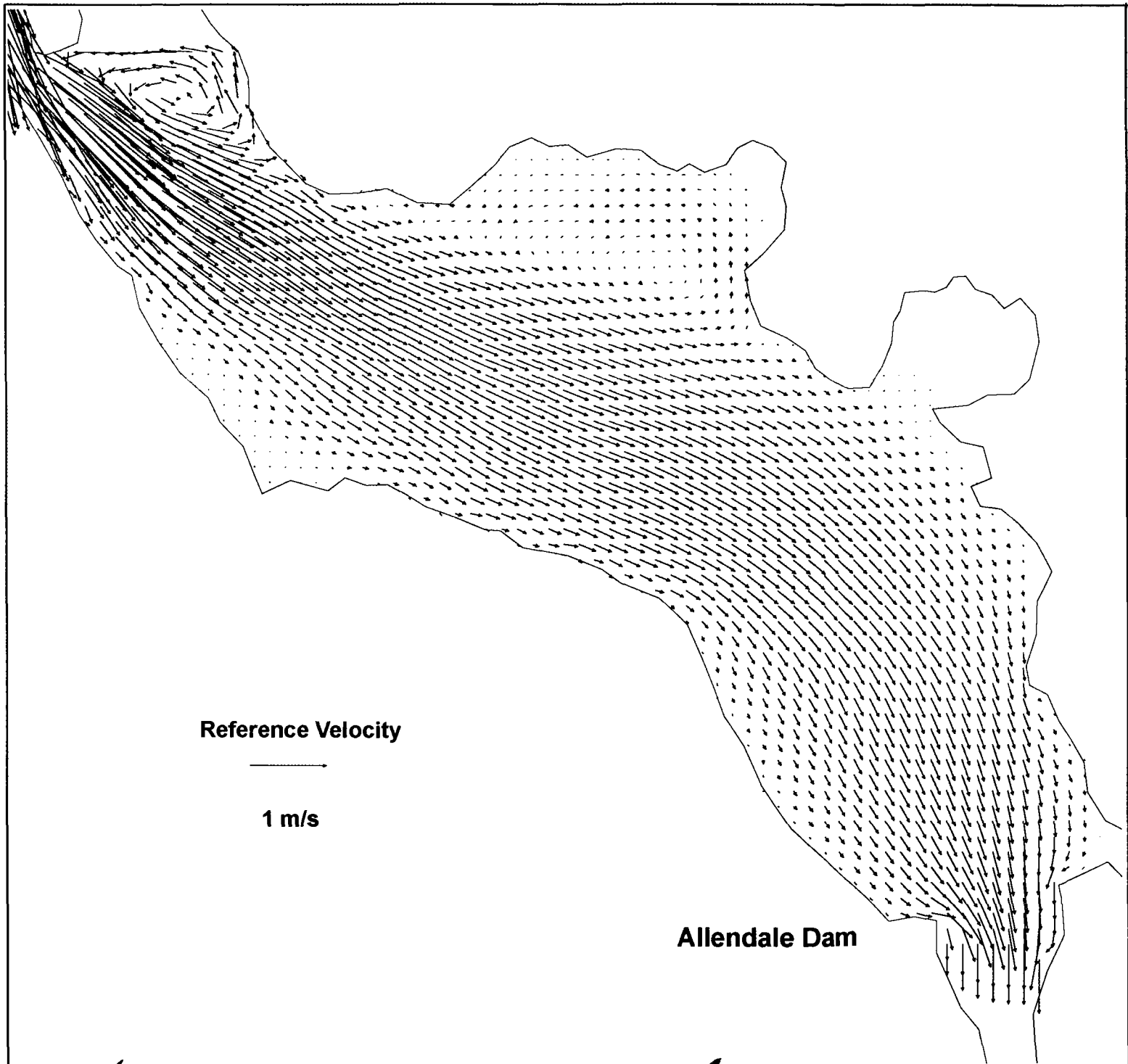

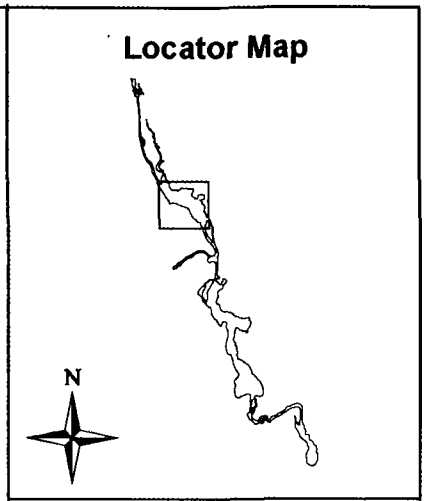

Graphic Scale

Meters

0 500 1,000 2,000

Legend

1997 Shoreline

Velocity vector

Figure 3-19.
Predicted current velocities during 100-year flood in Allendale Pond.

BATcen:110 November 2005

QEA
Quantitative Environmental Analysis, LLC

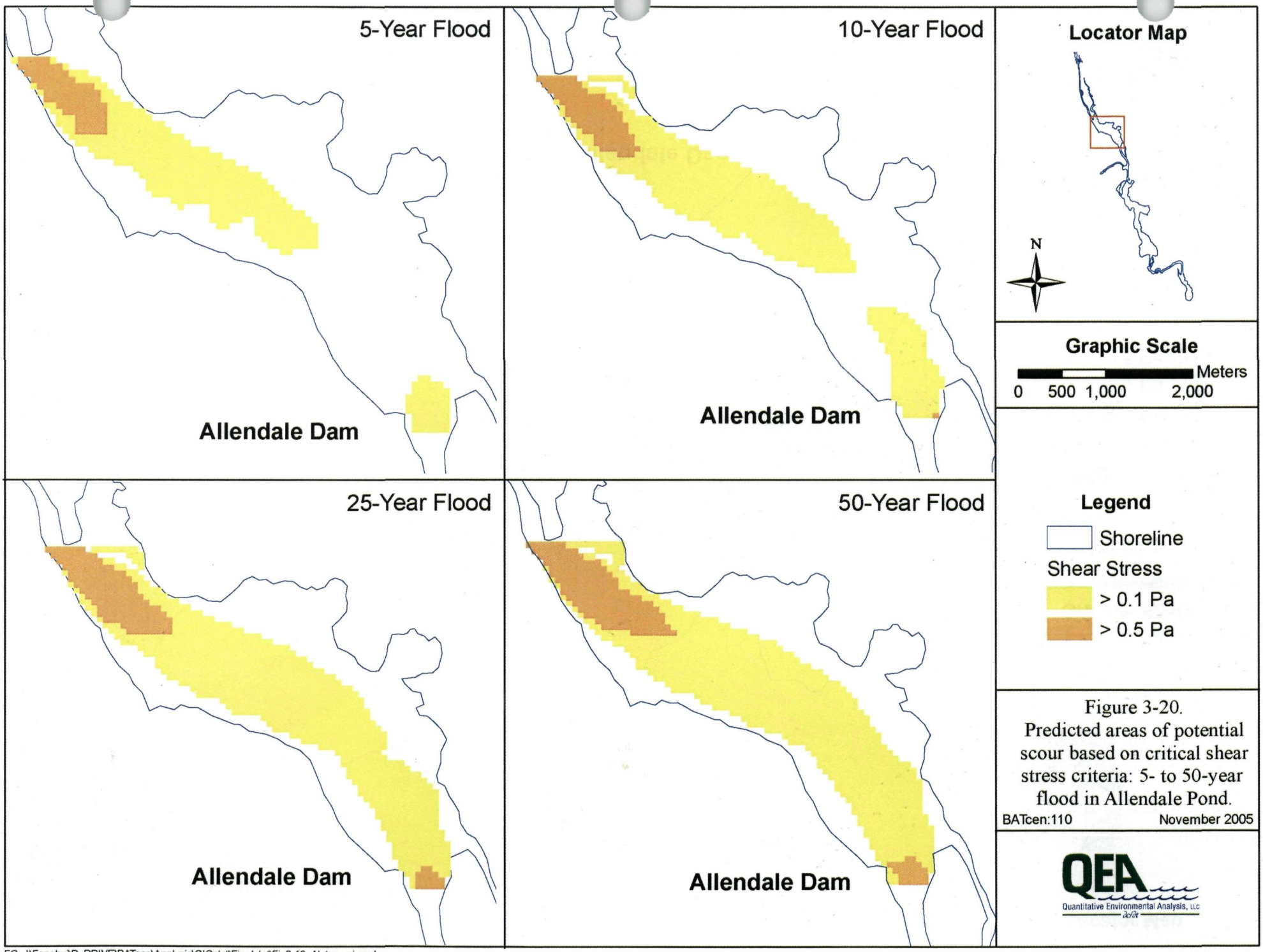

Figure 3-20.
Predicted areas of potential scour based on critical shear stress criteria: 5- to 50-year flood in Allendale Pond.

BATcen:110 November 2005

FC - \\Fanghui\D_DRIVE\BATcen\Analysis\GISplot\Finalplot\Fig3-18_Al_tao_cri.mxd

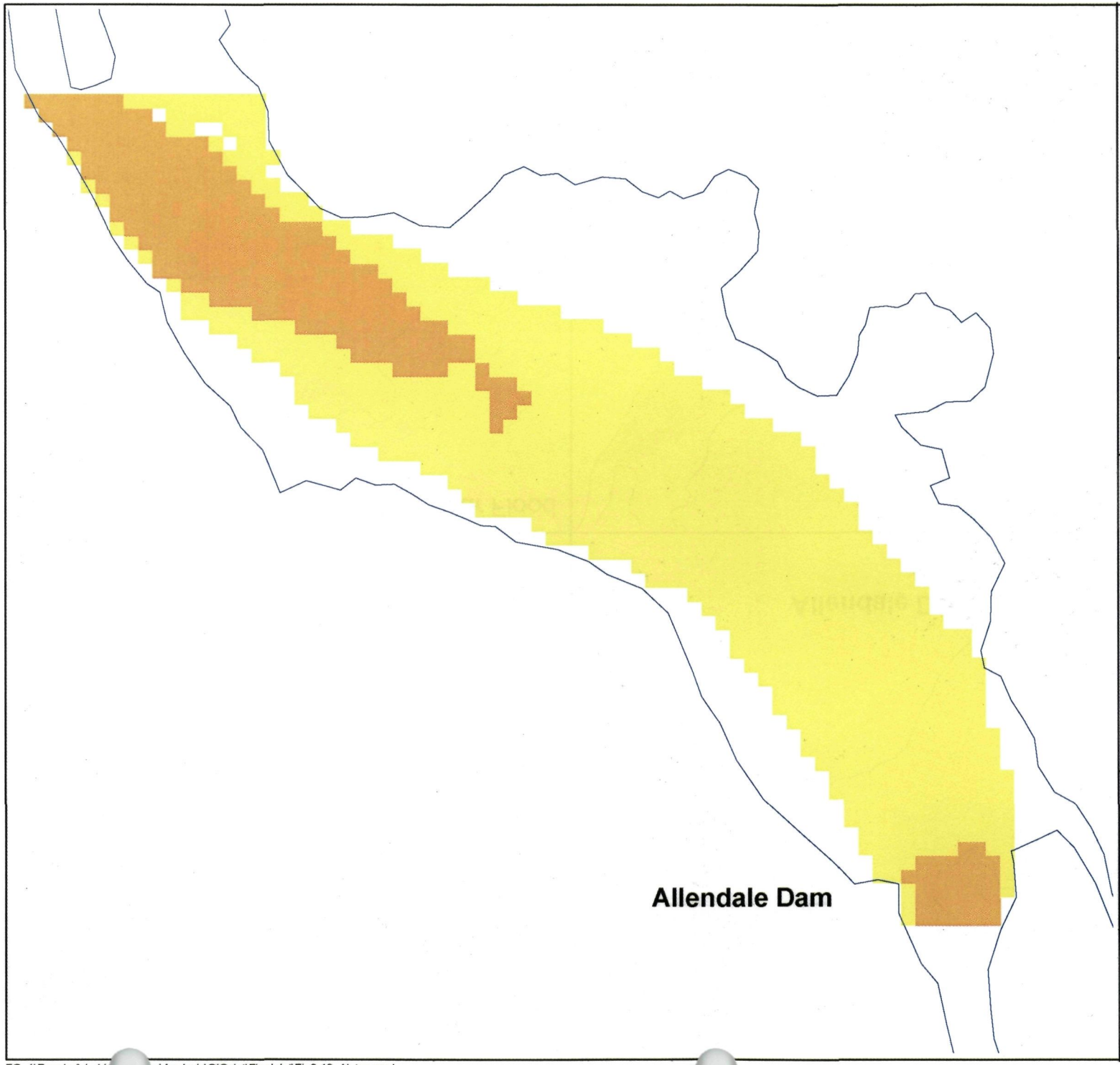

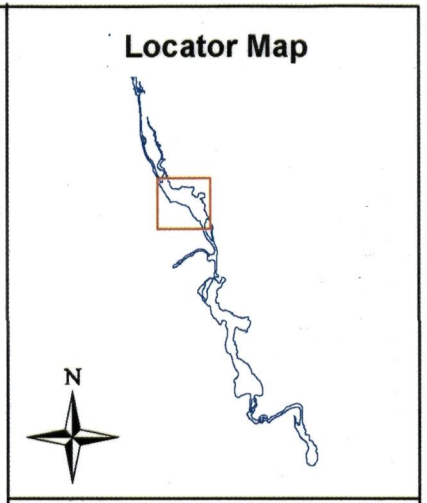

Graphic Scale

0 500 1,000 2,000 Meters

Legend

Shoreline

Shear Stress

> 0.1 Pa

> 0.5 Pa

Figure 3-21.
Predicted area of potential scour based on critical shear stress criteria: 100-year flood in Allendale Pond.

BATcen:110 November 2005

QEA
Quantitative Environmental Analysis, LLC

FC - \\Fanghui\d_dri\ en\Analysis\GISplot\Finalplot\Fig3-19_Al_tao.mxd

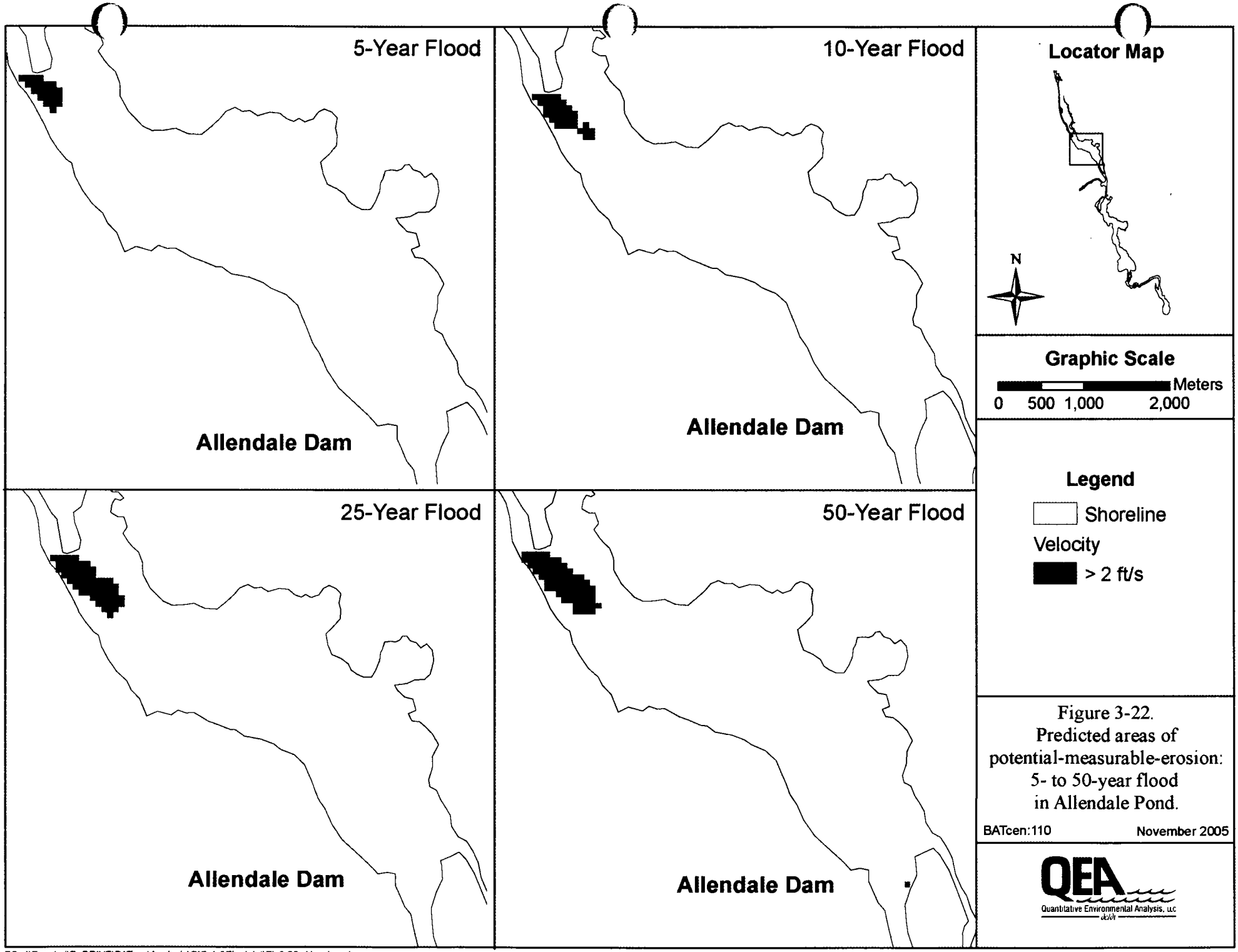

Figure 3-22.
Predicted areas of potential-measurable-erosion: 5- to 50-year flood in Allendale Pond.

BATcen:110 November 2005

FC - \\Fanghui\D_DRIVE\BATcen\Analysis\GISplot\Finalplot\Fig3-22_Al_vel.mxd

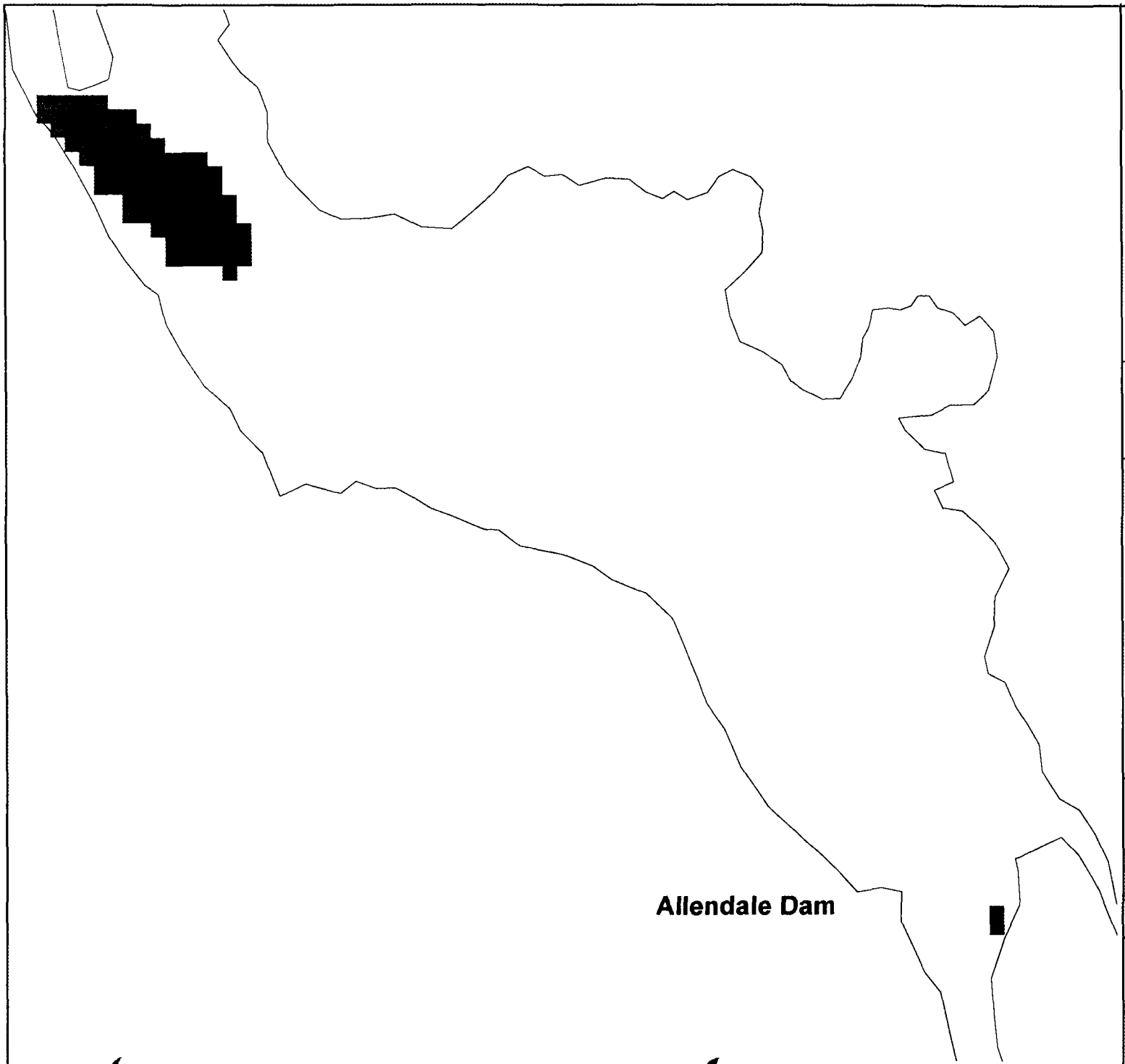

Locator Map

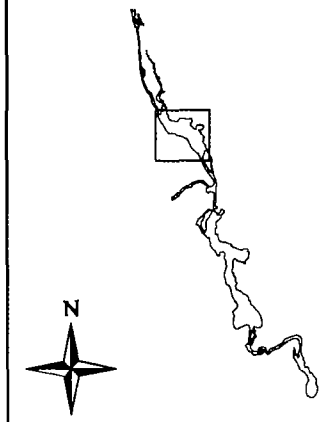

Graphic Scale

Meters

0 500 1,000 2,000

Legend

Shoreline

Velocity

> 2 ft/s

Figure 3-23.
Predicted areas of potential-measurable-erosion: 100-year flood in Allendale pond.

BATcen:110 November 2005

QEA
Quantitative Environmental Analysis, LLC

FC - \\Fanghui\d_dri n\Analysis\GISplot\Finalplot\Fig3-23_Al_vel.mxd

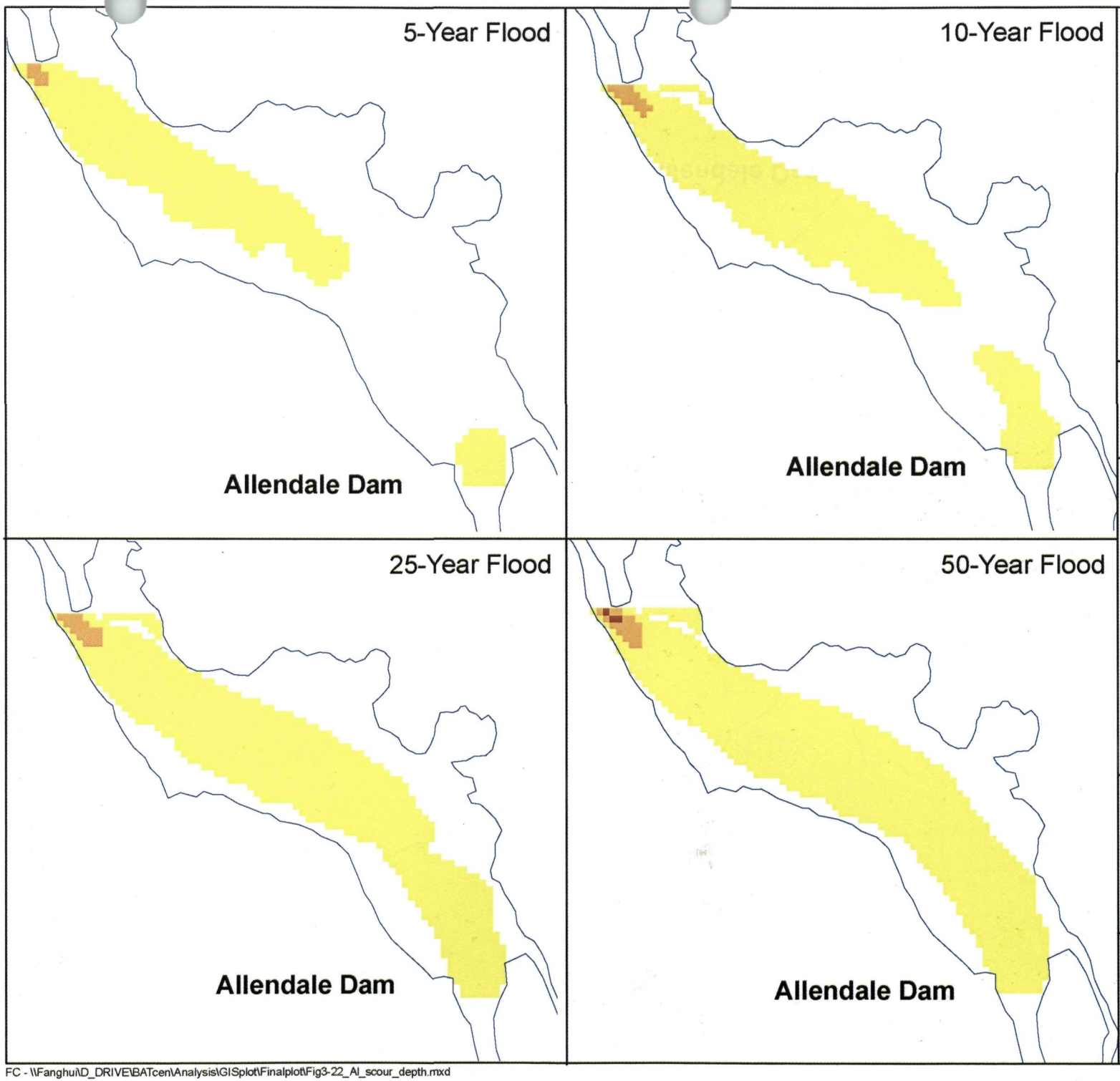

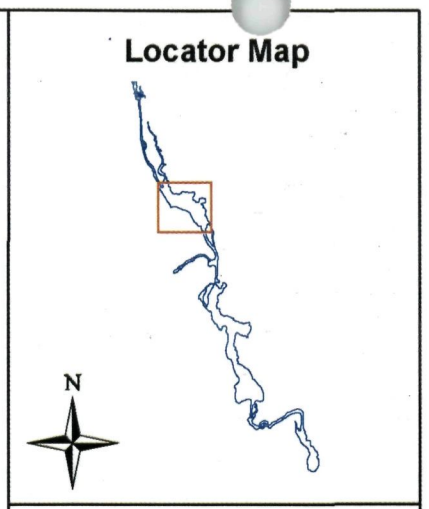

Graphic Scale

Meters

0 500 1,000 2,000

Legend

Shoreline

Scour Depth (cm)

0 - 1

1 - 5

> 5

Figure 3-24.
Spatial distribution of scour depth: 5- to 50-year flood in Allendale Pond.

BATcen:110 November 2005

QEA
Quantitative Environmental Analysis, LLC

FC - \\Fanghui\D_DRIVE\BATcen\Analysis\GISplot\Finalplot\Fig3-22_Al_scour_depth.mxd

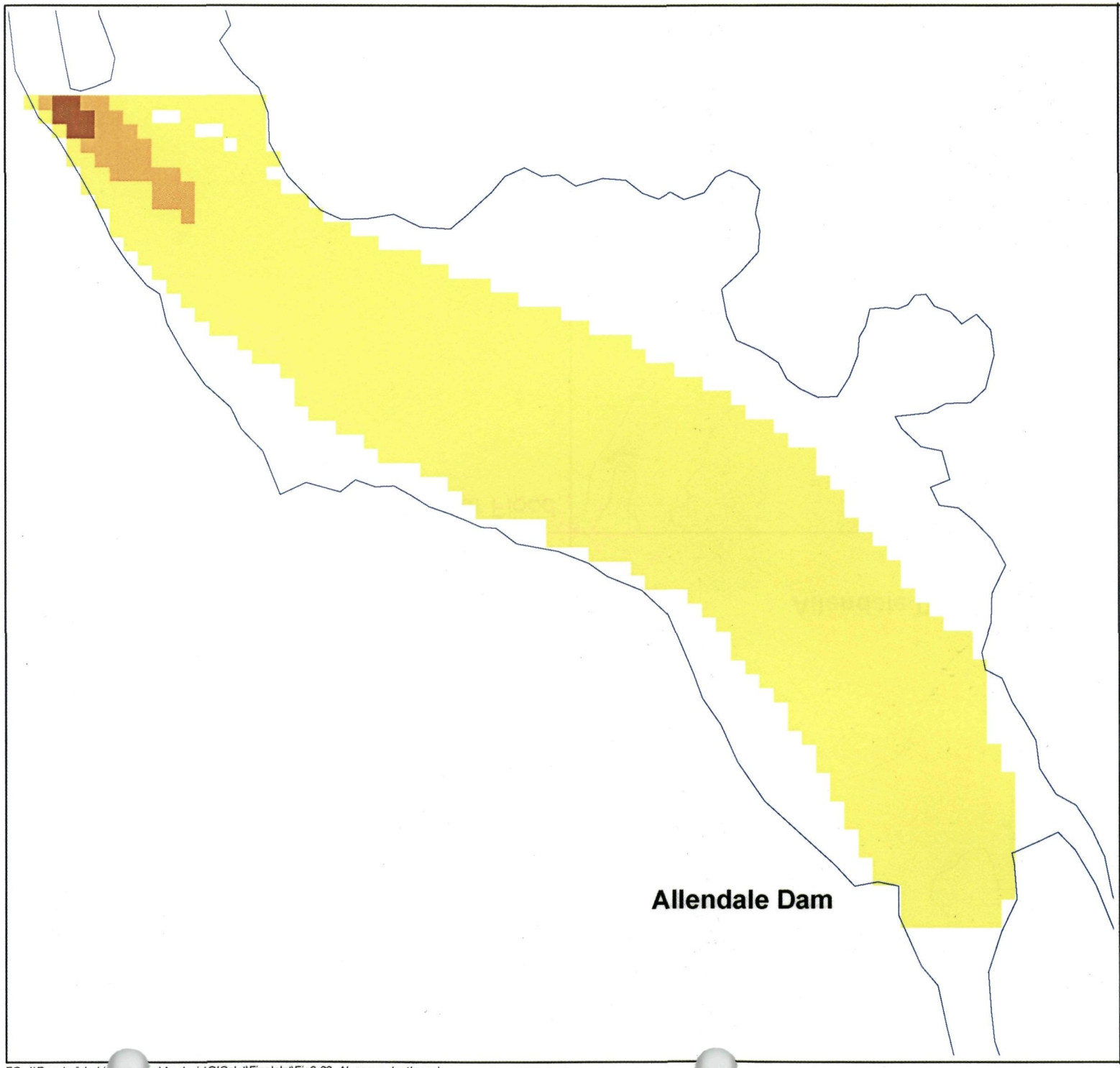

Locator Map

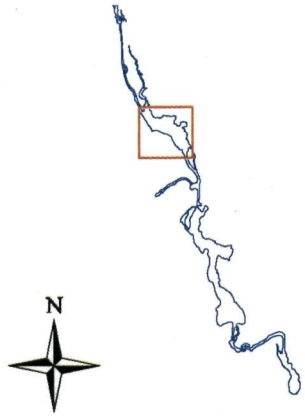

Graphic Scale

0 500 1,000 2,000 Meters

Legend

Shoreline

Scour depth (cm)

0 - 1

1 - 5

> 5

Figure 3-25.
Spatial distribution of scour depth: 100-year flood in Allendale Pond.

BATcen:110 November 2005

QEA
Quantitative Environmental Analysis, LLC

FC - \\Fanghui\d_dri en\Analysis\GISplot\Finalplot\Fig3-23_Al_scour_depth.mxd

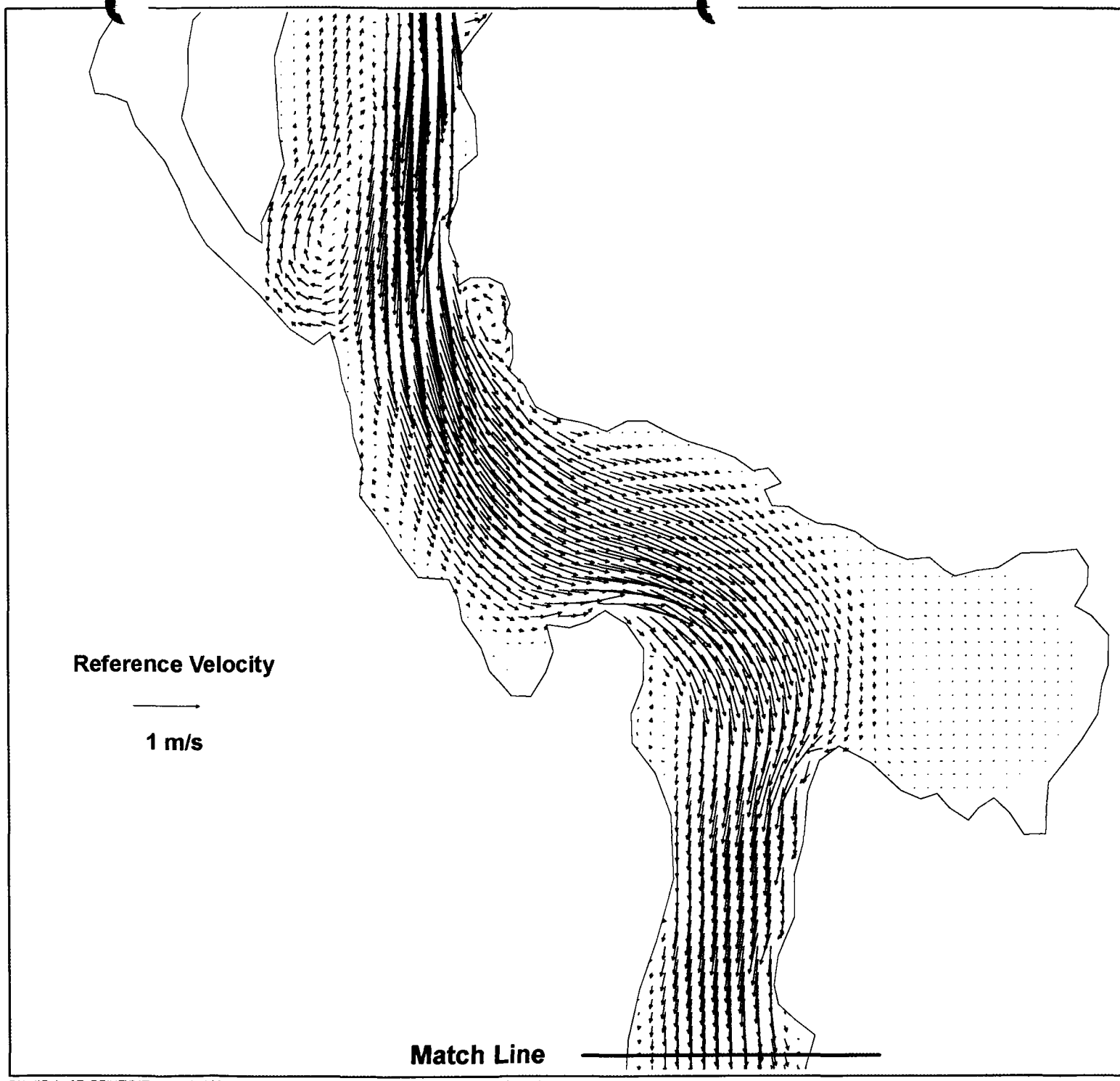

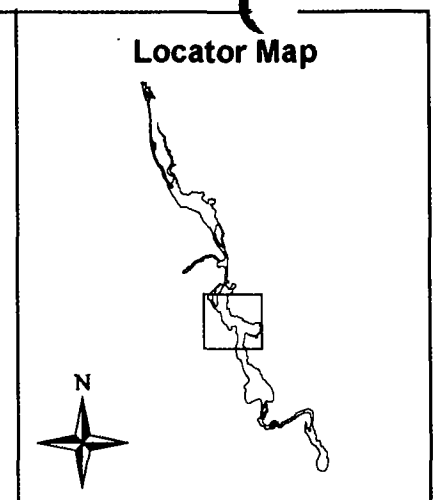

Graphic Scale

Meters

0 500 1,000 2,000

Legend

1997 Shoreline

Velocity Vector

Figure 3-26.
Predicted current velocities during 100-year flood in Lyman Mill Pond: northern portion.

BATcen:110 November 2005

QEA
Quantitative Environmental Analysis, LLC

DN - \\Daleel\E_DRIVE\BATcen\Analysis\Analysis\Model_Outputs\Get_vel_tau_scour\Figs_3-24_3-25.mxd

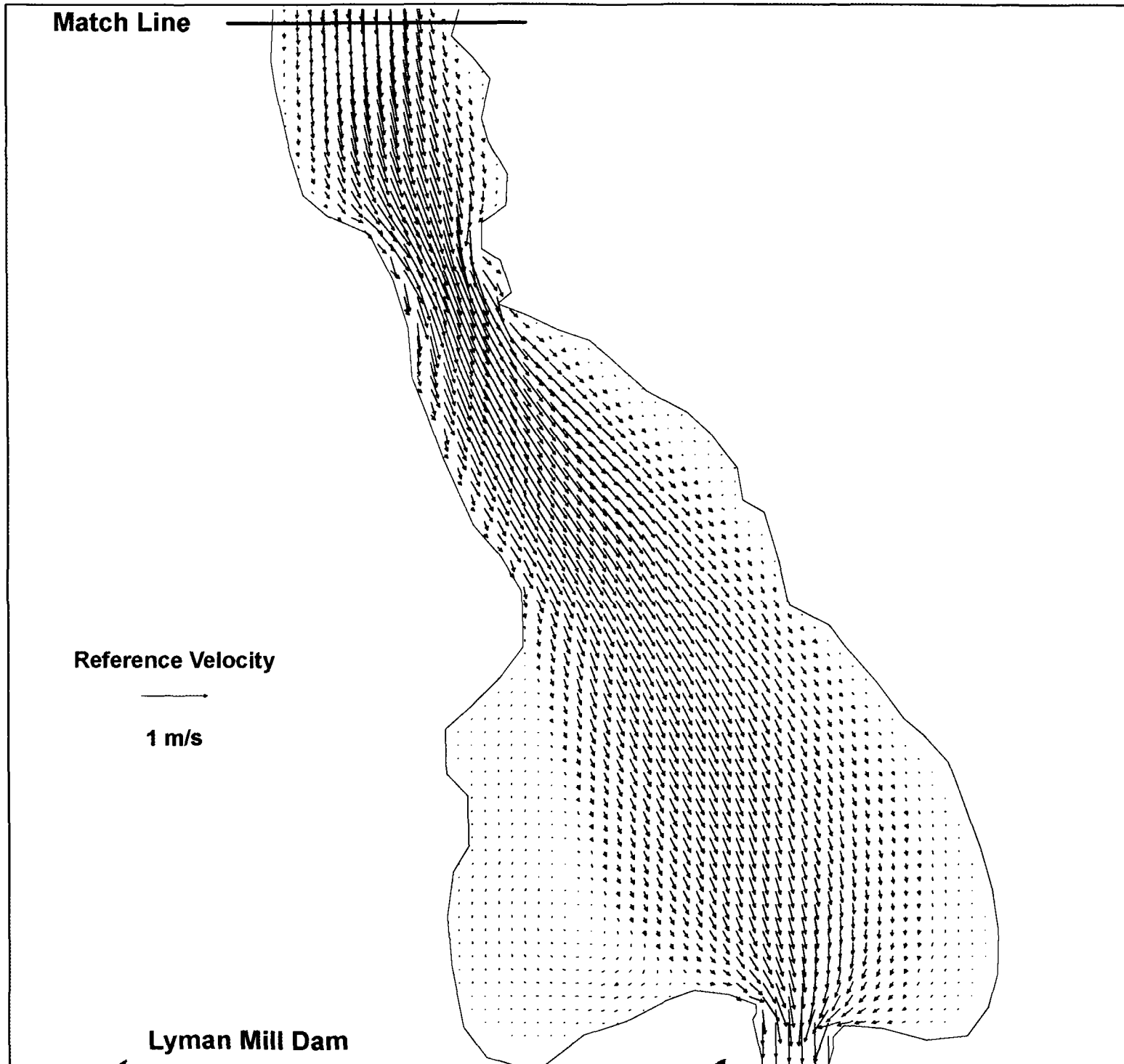

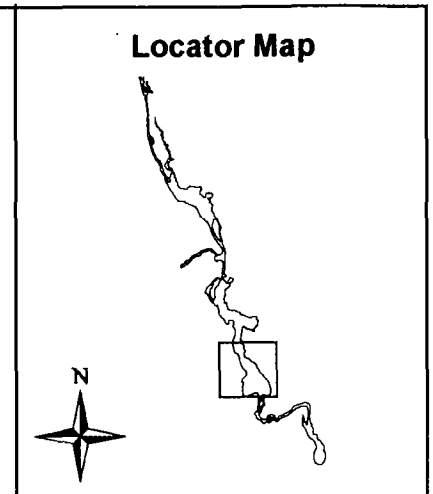

Graphic Scale

0 500 1,000 2,000 Meters

Legend

1997 Shoreline

Velocity Vector

Figure 3-27.
Predicted current velocities during 100-year flood in Lyman Mill Pond: southern portion.

BATcen:110 November 2005

QEA
Quantitative Environmental Analysis, LLC

DN - \\Daleel\E_DRIV ...en\Analysis\Analysis\Model_Outputs\Get_vel_tau_scour\Figs_3-24_3-25.mxd

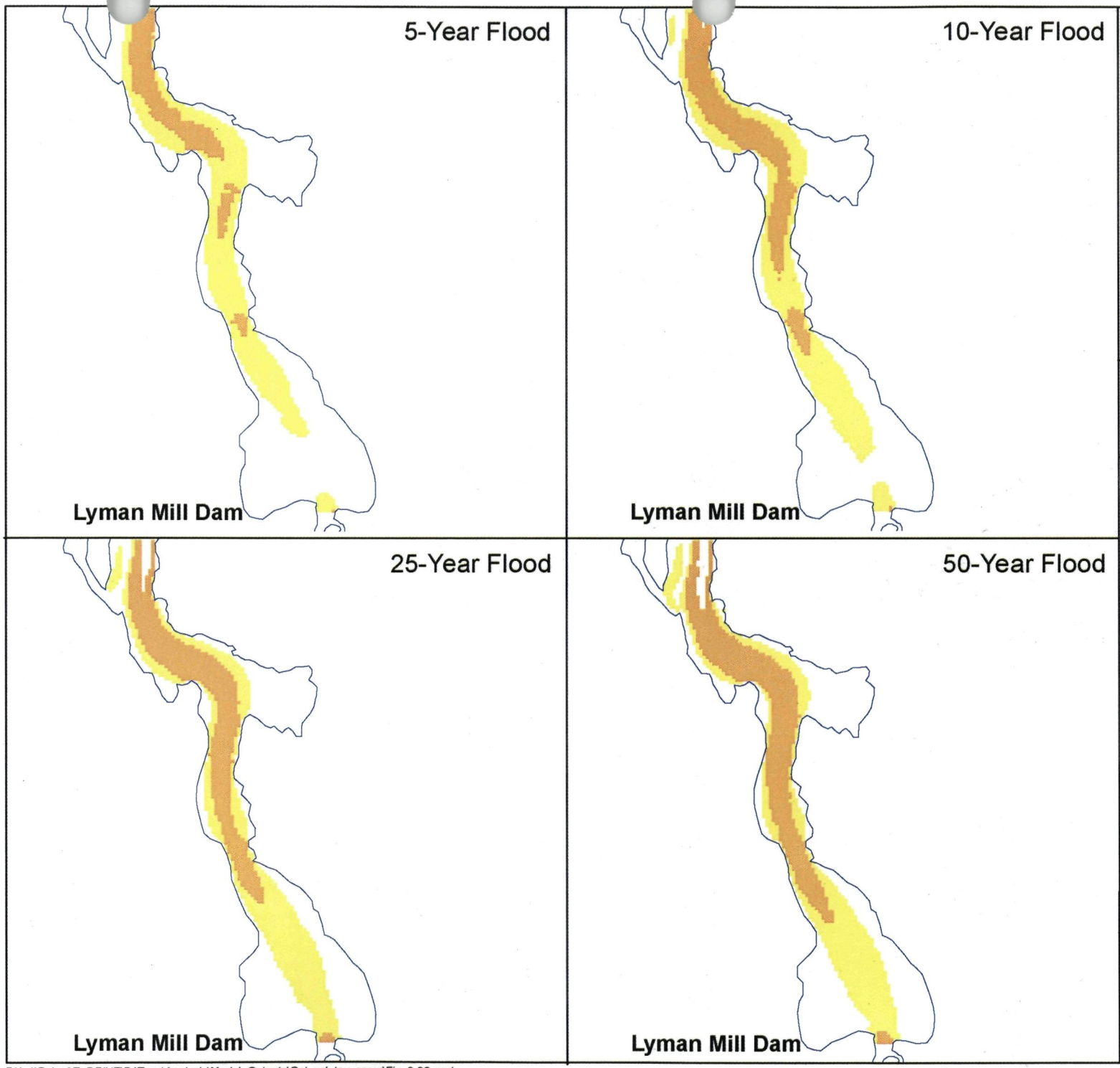

Locator Map

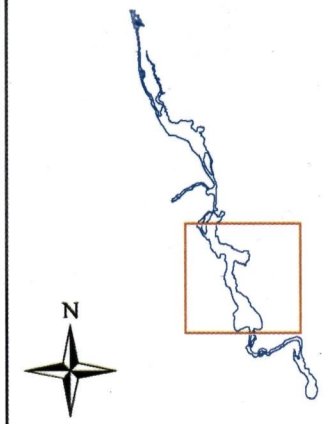

Graphic Scale

Meters

0 500 1,000 2,000

Legend

1997 Shoreline

Shear Stress

> 0.1 Pa

> 0.5 Pa

Figure 3-28.
Predicted areas of potential scour based on critical shear stress criteria: 5- to 50-year flood in Lyman Mill Pond.

BATcen:110 November 2005

QEA
Quantitative Environmental Analysis, LLC
$\partial c/\partial t$

DN - \\Daleel\E_DRIVE\BATcen\Analysis\Model_Outputs\Get_vel_tau_scour\Fig_3-26.mxd

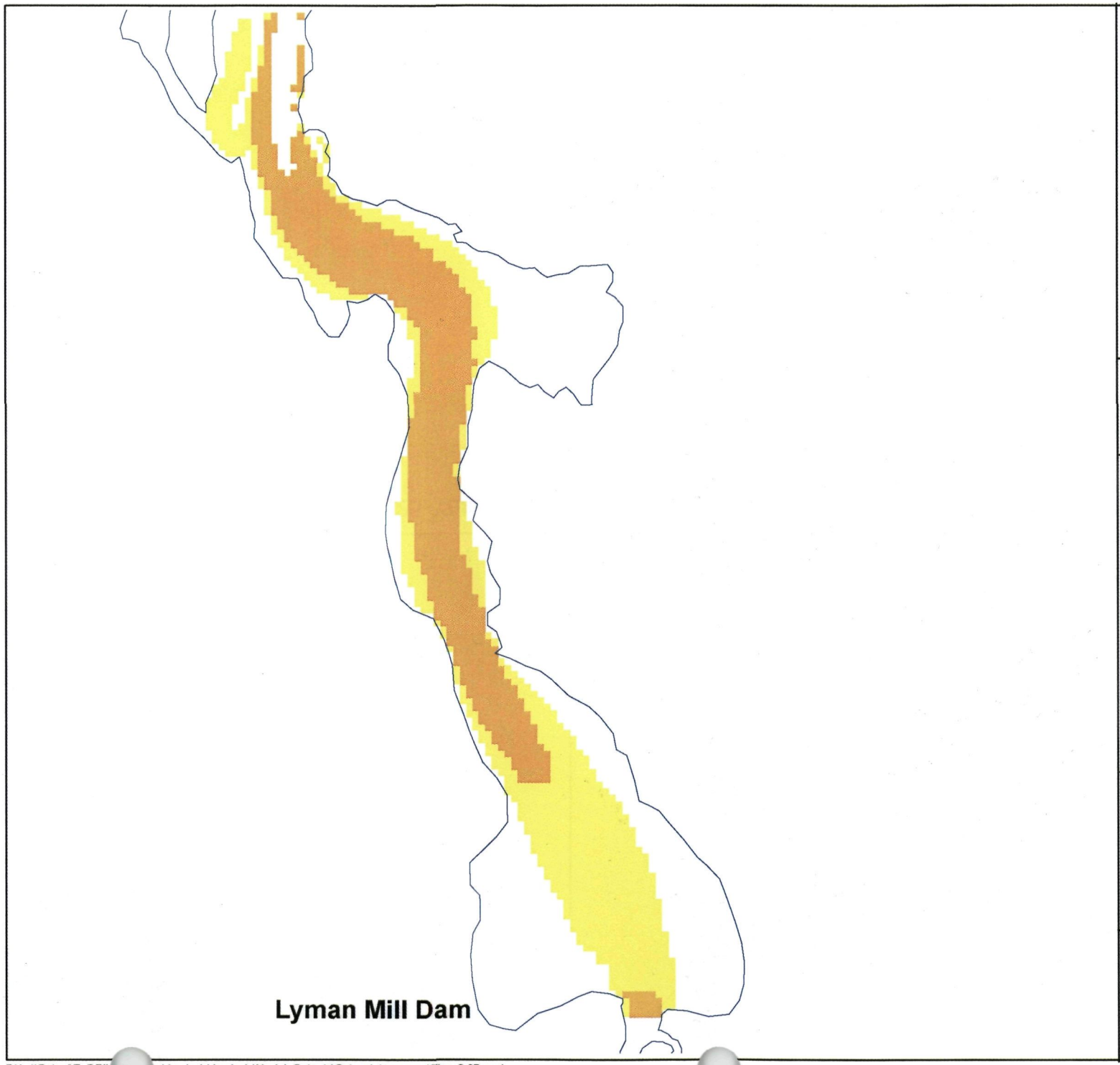

Locator Map

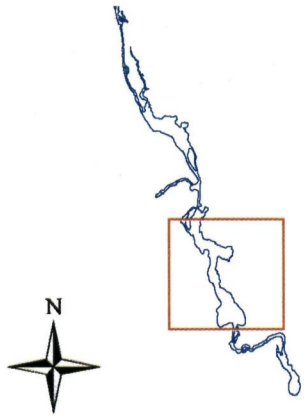

Graphic Scale

Meters

0 500 1,000 2,000

Legend

1997 Shoreline

Shear Stress

> 0.1 Pa

> 0.5 Pa

Figure 3-29.
Predicted areas of potential scour based on critical shear stress criteria: 100-year flood in Lyman Mill Pond.

BATcen:110 November 2005

QEA
Quantitative Environmental Analysis, LLC
$\partial c/\partial t$

DN - \\Daleel\E_DRI\ en\Analysis\Analysis\Model_Outputs\Get_vel_tau_scour\Figs_3-27.mxd

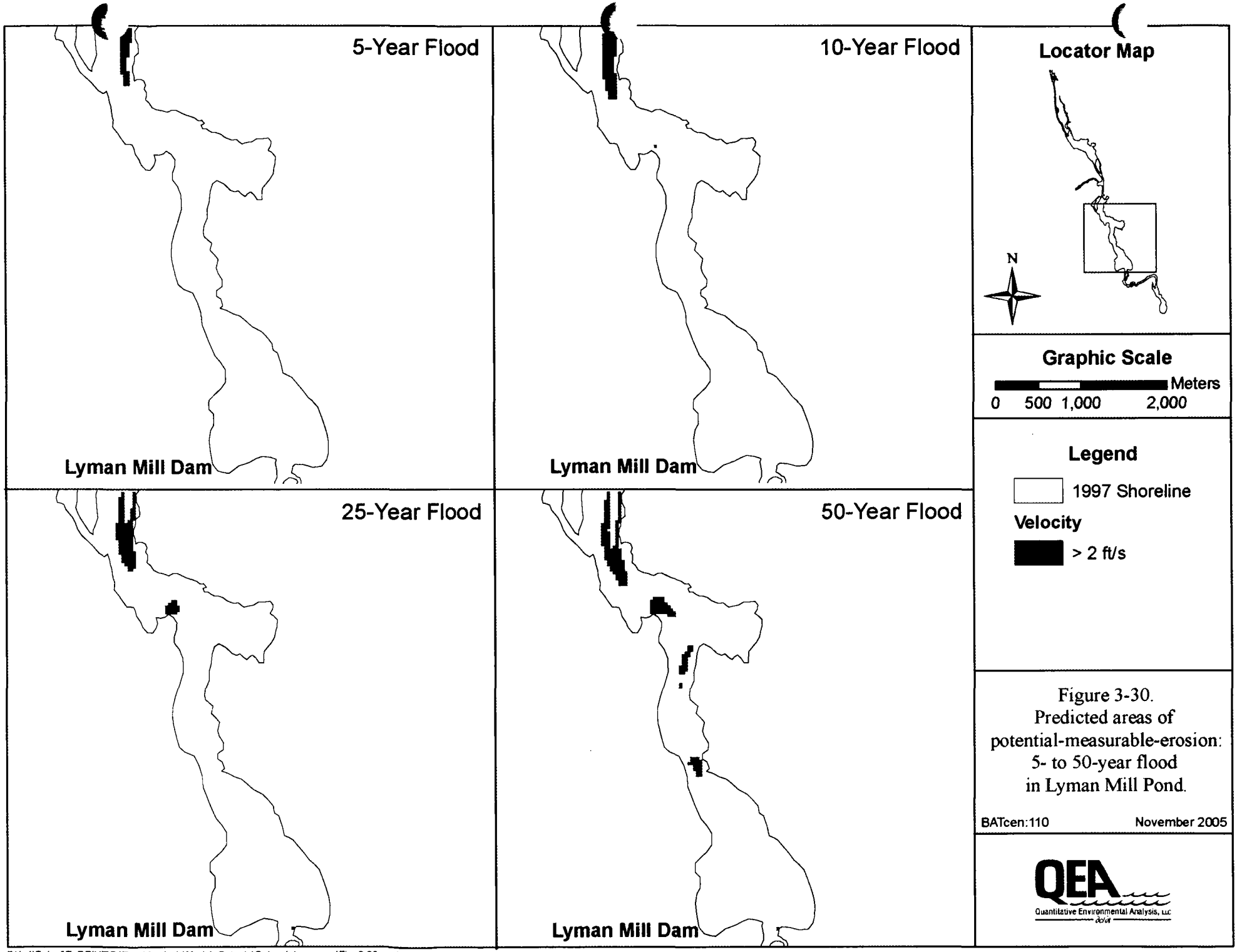

Figure 3-30.
Predicted areas of potential-measurable-erosion: 5- to 50-year flood in Lyman Mill Pond.

BATcen:110 November 2005

DN - \\Daleel\E_DRIVE\BATcen\Analysis\Model_Outputs\Get_vel_tau_scour\Fig_3-28.mxd

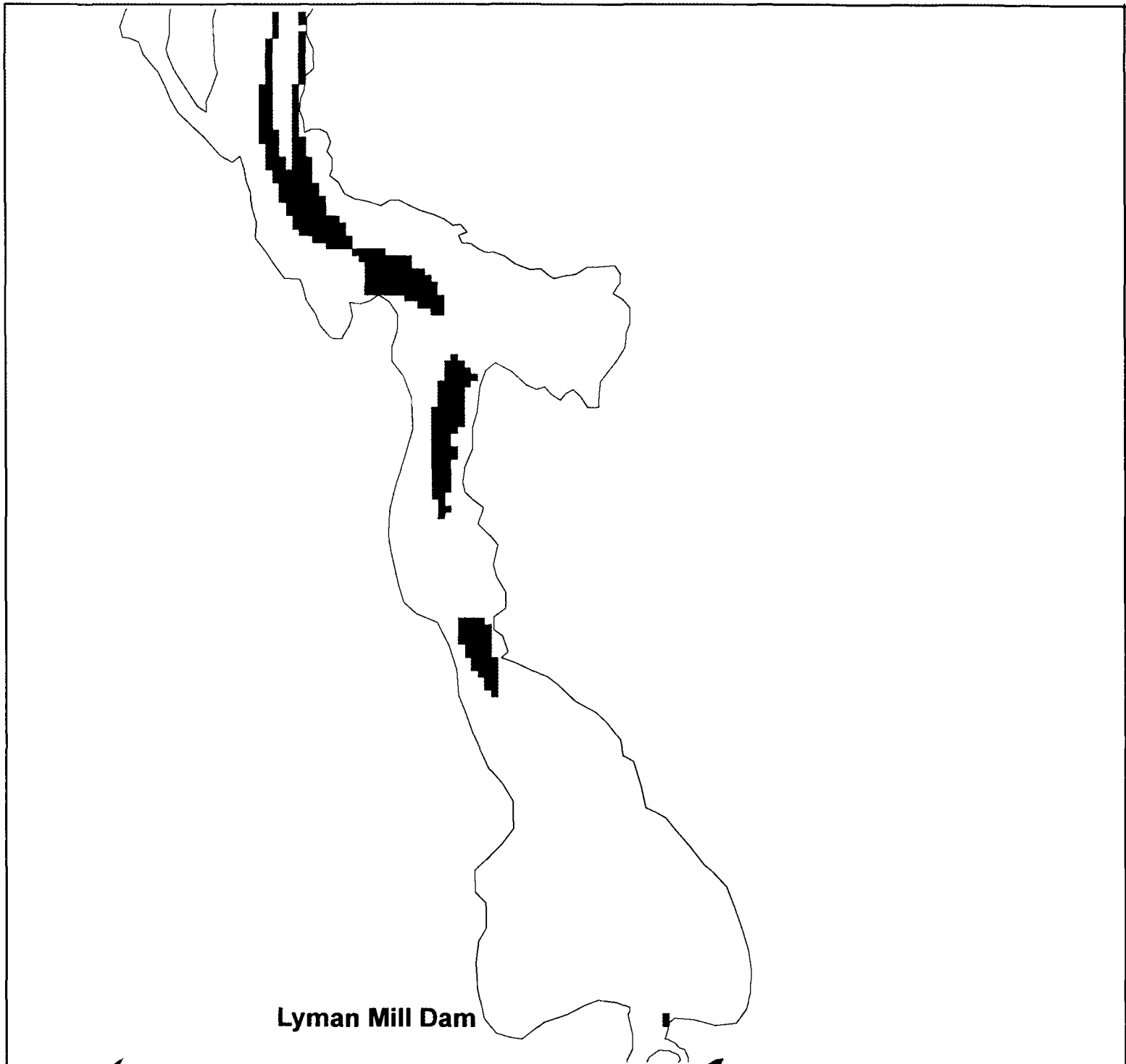

Locator Map

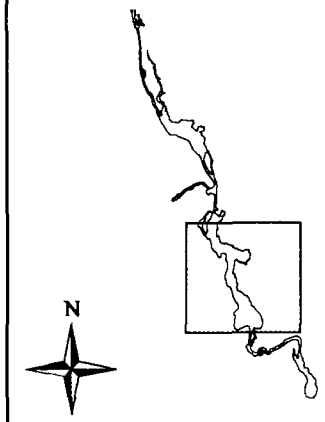

Graphic Scale

Meters

0 500 1,000 2,000

Legend

1997 Shoreline

Velocity

> 2 ft/s

Figure 3-31.
Predicted areas of potential-measurable-erosion: 100-year flood in Lyman Mill Pond.

BATcen:110 November 2005

QEA Quantitative Environmental Analysis, LLC

DN - \\Daleel\E_DRI\ en\Analysis\Analysis\Model_Outputs\Get_vel_tau_scour\Figs_3-29.mxd

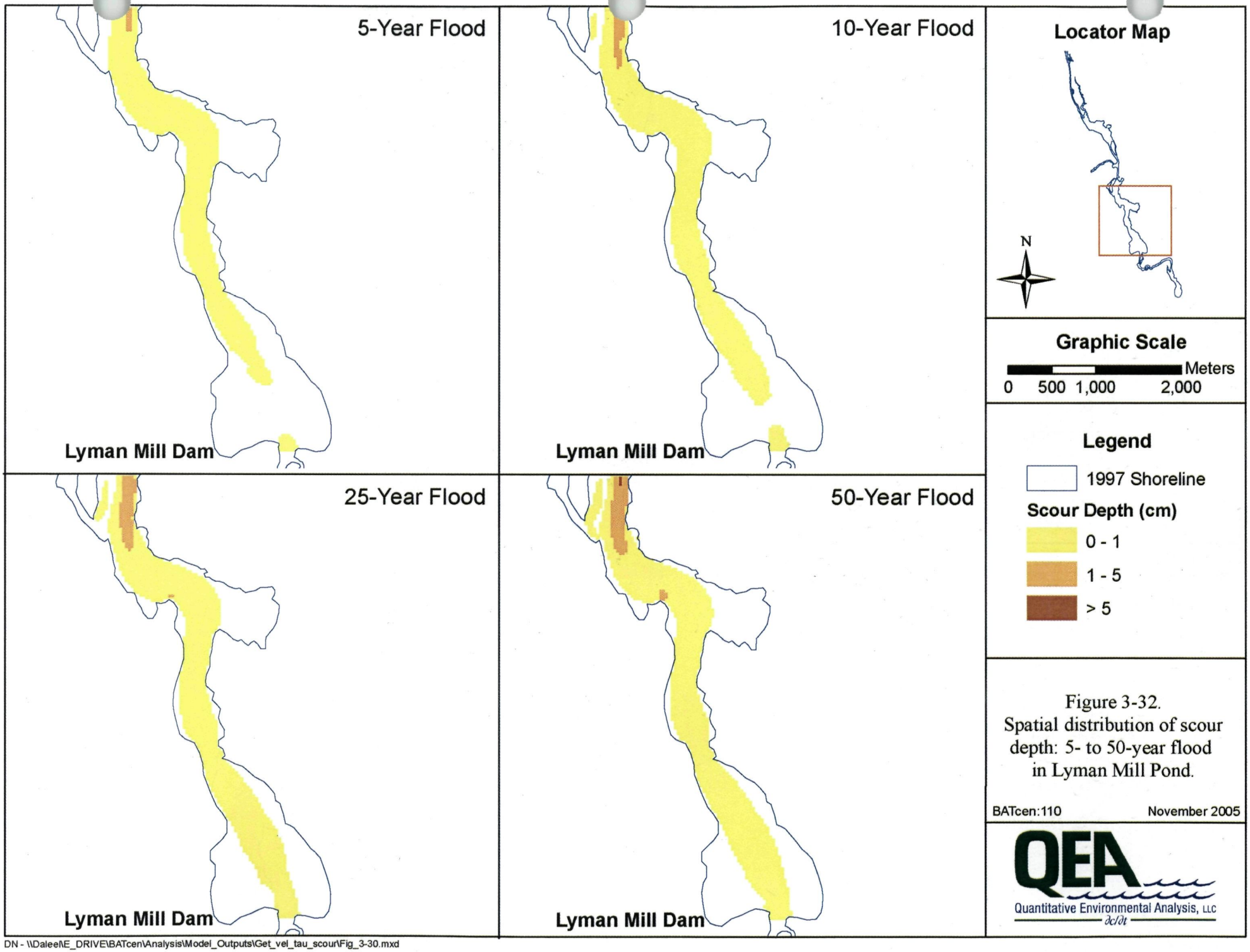

Figure 3-32.
Spatial distribution of scour depth: 5- to 50-year flood in Lyman Mill Pond.

DN - \\Daleel\E_DRIVE\BATcen\Analysis\Model_Outputs\Get_vel_tau_scour\Fig_3-30.mxd

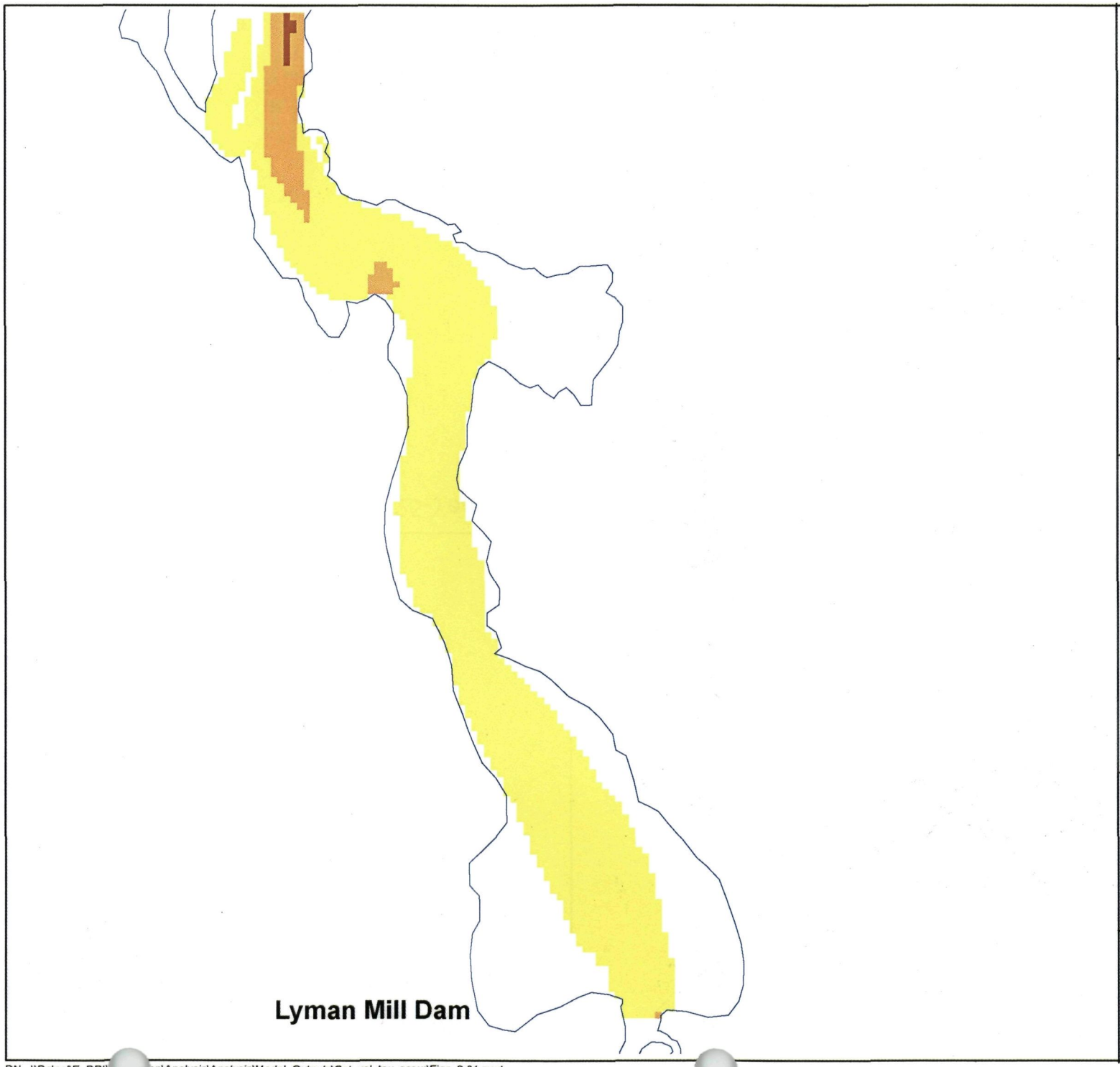

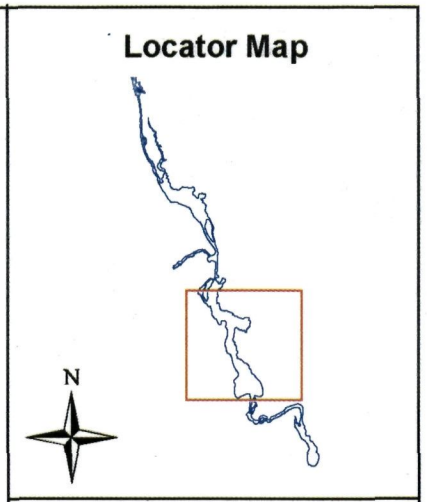

Graphic Scale

0 500 1,000 2,000 Meters

Legend

1997 Shoreline

Scour Depth (cm)

0 - 1

1 - 5

> 5

Figure 3-33.
Spatial distribution of scour depth: 100-year flood in Lyman Mill Pond.

BATcen:110 November 2005

QEA
Quantitative Environmental Analysis, LLC
$\partial c/\partial t$

DN - \\Daleel\E_DRI\ en\Analysis\Analysis\Model_Outputs\Get_vel_tau_scour\Figs_3-31.mxd

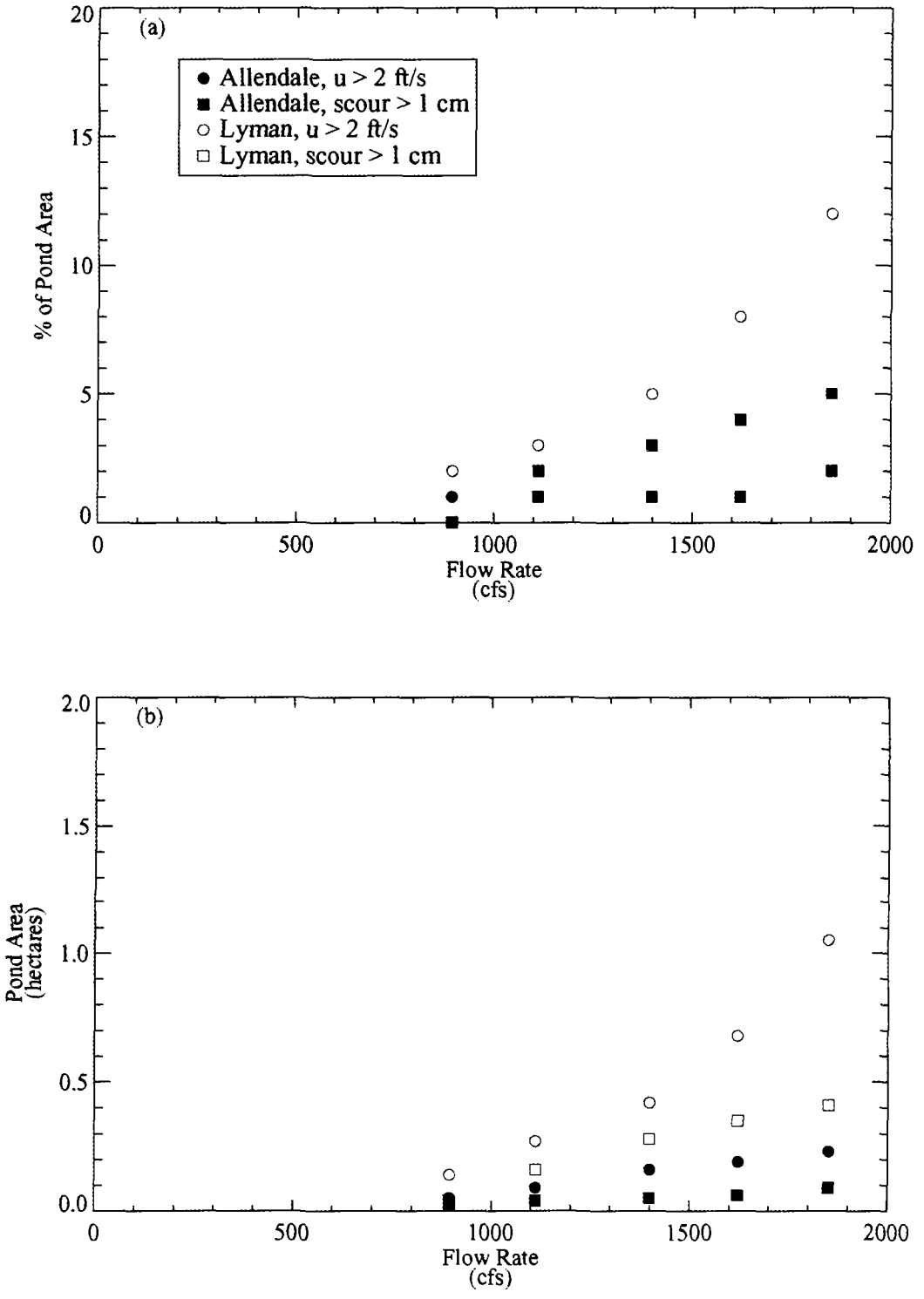

Figure 3-34. Comparison of areas of scour depth > 1 cm and velocity > 2 ft/s between the two ponds: (a) % of pond area vs. flow rate and (b) pond area vs. flow rate.

lz - D:\BATcen\Analysis\Model_Outputs\sensitivity_plots\plot_fig_3_34_051118.pro
Mon Nov 21 09:13:46 2005

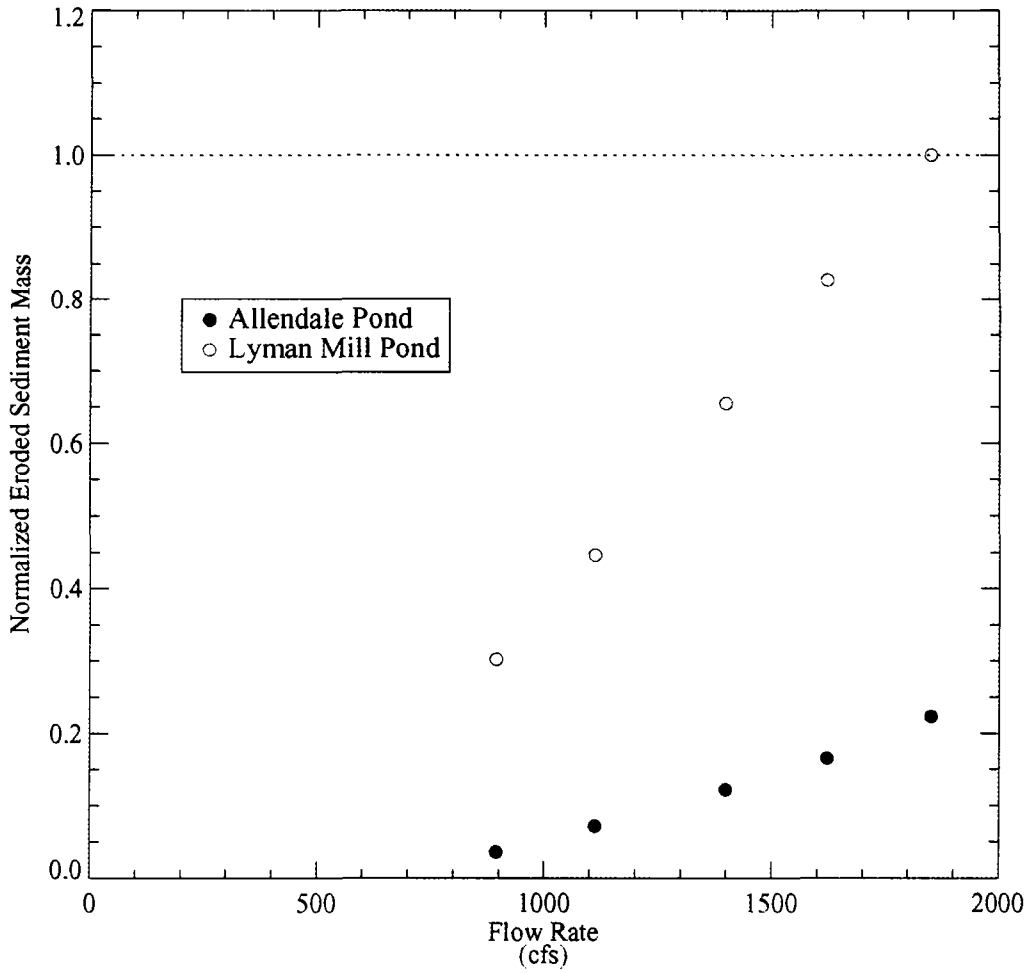

Figure 3-35. Comparison of variation in erosion mass with flow rate between the two ponds. Erosion mass is normalized with respect to the predicted mass for Lyman Mill Pond during a 100-year flood.

lz - D:\BATcen\Analysis\Model_Outputs\sensitivity_plots\plot_fig_3_35_051118.pro
Mon Nov 21 09:15:23 2005

APPENDIX B

POTENTIAL IMPACT OF UPSTREAM RESERVOIR RELEASES ON BED STABILITY IN ALLENDALE AND LYMAN MILL PONDS

Water is occasionally released from reservoirs that are located upstream of Allendale and Lyman Mill Ponds on the Woonasquatucket River. These reservoir releases cause flow rate increases in the river, with maximum flow rates of approximately 200 ft^3/s (cfs) occurring in the river during the releases (Anna Krasko, USEPA, personal communication). For comparison, the average flow rate in the river at the U.S. Geological Survey (USGS) gaging station near Centredale is 73 cfs. The 5-year flood has an estimated flow rate of 894 cfs. Thus, discharges associated with the upstream reservoir releases, which result in flow rates less than about 200 cfs, should not be characterized as floods, but are more appropriately viewed as moderate flow rates. Note that the flow rate range investigated in this study was specified by USEPA. An analysis of upstream reservoir releases was not conducted as part of this study.

The hydrodynamic model was used to simulate flow in Allendale and Lyman Mill Ponds for two flow conditions in the river: 1) 100 cfs and 2) 200 cfs. These two discharge rates correspond to the approximate range of flow conditions created by releases from upstream reservoirs. The model predicted spatial distributions of current velocity and bottom shear stress in the ponds for both flow rates. These results were used to assess the potential impacts on bed stability due to the upstream releases using two methods: 1) comparison of bottom shear stress and current velocity to critical values of those parameters; and 2) estimation of scour depth. Note that for the analysis conducted in this study, only the magnitude of river flow rate impacts the predicted scour depth. The process creating the increased river discharge, i.e., man-made release or natural watershed runoff, does not affect the estimated scour depths.

Areas in Allendale Pond where the bottom shear stress exceeds the upper- and lower-bound estimates of τ_{cr} (i.e., 0.1 and 0.5 Pa) for the two flow conditions are presented on Figures B-1 and B-2. For a 100 cfs flow rate, current velocities did not exceed the critical velocity criterion for potential-measurable-erosion (i.e., 2 ft/s). Current velocities exceeding the critical velocity criterion for potential-measurable-erosion (i.e., 2 ft/s) for a 200 cfs flow rate are predicted in the area shown on Figure B-3. These results indicate that bed erosion may occur in a relatively small portion of Allendale Pond, located near the upstream inlet of the pond, for flow rates less than 200 cfs.

In Lyman Mill Pond, bottom shear stress does not exceed the upper- and lower-bound estimates of τ_{cr} (i.e., 0.1 and 0.5 Pa) for the 100 cfs flow rate. Figure B-4 shows areas where bottom shear stress exceeds the upper- and lower-bound estimates of τ_{cr} (i.e., 0.1 and 0.5 Pa) for the 200 cfs flow rate. Current velocities exceeding the critical velocity criterion for potential-measurable-erosion (i.e., 2 ft/s) for the 200 cfs flow rate are predicted in the areas shown on Figure B-5. Potential-measurable-erosion is not predicted for the 100 cfs flow rate. Similar to Allendale Pond, bed erosion is predicted to occur in a relatively small portion of Lyman Mill Pond due to releases from upstream reservoirs.

A summary of estimated bed scour depths in the two ponds is presented in Table B-1. Consistent with the hydrodynamic results discussed above, minimal bed scour is predicted in the ponds for flow rates that occur during releases from upstream reservoirs.

Table B-1. Summary of Estimated Bed Scour Depths

Pond	Flow Rate (cfs)	Area with Scour > 1 cm (hectares)	% of Pond Area with Scour > 1 cm	Mass of Eroded Sediment (metric tons)	Maximum Scour Depth (cm)
Allendale	100	0	0	< 0.01	< 0.01
Allendale	200	0	0	0.11	0.06
Lyman Mill	100	0	0	< 0.01	< 0.01
Lyman Mill	200	0	0	1.5	0.12

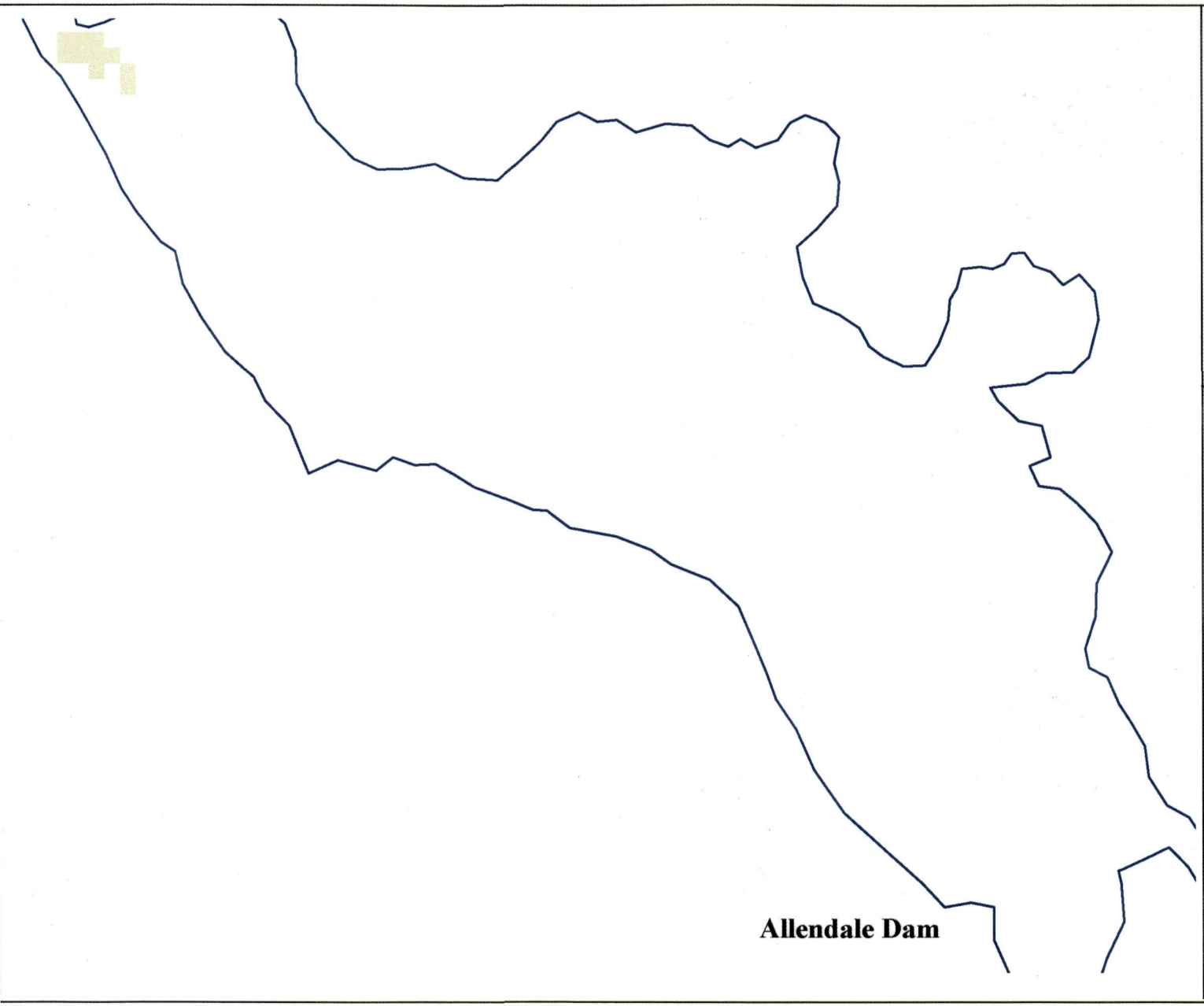

Locator Map

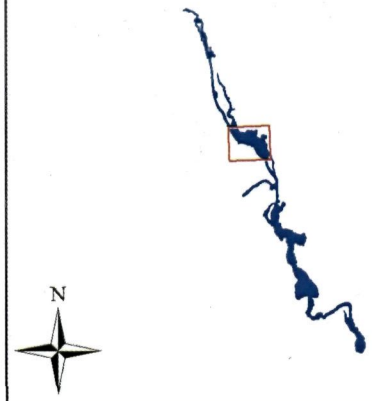

Legend

1997 Shoreline

Shear Stress

> 0.1 Pa

> 0.5 Pa

Figure B-1. Predicted areas of potential scour based on critical shear stress criteria: Flow rate = 100 cfs in Allendale Pond.

QEA
Quantitative Environmental Analysis, LLC

BATcen:121 **January 2005**

CO- C:\BATman\Maps\ArcGIS\shear_stress\batcen_allendale_tau_041220.mxd

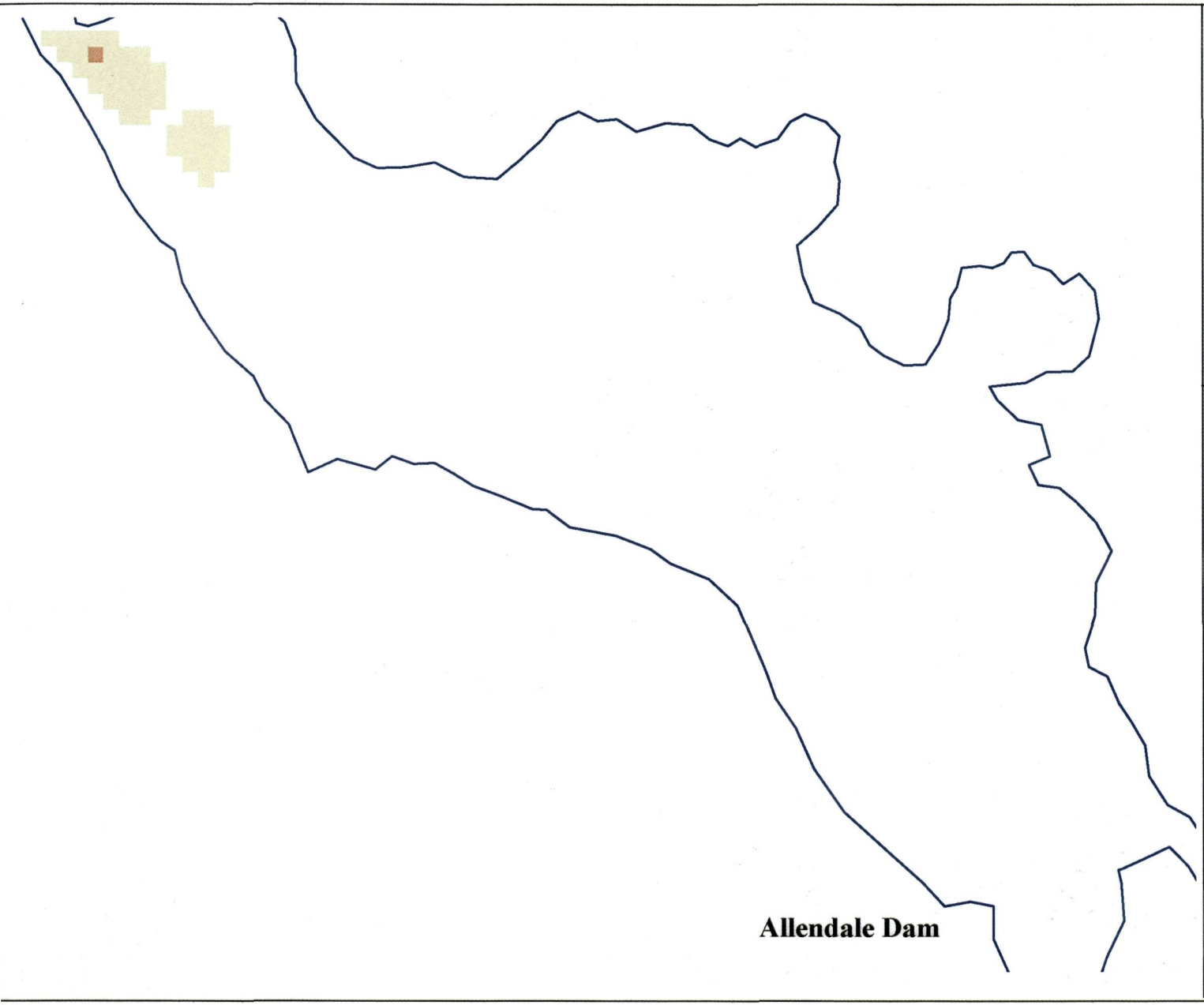

Locator Map

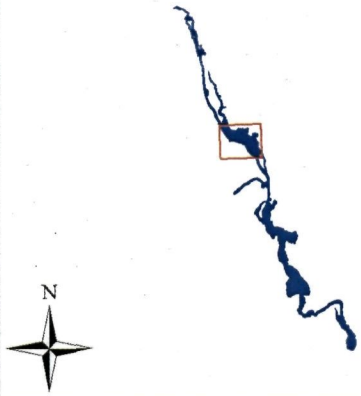

Legend

1997 Shoreline

Shear Stress

> 0.1 Pa

> 0.5 Pa

Figure B-2. Predicted areas of potential scour based on critical shear stress criteria: Flow rate = 200 cfs in Allendale Pond.

QEA Quantitative Environmental Analysis, LLC

BATcen:121 **January 2005**

CO- C:\BATman\Maps\ArcGIS\shear_stress\batcen_allendale_tau_041220.mxd

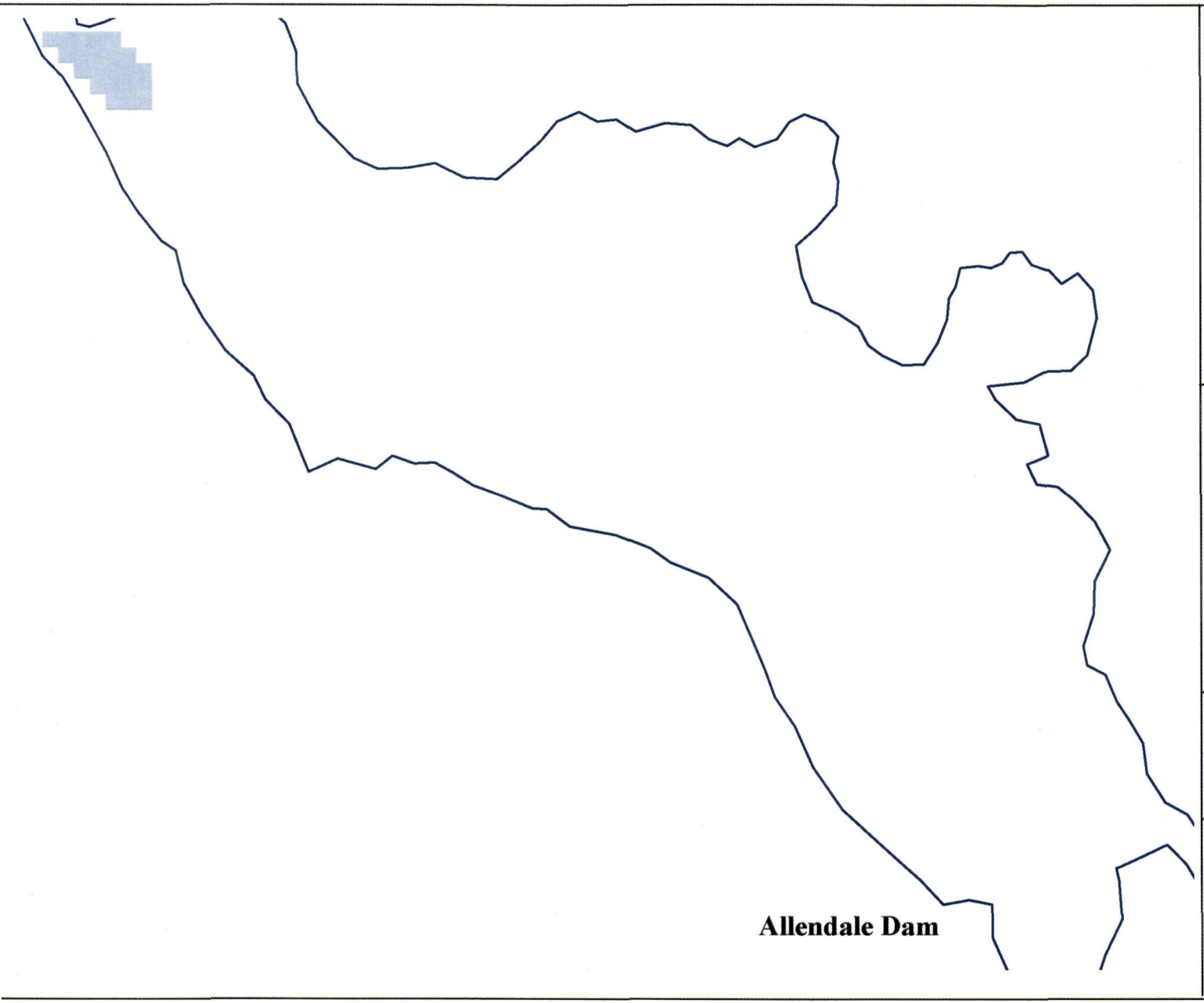

Locator Map

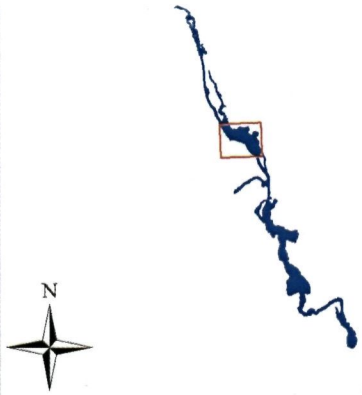

Legend

1997 Shoreline

Velocity

> 2 ft/s

Figure B-3. Predicted areas of potential significant scour based on 2 ft/s velocity criterion: Flow rate = 200 cfs in Allendale Pond.

QEA
Quantitative Environmental Analysis, LLC

BATcen:121 **January 2005**

CO- C:\BATman\Maps\ArcGIS\velocity\batcen_allendale_velocity_041220.mxd

Locator Map

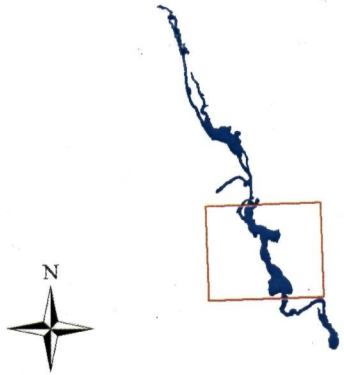

Legend

1997 Shoreline

Shear Stress

> 0.1 Pa

> 0.5 Pa

Figure B-4. Predicted areas of potential scour based on critical shear stress criteria: Flow rate = 200 cfs in Lyman Mill Pond.

QEA
Quantitative Environmental Analysis, LLC

BATcen:121 **January 2005**

CO- C:\BATman\Maps\ArcGIS\shear_stress\batcen_lyman_tau_041220.mxd

Locator Map

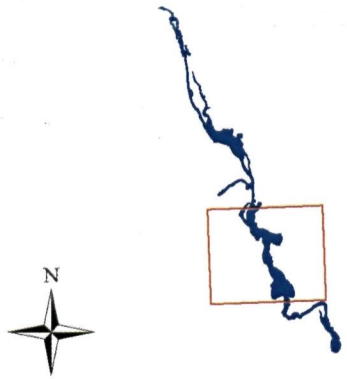

Legend

1997 Shoreline

Velocity

> 2 ft/s

Figure B-5. Predicted areas of potential significant scour based on 2 ft/s velocity criterion: Flow rate = 200 cfs in Lyman Mill Pond.

QEA
Quantitative Environmental Analysis, LLC

BATcen:121 **January 2005**

CO- C:\BATman\Maps\ArcGIS\velocity\batcen_lyman_velocity_041220.mxd